Electronic Thesis and Dissertation Repository

12-17-2019 3:00 PM

Self-healing of Concrete Under Diverse Environmental Exposure

Ahmed Ramadan Suleiman, *The University of Western Ontario*

Supervisor: Moncef L. Nehdi, *The University of Western Ontario*

A thesis submitted in partial fulfillment of the requirements for the Doctor of Philosophy degree in Civil and Environmental Engineering
© Ahmed Ramadan Suleiman 2019

Follow this and additional works at: https://ir.lib.uwo.ca/etd

Part of the Civil and Environmental Engineering Commons

ABSTRACT

Self-healing efficiency of cement-based materials has so far been evaluated mostly through the healing of surface cracks, without adequately capturing the dominant effects of environmental exposure or accurately quantifying the volume of cracks healed. In addition, the effects of diverse additions such as silica-based materials, swelling agents, superabsorbent polymers, and carbonating minerals on self-healing performance under different environmental exposure, remain largely unexplored.

In this dissertation, multiple test methods were used to investigate self-healing of cracks in cement mortar incorporating metakaolin, bentonite, fly ash, superabsorbent polymers, and calcium carbonate microfiller under different environmental exposure (i.e. cold and hot temperatures, high and low humidity, wet and dry cycles, and continuous underwater submersion). Change in crack width was monitored using optical microscopy. Scanning electron microscopy coupled with energy disperse X-ray analysis was used to identify healing compounds. Mercury intrusion porosimetry and water absorption were employed to assess porosity. X-ray computed micro-tomography (X-ray µCT) with 3-dimensional image processing was used to segment and quantify cracks before and after healing. The findings should stimulate concerted research efforts to bridge the gap between ideal laboratory conditions and realistic field exposure in future self-healing research endeavors.

Furthermore, an attempt was made to develop a hybrid artificial intelligence-based model to accurately predict the ability of concrete to heal its own cracks. A comprehensive database of concrete crack healing was created and used to train the proposed GA–ANN model. The results showed that the proposed GA–ANN model can capture the complex effects of various self-healing agents (e.g. biochemical material, silica-based additive, expansive and crystalline components) on the self-healing performance in cement-based materials. This could allow tailoring self-healing strategies for enhancing the durability design of concrete, thus leading to reduced maintenance and repair costs of concrete civil infrastructure.

Keywords: *Crack; Self-healing; X-ray computed tomography; Environmental exposure; Image processing; Model; Artificial intelligence.*

SUMMARY

Concrete is the second most used material on earth after water. The vast majority of the built civil infrastructure (i.e. bridges, tunnels, dams, etc.) is made of concrete. Although it is cost-effective and able to carry relatively high compressive loads, concrete is vulnerable to cracking. Therefore, harmful substances can easily penetrate into the concrete matrix, leading to premature damage. In addition, periodic inspection and maintenance of concrete structures is time consuming and often not effective.

Recently, inspired by the healing process of wounded skin, the concept of designing self-healing concrete has become an area of great interest. Self-healing of concrete implies that, without human intervention, cracks in concrete structures can automatically be filled. If successful, this could save billions of dollars in maintenance and repair costs, helping to build sustainable and more resilient infrastructure.

Despite the advent of abundant literature on the self-healing of concrete, there is currently lack of information on the effect of environmental exposure on the self-healing of concrete. Therefore, in the present study, the self-healing behavior of concrete incorporating various additives under different environments (i.e. cold and hot temperatures, high and low humidity, wet and dry cycles, and continuous underwater submersion) was investigated. In addition, several techniques such as CT scan, non-destructive mechanical testing, and 3D image analysis were used to evaluate and quantify the extent of self-healing in concrete. Moreover, an artificial intelligence-based model was developed to accurately predict the concrete's capability to heal its own cracks. This approach could exploit existing experimental findings for developing a predictive tool, which ultimately could form a basis for developing guidelines for the design and prediction of self-healing concrete.

Co-Authorship Statement

This thesis has been prepared in accordance with the regulation of integrated-article format stipulated by the Faculty of Graduate Studies at Western University. Substantial parts of this thesis have been published or submitted for publication to peer-reviewed technical journals. All experimental work, data analysis, and writing of the initial versions of publications listed below were carried out by the candidate. The research advisor and any other co-author provided guidance and supervision, and helped in the development of the final versions of publications:

- **A. R. Suleiman**, A. Nelson, and M. L. Nehdi, (2019) "Visualization and quantification of crack self-healing in cement-based materials incorporating different minerals", *Cement and Concrete Composites*", 103:49-58. **(Published)**

- **A. R. Suleiman** and M. L. Nehdi, (2019) "Self-healing behaviour of cracks in cement-based materials exposed to cyclic temperature and relative humidity", *The 7th International Conference on Engineering Mechanics and Materials*, Proceeding of the Annual Conference of the Canadian Society for Civil Engineering, Laval, Canada. **(Published)**

- **A. R. Suleiman** and M. L. Nehdi, (2018) "Effect of environmental exposure on autogenous self-healing of cracked cement-based materials", *Cement and Concrete Research*. 111:197-208. **(Published)**

- **A. R. Suleiman** and M. L. Nehdi, (2018) "Effect of environmental exposure on formation of self-healing product in cracked cement-based materials", *The 7th International Materials Specialty Conference*, Proceeding of the Annual Conference of the Canadian Society for Civil Engineering, Fredericton, Canada. **(Published)**

- **A. R. Suleiman** and M. L. Nehdi (2017) "Modeling self-healing of concrete using hybrid genetic algorithm–artificial neural network", *Materials*, 10: 135. **(Published)**

- **A. R. Suleiman** and M. L. Nehdi, (2017) "Predicting self-healing in concrete using artificial neural networks" *The 6th International Conference on Engineering Mechanics and Materials*, Proceeding of the Annual Conference of the Canadian Society for Civil Engineering, Vancouver, BC, Canada. **(Published)**

- **A. R. Suleiman** and M. L. Nehdi, (2019) "Exploring mechanical strength recovery of cement-based materials induced by self-healing using shear wave velocity", *Cement and Concrete Research* **(Submitted)**

- **A. R. Suleiman** and M. L. Nehdi, (2019) "Crack self-healing behaviour of cementitious materials incorporating superabsorbent polymers under simulated field conditions", *Cement and Concrete Composites* (**To be submitted)**

ACKNOWLEDGMENTS

TABLE OF CONTENTS

LIST OF TABLES

LIST OF FIGURES

xiii

NOTATIONS

ASTM	American Society for Testing and Materials
a	Exposed area of the specimens
a_1	Cross-sectional area of the pipe
A	Cross-sectional area subjected to flow
A_f	Activation function
GA	Genetic Algorithm
ANN	Artificial Neural Network
BN	Bentonite
CC	Calcium Carbonate
CSA	Canadian Standard Association
CT	Computerized Tomography
CSA	Canadian Standards Association
EDX	Energy Dispersive X-ray
FA	Fly Ash
k	Permeability coefficient
k_t	Water permeability coefficient after certain time
k_i	Initial water permeability
MIP	Mercury Intrusion Porosimtry
MK	Metakaolin
m_t	Change in mass at time t

OPC	Ordinary Portland Cement
R_C	Relative permeability coefficient
RH	Relative Humidity
SEM	Scanning Electron Microscopy
SAP	Superabsorbent Polymers
SWV	Shear Wave Velocity
T	Temperature
t	Time
PRA	Piezoelectric Ring Actuator
W_{nj}	Weight between neuron
y_n	Output of the neuron
δ	Density of water

CHAPTER ONE

Overview

1.1   Status of Current Infrastructure

Concrete is the world's most widely used construction material. Although it is cost-effective and able to carry relatively high compressive loads, it is susceptible to micro-cracks, which can jeopardize the durability of civil infrastructure, inflicting multibillion dollar losses in premature degradation. Several factors can lead to crack formation in a concrete matrix, including mechanical load, restrained shrinkage or thermal deformation, differential settlement, poor construction methods and faulty workmanship. Therefore, harmful substances such as chloride ions, sulfates, and carbon dioxide can easily ingress into to the concrete matrix, leading to reinforcing steel corrosion and concrete damage. Moreover, conventional concrete repairing and rehabilitation techniques are time-consuming and often not effective. According to Herbert and Li (2013), the cost of repair and rehabilitation of existing civil infrastructure, especially in developed countries, has exceeded the cost of building new infrastructure.
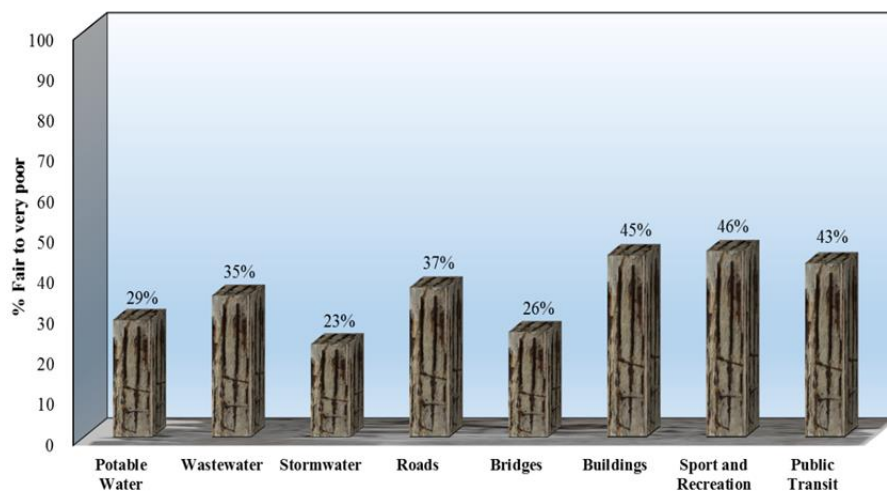
Figure 1.1: Proportion of Canadian civil infrastructure that is in (fair to very poor) physical condition.

For instance, **Figure 1.1** shows the recent percentage of Canadian civil infrastructure with an average physical condition of fair to very poor. According to the 2019 Canadian Infrastructure Report Card, the state of Canada's public infrastructure is at risk, which require immediate attention. In the USA alone, the infrastructure deficit was estimated to reach $US 3.6 trillion by year 2020. Indeed, the deteriorated civil infrastructure not only drains financial resources, but also has social and environmental implications.

1.2   Recent Research on Self-healing of Concrete

Recently, the self-healing behavior of cement-based materials has received increasing attention as a promising tool to mitigating damage inflicted to concrete civil infrastructure (e.g. Van Tittelboom and De Belie, 2013; Edvardsen 1999; Şahmaran *et al*., 2008; Azarsa *et al*., 2019; Wu *et al*., 2012; Snoeck and De Belie, 2015; Ferrara *et al*., 2014; Kempl and Çopuro, 2016; Huang *et al*., 2013; Huang *et al*., 2014; Jonkers *et al*., 2010; Wiktor and Jonkers, 2011; Van Tittelboom *et al*., 2010; Wang *et al*., 2014). Several studies have reported that surface cracks in concrete can self-heal autogenously. For instance, Edvardsen (1999) investigated the autogenous self-healing in concrete using a water permeability test. Results showed that formation of calcite in cracks is the sole cause for the autogenous healing. Huang *et al*., 2013 characterized and quantified the autogenous crack healing in concrete using techniques such as back-scattered electron (BSE), Fourier transform infrared spectroscopy (FTIR), and thermogravimetric analysis (TGA). However, in their study, instead of generating real cracks, artificial planar gaps were made to characterize the self-healing products. All specimens were submerged in water prior to testing. Experimental results showed that crystal and gel like minerals formed as healing product mainly consisting of calcium hydroxide CH and calcium silicate hydrate C-S-H. In addition, it was found that the percentage of CH formed as a healing product was much higher than that of C-S-H.

Other studies also showed that autogenous self-healing of cracks in concrete can be improved using agents capable to promote further hydration or carbonation (e.g. Van Tittelboom and De Belie, 2013; Rahmani and Bazrgar, 2015; Termkhajornkit *et al*., 2009; Sisomphon *et al*., 2012; Ferrara *et al*., 2016; Qureshi and Al-Tabbaa, 2016; Huang *et al*., 2014; Jonkers *et al*., 2010; Wiktor and Jonkers, 2011; Wang *et al*., 2014). For instance, Rahmani and Bazrgar (2015) investigated the effect of using coarse cement particles on the autogenous self-healing of concrete submerged in tap water.

Coarse cement particles were added to the mixtures as a self-healing agent. Their results showed that, after 12 weeks of curing, the use of coarse cement particles decrease the water passing rate in the cracked specimens by 100%.

Sisomphon *et al.* (2012) studied the influence of both expansive and crystalline additives on the self-healing of cracks in cement-based mortars. In their study, mortar specimens were pre-cracked and subsequently immersed in water. Results showed that surface cracks with width of around 400 µm exhibited complete healing in cement mortars incorporating expansive and crystalline additives, whereas in the case of control specimens, the maximum crack width that fully self-healed was 150 µm. It was concluded that calcium carbonate ($CaCO_3$) was the main healing product filling surface cracks. Similar results were reported by Azarsa *et al.*, (2019) when they studied the self-healing and durability parameter of concrete incorporating crystalline admixtures and portland limestone cement. Jonkers *et al.,* (2010) investigated the feasibility to use a specific group of alkali-resistant spore-forming bacteria related to the genus *Bacillus* as a self-healing agent in concrete. In their study, bacterial spores were directly added to the cement paste mixture. Their results showed that specimens incorporating bacteria produced significantly more crack-plugging minerals than the control specimens. However, continuous decrease in pore size due to cement hydration has limited the lifespan of the bacterial spores. In order to protect and increase the service life of bacterial spores, Wiktor and Jonkers (2011) implemented two-component bio-chemical self-healing agent into concrete, consisting of a mixture of bacterial spores and calcium lactate in expanded clay particles. They found that applying two-component of biochemical self-healing agent in pores expanded clay particles prior to addition to concrete mixtures could promote and improve the self-healing of surface cracks. Similarly, their results showed that $CaCO_3$ was the main healing product filling cracks.

Incorporating supplementary cementitious materials further enhanced the autogenous self-healing of concrete (e.g. Van Tittelboom *et al.*, 2012; Termkhajornkit *et al.*, 2009; Huang *et al.*, 2014; Şahmaran *et al.*, 2008; Hung and Su, 2016; Özbay *et al.*, 2013). For instance, Huang *et al.* (2014) investigated the effect of activated blast furnace slag on the self-healing of microcracks in cementitious materials. Their results showed that cement paste containing a high percentage of slag had a higher potential of self-healing than that of portland cement paste. Van Tittelboom *et al.* (2012) investigated using both

blast furnace slag and fly ash and found that they can enhance the autogenous healing of cracked mortar and cement paste submerged in water. Similarly, Özbay *et al.* (2013) reported improved healing of cracked engineered cementitious composites incorporating high volume fly ash. Termkhajornkit *et al.* (2009) investigated the effect of incorporating different percentages of fly ash on the self-healing efficiency of cement paste. Although no cracks were generated in their experiments, the self-healing was interpreted through changes of mechanical strength, porosity, effective chloride diffusion coefficient, and hydrated products upon increasing the fly ash content.

1.3 Research Needs and Motivation

Despite abundant literature on self-healing of cement-based materials, there is dearth of information on how environmental exposure affects self-healing. For example, in the above studies, self-healing was essentially explored through surface crack and mostly under submerged conditions. However, The self-healing of **(a)** internal cracks, **(b)** the effects of exposure to realistic curing conditions that better mimic field environmental conditions on the effectiveness of self-healing, **(c)** the effects of diverse additions such as silica-based materials, swelling agents, superabsorbent polymers, and carbonating minerals on self-healing performance under different environmental exposure, and **(d)** the depth of the self-healing effect remain largely unexplored.

Furthermore, an extensive survey of pertinent studies in the open literature shows that self-healing in cement-based materials has been mainly investigated from a durability prospective, particularly considering crack closure behavior, chloride ions diffusion, and recovery of liquid and gas tightness. On the other hand, mechanical strength recovery due to self-healing has been less reported (Ferrara *et al.*, 2014; Li *et al.*, 2017). According to Li *et al.* (2017), the self-healing mechanism is a localized phenomenon on a micro-scale level that can hardly be captured through conventional destructive testing methods. Therefore, it requires a non-destructive technique that is sufficiently sensitive to detect strength recovery specifically due to self-healing.

Finally, there has been so far no attempt to develop a model that can predict the crack self-healing due to autogenous and improved autogenous self-healing in cement-based materials. This warrants further research to bridge the gap between laboratory findings on self-healing and actual field performance of ageing civil infrastructure.

1.4   Specific Research Objectives

This research investigates the self-healing behaviour of concrete incorporating different additives and exposed to various environmental conditions. The specific objectives of the current thesis address the research needs identified in section 1.3 and include:

- Finding the healed width and depth of cracks in concrete incorporating various additives and exposed to diverse environmental conditions.

- Investigating the effects of various additives (i.e., silica-based materials, swelling agents, superabsorbent polymers, and carbonating minerals) on the self-healing performance of concrete under realistic field exposure.

- Identifying the main healing product formed within cracks via scanning electron microscopy (SEM) coupled with energy dispersive X-ray analysis (EDX).

- Studying the effect of microstructure densification due to ongoing hydration on the self-healing of cracks in cement-based materials.

- Employing X-ray computed micro-tomography (X-ray µCT) with 3-D image processing to visualize cracks before and after healing.

- Segmenting and quantifying the change in crack volume owing to self-healing through using 3D rendering software.

- Determining the variation in permeability and water absorption of cracked concrete specimens due to self-healing under different environmental exposure.

- Measuring the mechanical strength recovery due to self-healing of cementitious materials exposed to various environments by using a non-destructive shear wave velocity technique.

- Developing a hybrid artificial intelligence-based model to accurately predict the ability of concrete to heal its own cracks.

1.5   Original Contributions

To reap real benefits from the emerging studies on self-healing of cement-based materials, there is need to accurately quantify the healing of both surface and internal cracks, along with delineating the effects of variable curing conditions and environmental exposure on the effectiveness of self-healing. While in previous studies,

self-healing efficiency was essentially evaluated through the change of crack width on the surface of specimens mostly submerged in water, the current research demonstrates that precise segmentation of cracks is essential to characterize the self-healing efficiency of cement-based materials. Thus, visualizing and quantifying the combined influence of adding various minerals under variable environmental exposure conditions on the change in size of the entire crack volume owing to self-healing, while identifying the main healing compound, is novel in this thesis and should be pursued further.

Another novel aspect of the current thesis is to investigate the self-healing efficiency in terms of mechanical strength recovery and the associated effects of varying the environmental exposure conditions using shear wave velocity measurements. The results should stimulate a new critical look into the state-of-the-art of self-healing testing protocols and highlight the need for capturing the dominant effects of environmental exposure, and the relationship between the rate of mechanical strength recovery and the crack closing mechanism due to self-healing. Finally, this study provides a novel approach to predicting the self-healing in concrete using a hybrid genetic algorithm–artificial neural network.

1.6   Thesis Structure

The present thesis has been structured and organized according to the integrated-article format predefined by the Faculty of Graduate Studies at Western University, London. Ontario, Canada. It consists of seven chapters covering the scope of this study: Self-healing of concrete under diverse environmental exposure. Substantial parts of the current thesis have been published, accepted for publication, or submitted for possible publication in peer-reviewed technical journals and conference proceedings.

Chapter 1 presents an overview of the current status of Canadian and U.S. infrastructure. It also reviews recent research on self-healing concrete and provides the research needs and motivation along with the objectives and original contributions of the present thesis.

Chapter 2 investigates the effects of environmental exposure on autogenous self-healing of cracked cement-based materials.

Chapter 3 discovers the effects of various additions (i.e., silica-based materials, swelling agents, and carbonating minerals) on the self-healing performance of cementitious materials under different environmental exposure.

Chapter 4 explores the mechanical strength recovery of cement-based materials induced by self-healing using shear wave velocity under different environmental exposure.

Chapter 5 examines the self-healing behaviour of cementitious materials incorporating superabsorbent polymers under simulated field conditions

Chapter 6 presents an approach to predicting the self-healing in concrete using a hybrid genetic algorithm–artificial neural network (GA–ANN).

Finally, **Chapter 7** summarizes the conclusions drawn from the research and recommends future research directions.

1.7 References

C. Edvardsen, (1999) "Water permeability and autogenous healing of cracks in concrete" ACI Materials Journal, 96: 448–454.

C. Hung and Y. Su (2016) "Medium-term self-healing evaluation of Engineered Cementitious Composites with varying amounts of fly ash and exposure durations", *Construction and* Building Materials, 118: 194-203.

Canadian Construction Association, Canadian Public Works Association, Canadian Society for Civil Engineering, and Federation of Canadian Municipalities (2019) "In forming the future: Canadian Infrastructure Report Card", *http://www.canadainfrastructure.ca/*.

D. Snoeck and N. De Belie (2015) "From straw in bricks to modern use of microfibers in cementitious composites for improved autogenous healing – A review", *Construction and Building Materials*, 95(1): 774-787.

E. Herbert and V. Li, (2013) "Self-healing of microcracks in engineered cementitious composites (ECC) under a natural environment", *Materials*, 6: 2831–2845.

E. Özbay, M. Şahmaran, M. Lachemi, and H. E. Yücel (2013) "Self-Healing of microcracks in high-volume fly-ash-incorporated engineered cementitious composites", *ACI Materials Journal*, 110 (1): 33-43.

H. Huang, G. Ye, and D. Damidot (2014) "Effect of blast furnace slag on self-healing of microcracks in cementitious materials", *Cement and Concrete Research*, 60: 68-82.

H. Huang, G. Ye, and D. Damidot (2013) "Characterization and quantification of self-healing behaviors of microcracks due to further hydration in cement paste", *Cement and Concrete Research*, 52: 71-81.

H. Rahmani and H. Bazrgar (2015) "Effect of coarse cement particles on the self-healing of dense concretes", *Magazine of Concrete Research*, 67(9): 476-486.

H. M. Jonkers, A. Thijssena, G. Muyzerb, O. Copuroglua, E. Schlangena (2010) "Application of bacteria as self-healing agent for the development of sustainable concrete", *Ecological Engineering*, 36(2): 230-235.

J. Kempl and O. Çopuroğlu (2016) "EH-pH- and main element analyses of blast furnace slag cement paste pore solutions activated with sodium monofluorophosphate - Implications for carbonation and self-healing", *Cement and Concrete Composites*, 71: 63-76.

J.Y. Wang, H. Soens, W. Verstraete, and N. De Belie (2014) "Self-healing concrete by use of microencapsulated bacterial spores", *Cement and Concrete Research*, 56: 139-152.

K. Sisomphon, O. Copuroglu, and E.A.B. Koenders (2012) "Self-healing of surface cracks in mortars with expansive additive and crystalline additive", *Cement and Concrete Composites*, 34(4): 566-574.

K. Van Tittelboom, N. De Belie, W. De Muynck, and W. Verstraete (2010) "Use of bacteria to repair cracks in concrete", *Cement and Concrete Research*, 40(1): 157-166.

K. Van Tittelboom, E. Gruyaert, H. Rahier, and N. De Belie (2012) "Influence of mix composition on the extent of autogenous crack healing by continued hydration or calcium carbonate formation", *Construction and Building Materials*, 37: 349-359.

K. Van Tittelboom and N. De Belie (2013) "Self-healing in cementitious materials - A review". *Materials*, 6: 2182-2217.

L.W. Li, Z. Jiang, and Z. Yang (2017) "Acoustic characterization of damage and healing of microencapsulation-based self-healing cement matrices", *Cement and Concrete Composites*, 84(15): 48-61.

L. Ferrara, V. Krelani, and M. Carsana (2014) "A ''fracture testing'' based approach to assess crack healing of concrete with and without crystalline admixtures", *Construction and Building Materials*, 68(15): 535-551.

L. Ferrara, V. Krelani and F. Moretti (2016) "On the use of crystalline admixtures in cement based construction materials: from porosity reducers to promoters of self healing", *Smart Materials and Structures*, 25: 17 p.

M. Şahmaran, S. B. Keskin, G. Ozerkan, and I. O. Yaman (2008) "Self-healing of mechanically-loaded self consolidating concrete with high volumes of fly ash", *Cement and Concrete Composites*, 30 (10): 872-879.

M. Wu, B. Johannesson, and M. Geiker (2012) "A review: Self-healing in cementitious materials and engineered cementitious composite as a self-healing material", *Construction and Building Materials,* 28(1): 571-583.

P. Azarsa, R. Gupta, A. Biparva, (2019) "Assessment of self-healing and durability parameters of concretes incorporating crystalline admixtures and Portland Limestone Cement" *Cement and Concrete Composites*, 99: 17-31.

P. Termkhajornkit, T. Nawab, Y. Yamashiro, and T. Saito (2009) "Self-healing ability of fly ash–cement systems", *Cement and Concrete Composites*, 31(3): 195-203.

T.S. Qureshi and A. Al-Tabbaa (2016) "Self-healing of drying shrinkage cracks in cement-based materials incorporating reactive MgO", Smart Materials and Structures, 25: 16p.

V. Wiktor and H. M. Jonkers (2011) "Quantification of crack-healing in novel bacteria-based self-healing concrete", *Cement and Concrete Composites*, 33(7): 763-770.

CHAPTER TWO

Effect of Environmental Exposure on Autogenous Self-Healing of Cracked Cement-Based Materials*

2.1   Introduction

In this chapter, the self-healing of both surface and interior cracks and the effects of different curing conditions on the self-healing of cracks were duly explored. Pre-cracked mortar specimens were submerged in water, while identical specimens were exposed to cyclic temperature and relative humidity. Change in crack width was examined using optical microscopy. SEM coupled with energy dispersive X-ray analysis was used to identify healing compounds. Mercury intrusion porosimetry, water absorption and permeability were employed to assess porosity. X-ray computed tomography was deployed to explore healing of internal cracks.

2.2   Experimental Program

2.2.1 Materials and Specimen Preparation

Mortar specimens were made with ordinary portland cement compliant with CSA A3001 and ASTM C150 standards, along with 20% CSA A3000 Type CI fly ash (ASTM C618 Class C) to promote autogenous self-healing. Water-to-cementitious materials ratio (w/cm) of 0.35 and sand-to-cementitious materials mass ratio (s/c) of 2 were used. The physical and chemical properties of the cement fly ash and sand are summarized in **Tables 2.1** and **2.2**. The specimens were cast in 10 cm diameter and 5 cm height plastic containers reinforced with a galvanized steel mesh (6 mm × 6 mm with Ø = 1 mm), which was embedded at the centre of the tested (100 diameter and 50 mm height) mortar specimens. After demolding at 1-d, specimens were cured for 28-d in a moist room at RH ≥ 95% and T = 21 ± 1°C. The curing was carried out according

to ASTM C511 (Standard Specification for Mixing Rooms, Moist Cabinets, Moist Rooms, and Water Storage Tanks Used in the Testing of Hydraulic Cements and Concretes). At the age of 28-d, specimens were removed from the moist room and cracked, as displayed in **Figure 2.1**.

Table 2.1: Physical and chemical properties of cement and fly ash

Components /Property	Cement Type (10)	Fly ash CI
Silicon oxide (SiO_2) (%)	19.6	42.4
Aluminum oxide (Al_2O_3) (%)	4.8	21.2
Ferric oxide (Fe_2O_3) (%)	3.3	7.1
Calcium oxide (CaO) (%)	61.50	16
Magnesium oxide (MgO) (%)	3.0	-
Sulfur trioxide (SO_3) (%)	3.50	2.40
Loss on ignition (%)	1.90	1.60
Insoluble residue (%)	0.44	-
Equivalent alkalis (%)	0.7	-
Tricalcium silicate (C_3S) (%)	55	-
Dicalcium silicate (C_2S) (%)	15	-
Tricalcium aluminate (C_3A) (%)	7	-
Tetracalcium aluminoferrite (C_4AF) (%)	10	-
Blaine fineness (m^2/kg)	371	-
Autoclave expansion (%)	0.09	-
Compressive strength 28 days (MPa)	40.9	-
Specific gravity	3.15	2.60
Time of setting (min) Vicat Initial	104	-
Pozzolanic activity index (%)	-	100

Table 2.2: Physical and chemical properties of sand

Property	Value
Absorption (%)	1.09
Specific gravity (apparent) (%)	2.72
Specific gravity (dry) (%)	2.65
Specific gravity (SSD) (%)	2.68
Unit weight (kg/m^3)	1512
Materials finer than 75-μm (sieve # 200) (%)	2.10

All 100 x 50 mm cylindrical specimens were pre-cracked (longitudinal crack) at the age of 28 days by means of a splitting test at a constant loading rate of 0.01 mm/s. The crack width was controlled during the splitting test via a calibration ruler as per the method described by Roig-Flores *et al*. (2015). For each environmental condition, three groups of specimens with three different values of crack width were tested. The first group consisted of three specimens with an average crack width in the range of 50 – 150 µm. For the second and third groups, the average crack widths were 150 – 300 µm and 300 – 500 µm, respectively.
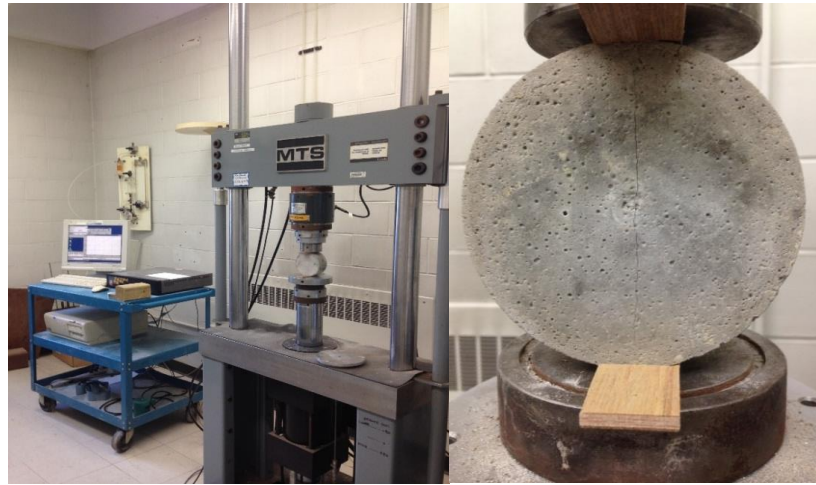
Figure 2.1: Cracking of specimens using MTS machine.

2.2.2 Environmental Exposure

The effect of environmental exposure on the development of self-healing in mortar specimens was investigated. Cracked specimens were divided into two groups. Specimens of the first group were fully submerged in deionized water at a constant temperature of T = 19°C. Barnstead easypure rodi water purification system model was used as shown in the **(Fig. 2.2)**. The second group of specimens was placed inside a walk-in environmental chamber and exposed to cyclic temperature ranging from 10°C to 40°C and relative humidity in the range of 20% to 90% (**Table 2.3** and **Fig. 2.3**).

Table 2.3: Duration of each temperature/humidity cycle

Cycle #	Relative Humidity %	Temperature (C°)	Duration (days)
1	90	20	4
2	20	-10	4
3	60	40	4

Figure 2.2: Water purification system.

Figure 2.3: Test specimens in environmental chamber.

2.2.3 Mercury Intrusion Porosimetry (MIP)

Fragments from the cracked specimens (before and after self-healing) were retrieved and dried inside a desiccator until reaching a constant mass as shown in the **(Fig. 2.4 (a))**. The pore size distribution for each specimen was determined using a Micrometrics AutoPore IV 9500 Series porosimeter allowing a range of pressures from 0 to 414 MPa as shown in the **(Fig. 2.4 (b))**. The assumed surface tension of mercury was 0.484 N/m at 25°C according to ASTM D4404 (Standard Test Method for Determination of Pore Volume and Pore Volume Distribution of Soil and Rock by Mercury Intrusion Porosimetry).

(a)

(b)

Figure 2.4: (a) desiccator and (b) illustration of MIP test apparatus.

2.2.4 Water Absorption Test

The rate of water absorption of the cracked specimens was measured according to ASTM C-1585 (Standard Test Method for Measurement of Rate of Absorption of Water by Hydraulic Cement Concretes). Before the test, specimens were oven-dried at a temperature of T = 50 °C until constant mass. Subsequently, the side surface of each specimen was sealed with a silicone and placed in contact with water to a depth of 3 to 5 mm. Only one surface of each tested mortar specimen was allowed to be in contact with water. The water absorption rate was measured before cracking, upon cracking, and after exposing to controlled environmental conditions. Water absorption before cracking represents the absorption rate of uncracked specimens at the age of 28 days. The specimens were then cracked via a splitting test and divided into groups based on their average crack width. The absorption rate was measured again thereafter. The mass of specimens versus time was recorded. Absorption was calculated using **Eq. (2.1)**. The sorptivity coefficient, S was estimated as the slope of the best fit line between absorption, I and the square root of time, t as per **Eq. (2.2)**.

$$I = \frac{m_t}{a \times \delta} \tag{2.1}$$

$$S = \frac{I}{\sqrt{t}} \tag{2.2}$$

Where; m_t = change in specimen mass in grams at the time t; a = exposed area of the specimen in mm^2; and δ = density of the water in g/mm^3.

2.2.5 Permeability Test

Water passing through cracked specimens was measured before and after healing. The RILEM Test Method II.4 (Measurement of Water Absorption under Low Pressure) was adopted (**Fig. 2.5**) to estimate the water permeability coefficient, k (cm/s) based on **Eq. (2.3)**. To evaluate the self-healing efficiency in cracked specimens, the relative permeability coefficient was calculated based on **Eq. (2.4),** where; k_i = initial water permeability coefficient (cm/s); k_t = water permeability coefficient after certain time (cm/s).

$$k = \frac{a_1 \times L}{A \times t} \ln\left[\frac{h_1}{h_2}\right] \qquad \text{(2.3)}$$

$$R_c = \frac{k_t}{k_i} \qquad \text{(2.4)}$$

Where; a_1 = cross-sectional area of the pipe (cm^2); L = specimen thickness (cm); A = cross-sectional area subjected to flow (cm^2); t = time (s); h_1 = initial water head (cm); h_2 = water head (cm).
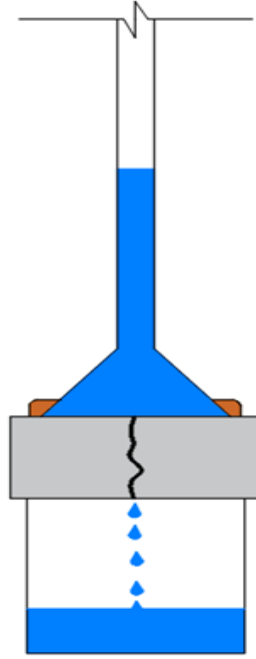
Figure 2.5: Water permeability test.

2.2.6 SEM and EDX analysis

The morphology of the healing products formed in the surface cracks was investigated using scanning electron microscopy (SEM) coupled with energy dispersive X-ray analysis (EDX) using a Hitatchi SU-3500 Field Emission SEM housed in Surface Science Centre at the University of Western Ontario (**Fig. 2.6).** Specimens for SEM analysis were dried using a desiccator and then coated with osmium or gold before testing.
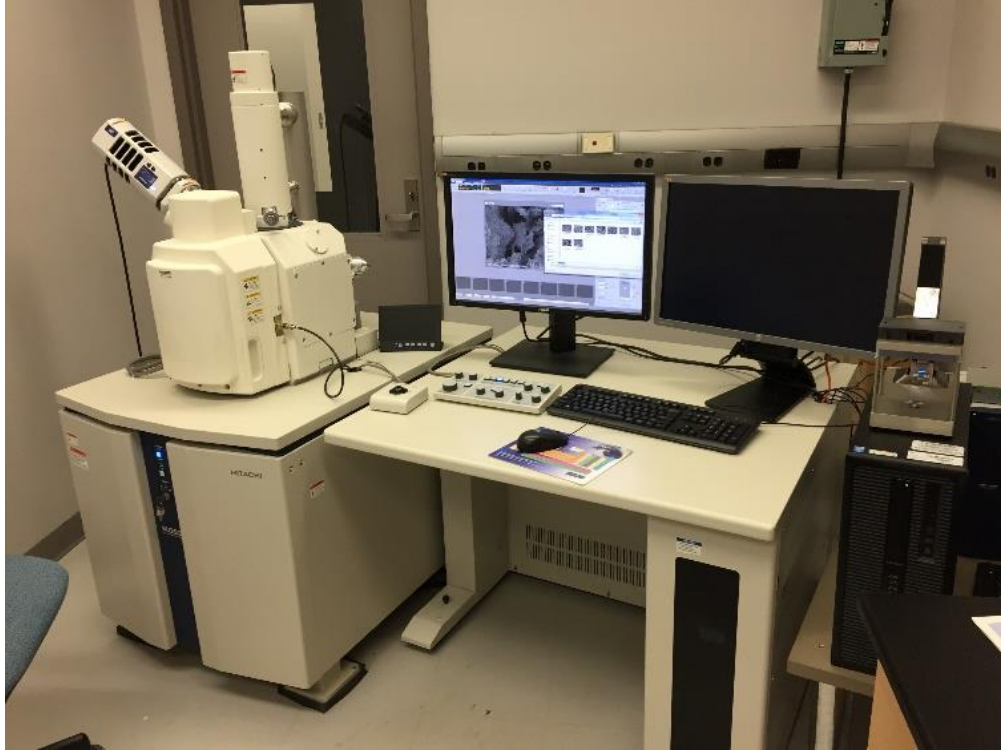
Figure 2.6: SEM coupled with energy dispersive X-ray analysis EDX.

2.2.7 Optical Microscopy

The change in surface crack width of mortar specimens owing to self-healing was monitored using a Carton 40x microscope as shown in the (**Fig. 2.7**). For each environmental exposure, the width of surface cracks was measured over a period of one year. The crack healing capacity was evaluated based on measurements of the crack width change, similar to previous studies by Ferrara *et al*. (2016; 2017) and Borg *et al.* (2018). The crack sealing index was calculated based on the following equation:

$$CSI = 1 - \frac{Cw_t}{Cw_i} \qquad \textbf{(2.5)}$$

Where; *CSI* = crack sealing index; Cw_i = initial crack width; and Cw_t = crack width at time *t*.

Figure 2.7: Optical Microscopy.

2.2.8 X-ray Computed Tomography

Several studies have explored the self-healing of internal cracks indirectly using non-destructive techniques, such as ultrasonic pulse velocity (UPV), diffusion in ultrasound, coda wave interferometry, and acoustic emission (AE) (e.g. Ferrara *et al*., 2014; Van Tittelboom *et al*., 2010; Liu *et al*., 2016; Tsangouri *et al*., 2016). For instance, Liu *et al*. (2016) evaluated self-healing of internal cracks in biomimetic mortar using coda wave interferometry. Their results indicated that cracked mortar specimens exhibited strength development and higher relative velocity change. Another study by Ferrara *et al*. (2014) used UPV to investigate the effects of self-healing of cracks on the recovery of stiffness and load bearing capacity in pre-cracked concrete. Tsangouri *et al*. (2016) used eight AE sensors attached on concrete surface to investigate crack healing. Their results showed that transmitter localization loses its accuracy in the presence of 300 µm wide crack and improves as the crack heals. Although these techniques provide useful information regarding the internal self-healing process, they do not measure change in the crack width. In the present study, X-ray computed microtomography (X-ray µCT), a non-destructive technique, was used to investigate the change in internal crack width with progress of self-healing.

To evaluate the self-healing of internal cracks, a Nikon XT-H-225-ST µCT scanner housed at Sustainable Archaeology, Western University, was deployed as shown in the

Figure 2.8. The X-ray computed tomography scanner generates micrometer scale high resolution 3D and 2D images of both the sample's interior and exterior. The X-ray images are subsequently deployed to reconstruct the exterior and interior of the sample via computed tomography. X-ray µCT provides non-destructively detailed 3D images of the internal structure of material by combining a series of cross-sectional images. In the 3-D image, resolution was 62.26u voxel size. Parameters of the scan were defined as follows: - 225 kVp -100 µA-22.5 watts; panel gain = 24; 3141 images; 150 frames/projection on shading correction; panel at -116.517; 2.5mm Cu filter - fast CT - 53 min scan.

Figure 2.8: X-ray µCT scanning.

2.3   Results and Discussion

2.3.1 Optical Microscopy

Surface cracks in mortar specimens before and subsequent to self-healing were investigated using optical microscopy. For specimens submerged in water (**Figure 2.9**), surface cracks with different widths were filled with self-healing products. The maximum width of cracks healed in specimens submerged in water was 300 µm. However, for identical cracked specimens exposed to cyclic T and RH, no healing products in cracks were observed (**Figure 2.10). Figure 2.11** represents the crack sealing index of specimens exposed to different environments. The results are plotted in terms of evolution of the crack sealing index over time. Submerged specimens with maximum crack width 300 µm feature complete crack closing after 60 days from

cracking. However, cracks with width larger than 300 µm did not exhibit crack closing up to a one year.
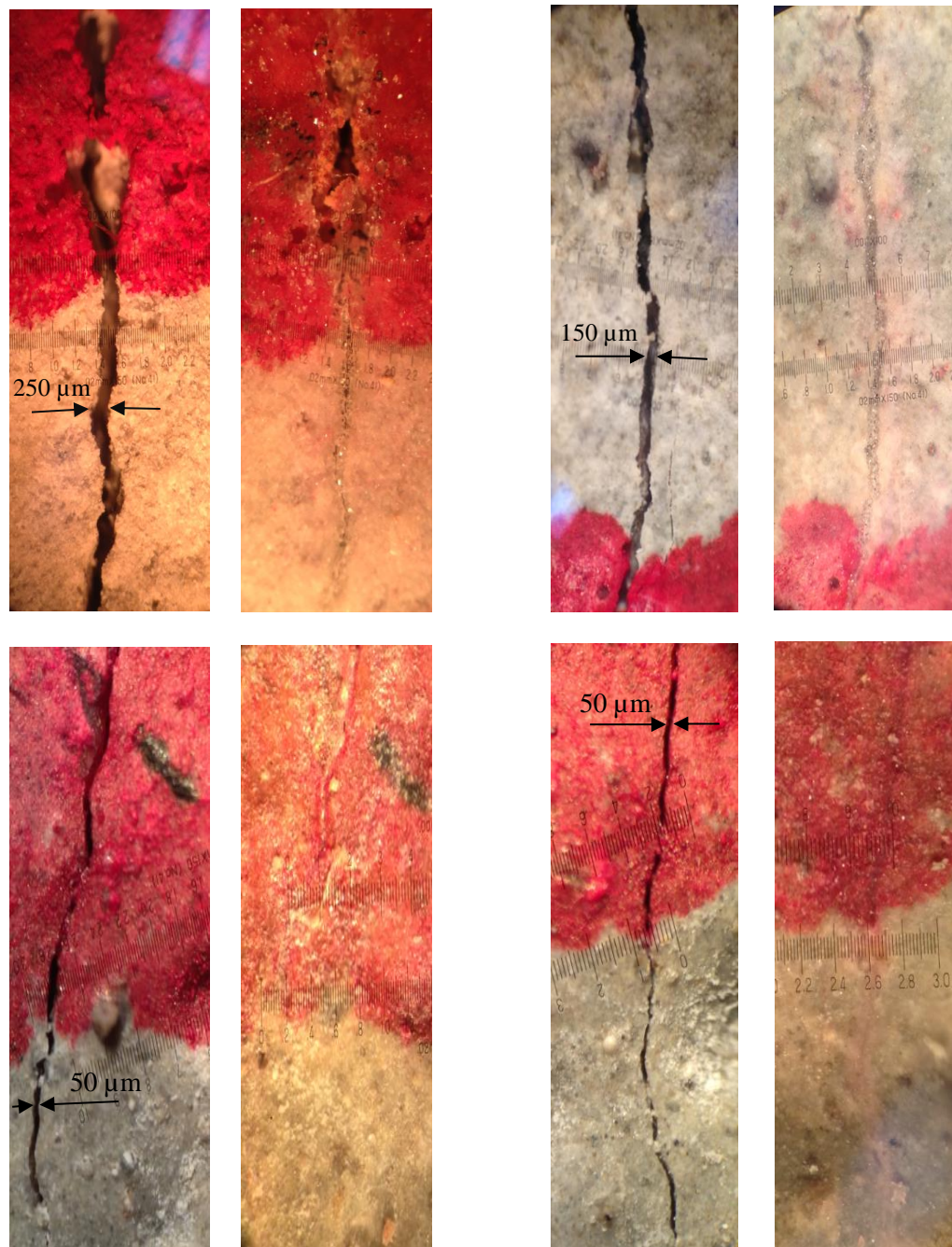
Figure 2.9: Surface cracks before and after water submersion showing self-healing.
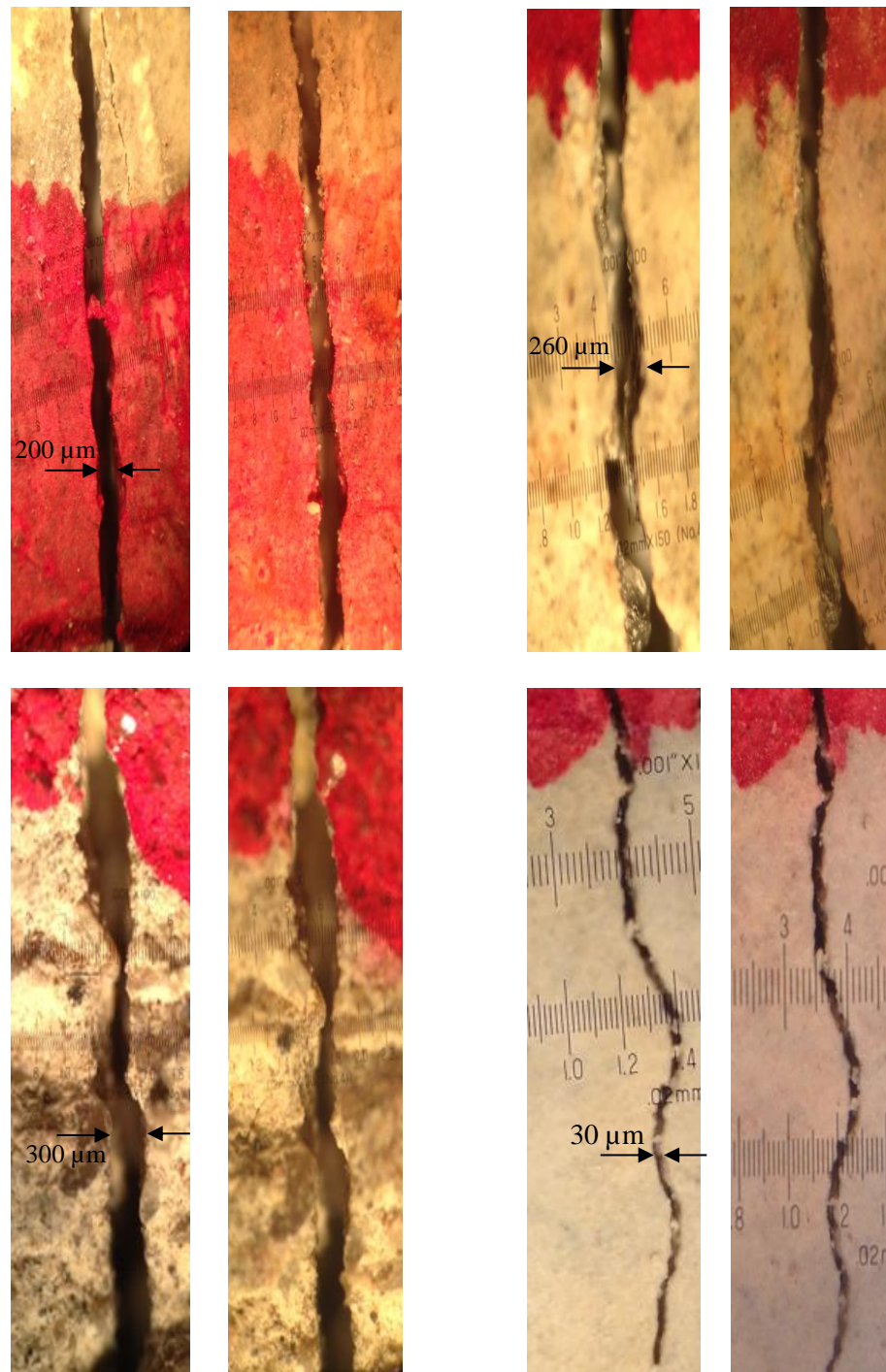
Figure 2.10: Surface cracks before and after exposure to cyclic T and RH showing no significant healing.

(a)

(b)

(c)
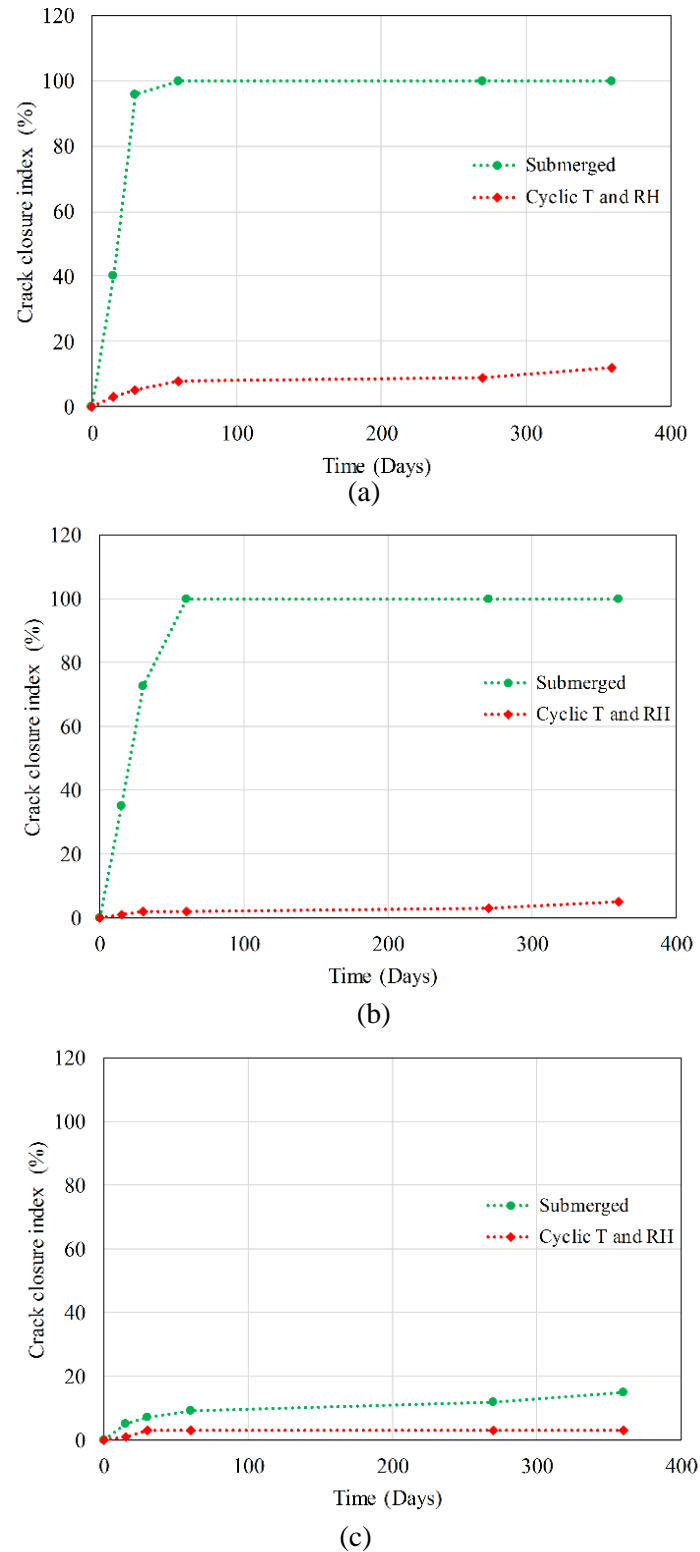
Figure 2.11: Change in surface crack width of specimens exposed to different environments with initial crack width (a) 50-150 µm; (b) 150-300 µm; and (c) 300-500 µm.

2.3.2 MIP and Pore Structure Results

The evolution of pore structure with time was assessed using MIP. Specimens from each environmental exposure were tested at ages of 28, 45, 60, 270, and 360 days. The results were then cross-checked with the crack sealing index, as shown in the **Figure 2.12**. **Figure 2.13** shows the cumulative mercury intrusion curves as a function of the pore diameter for cracked mortar specimens before and after each environmental exposure. It can be observed that in both exposures, cracked specimens exhibited reduction in and refinement of pore size after 2 months. For example, the volume of pores with diameters from 2 µm to 0.05 µm was noticeably decreased compared to that of specimens before exposure. In addition, the percentage of pores with diameter smaller than 0.05 µm increased, indicating a refinement of pore structure. For those specimens submerged in water, the percentage of pores with diameter smaller than 0.015 µm increased in comparison to that of identical specimens exposed to cyclic T and RH. **Figure 2.14** illustrates the cumulative intruded pore volume vs. pore diameter for submerged specimens at different ages. It can be observed that specimens fully submerged in water continued to exhibit reduction in porosity, leading to microstructural densification, likely owing to ongoing cement hydration and pozzolanic reactions of fly ash.
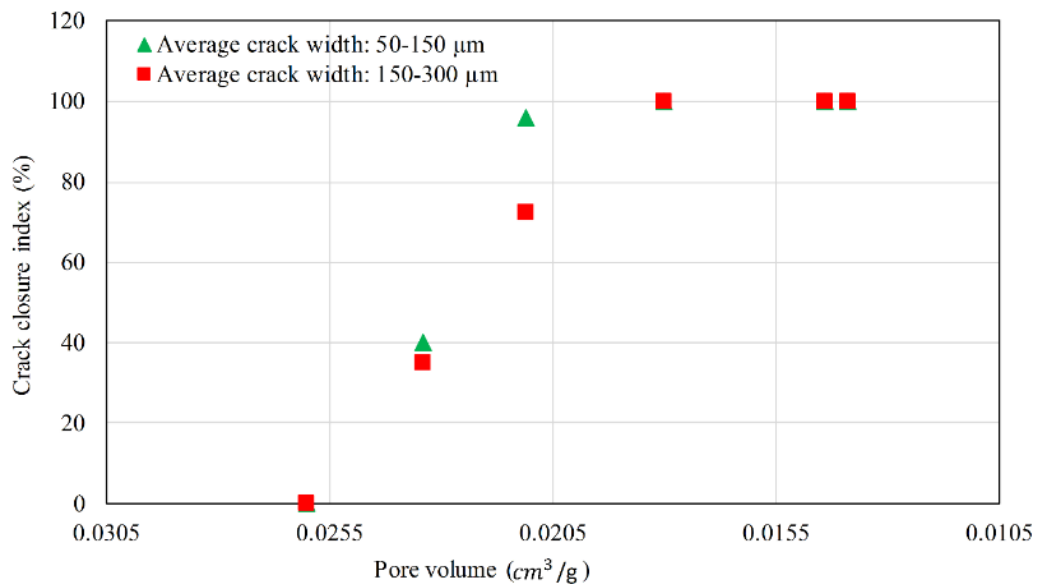
Figure 2.12: Crack closure index vs. pore volume.
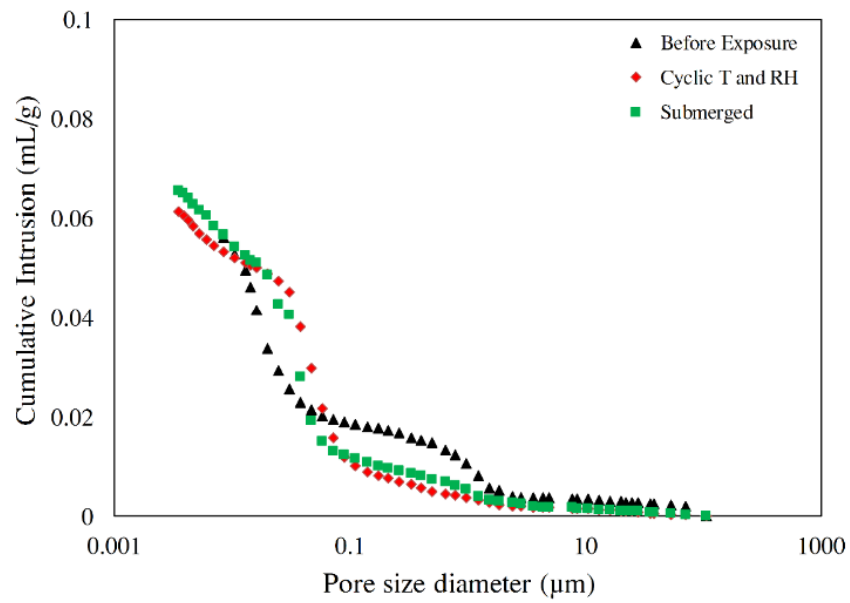
Figure 2.13: Cumulative intruded pore volume vs. pore diameter for cracked specimens exposed to different environments for a period of 2 months.
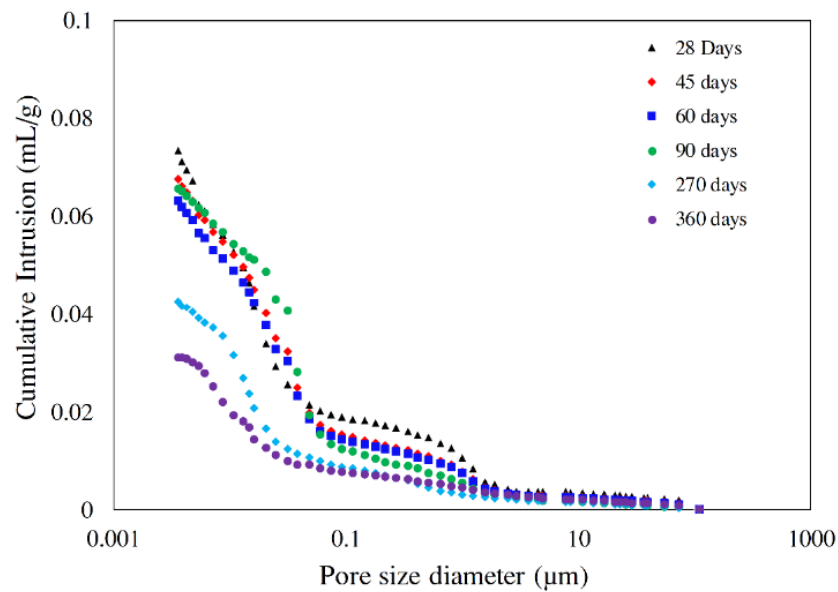
Figure 2.14: Cumulative intruded pore volume vs. pore diameter for submerged specimens at different ages.

2.3.3 Capillary Water Absorption

Figures 2.15 to 2.18 show capillary water absorption results of cracked mortar specimens before and after each environmental exposure.
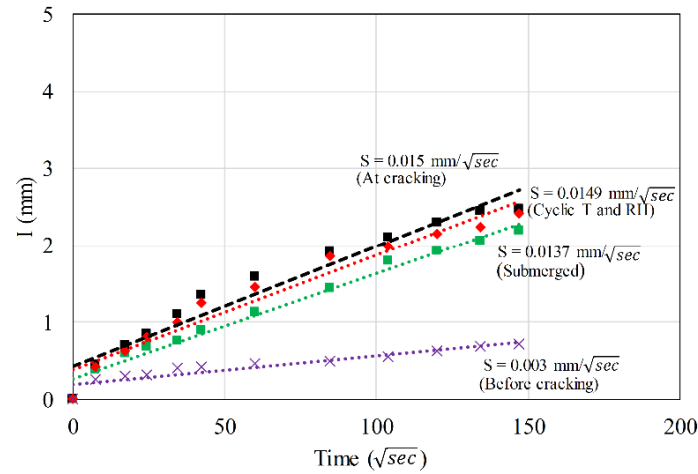
(a)
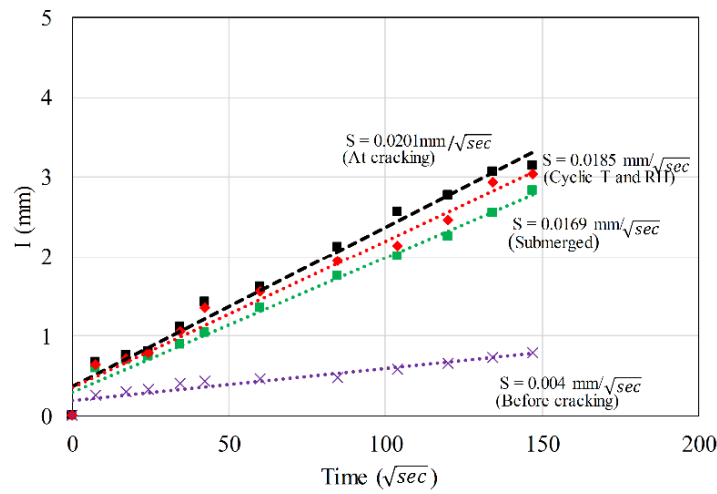
(b)
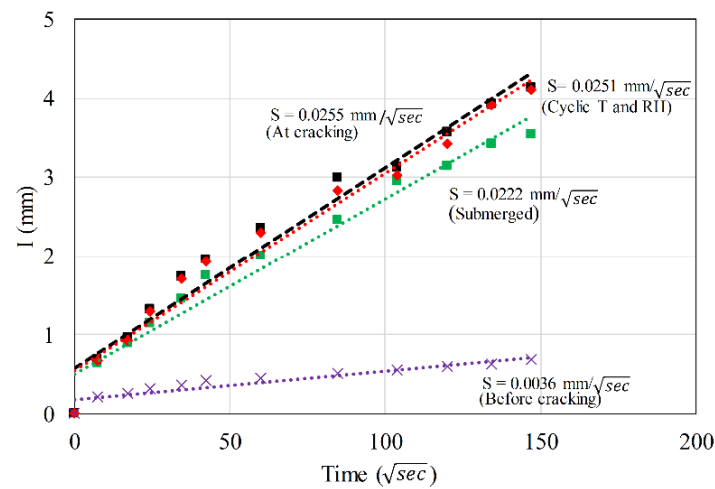
(c)

Figure 2.15: Change in water absorption of cracked specimens exposed to different environments for a period of 15 days with average crack width (a) 50-150 µm; (b) 150-300 µm; and (c) 300-500 µm.

(a)

(b)

(c)
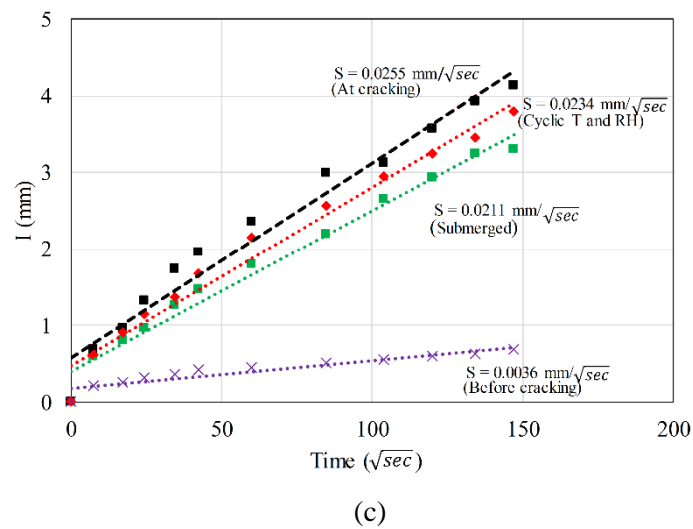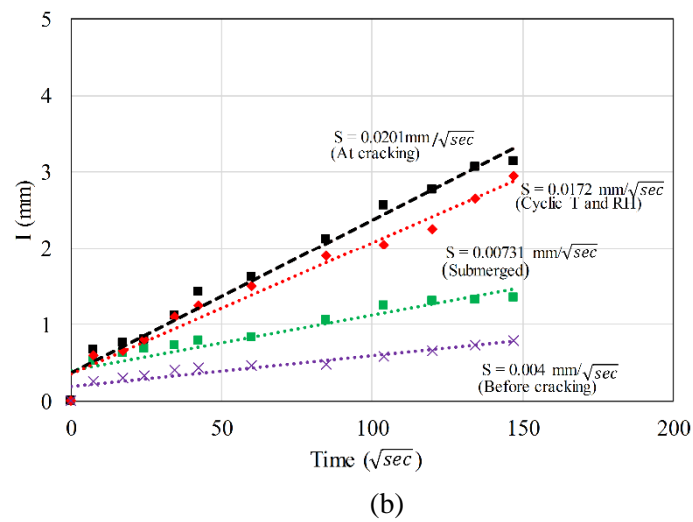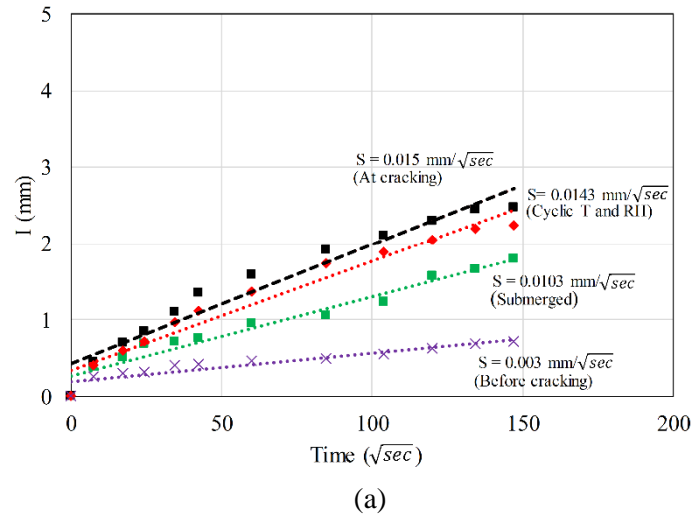
Figure 2.16: Change in water absorption of cracked specimens exposed to different environments for a period of 1 month with average crack width (a) 50-150 µm; (b) 150-300 µm; and (c) 300-500 µm.
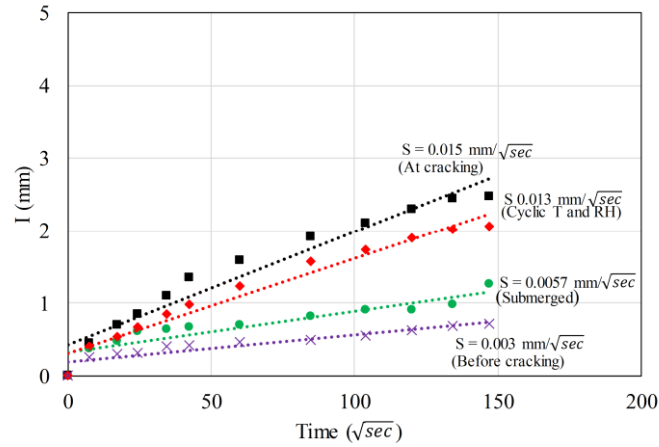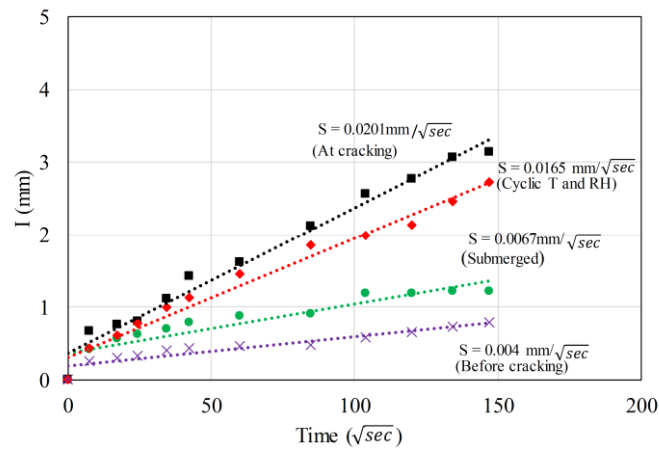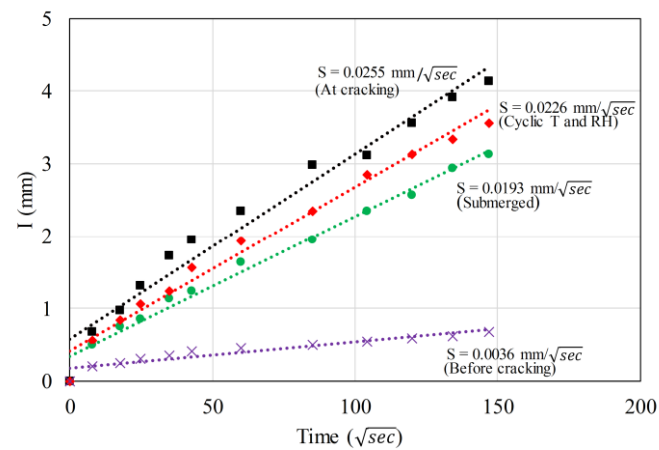
Figure 2.17: Change in water absorption of cracked specimens exposed to different environments for a period of 2 months with average crack width (a) 50-150 µm; (b) 150-300 µm; and (c) 300-500 µm.

(a)

(b)

(c)
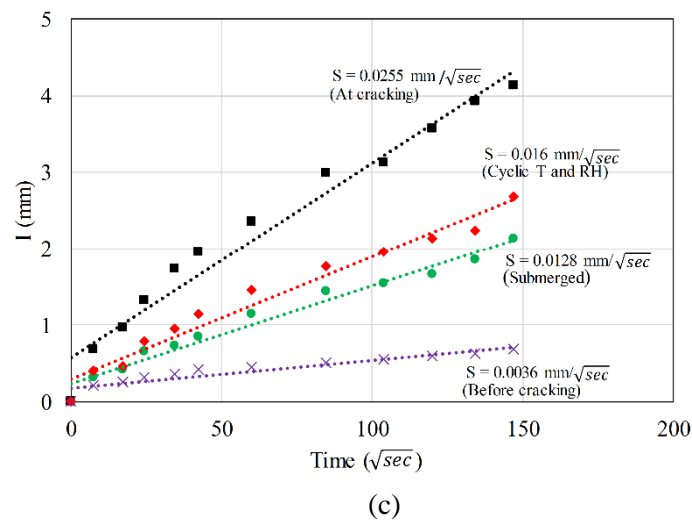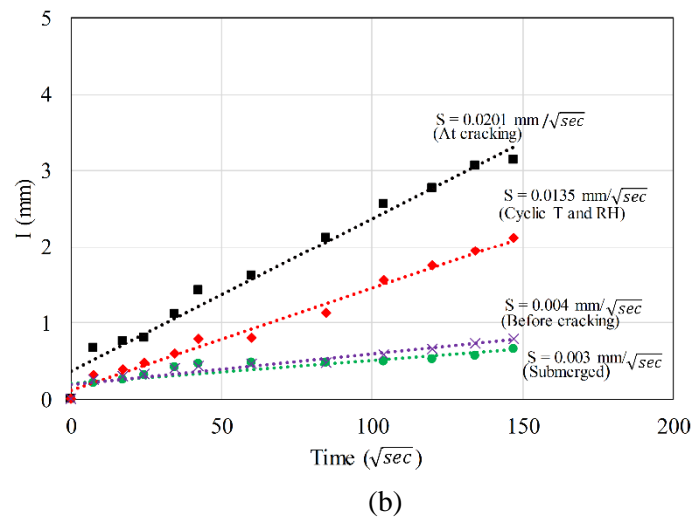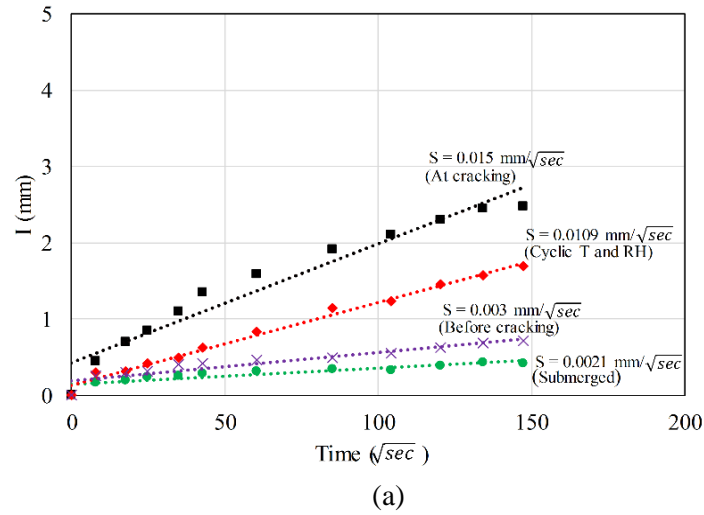
Figure 2.18: Change in water absorption of cracked specimens exposed to different environments for a period of 1 year with average crack width (a) 50-150 µm; (b) 150-300 µm; and (c) 300-500 µm.

The rate of water absorption was measured before, upon, and after cracking. The results were then cross-checked with the crack sealing index, as shown in the **Figure 2.19**. Results showed that water sorptivity coefficient increase apparently due to crack formation. For instance, for the first group, the sorptivity index of the uncracked specimens was 0.0035 mm/√sec, whereas at cracking was 0.015 mm/√sec as shown in the **Figure 2.15**. In addition, as the crack width increases, the sorptivity index increases. Hence, the value o the crack width significantly alters the transport property of the tested specimens.

Results also indicated that cracked specimens that were fully submerged in water exhibited higher reduction in absorption compared to that of identical specimens placed inside a walk-in environmental chamber and exposed to cyclic T and RH. For instance, after one year, the sorptivity index of the submerged specimens was 0.0021 mm/$\sqrt{sec}$, whereas that of specimens with similar initial crack width and exposed to cyclic T and RH was 0.0109 mm/$\sqrt{sec}$. It is believed that the reduction in absorption for submerged specimens reflects the observed microstructure densification owing to the development of hydration products and possibly self-healing of cracks. Interestingly, in both environments, specimens with initial crack width larger than 300 µm did not exhibit significant reduction in absorption in comparison to specimens with crack widths smaller than 300 µm.
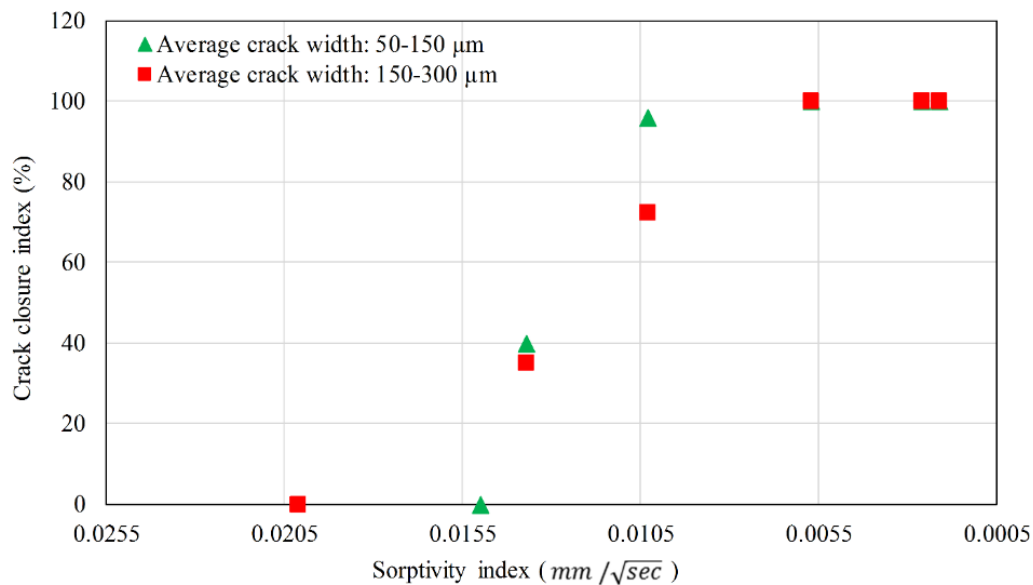
Figure 2.19 Crack closure index vs. sorptivity index.

2.3.4 Water Permeability

Figure 2.20 exhibits the change in relative permeability of the pre-cracked mortar specimens submerged in water. It can be observed that the permeability coefficient of the cracked specimens dropped by up to 71% when they were fully submerged in water for 60 days. However, only 6% reduction in permeability was observed for the pre-cracked specimens exposed to cyclic T and RH. Again, this can be attributed to coupled microstructure densification through portland cement hydration and pozzolanic reactions of fly ash and formation of self-healing products that sealed cracks in the case of complete water submerging. Previous study by Jiang *et al*. (2015) reported that pre-cracked mortar specimens exposed to cyclic drying and wetting did not exhibit decrease in permeability, which could be related to the formation of microcracks upon exposing pre-cracked specimens to cyclic drying and wetting.
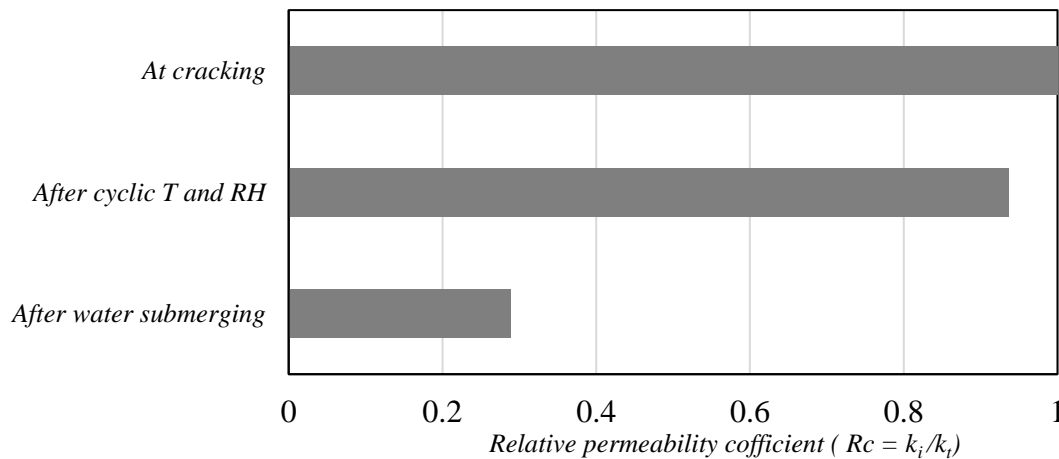
Figure 2.20 Change in relative permeability coefficient of cracked specimens with average crack width (150 to 300 µm) exposed to different environments for a period of 2 months.

Roig-Flores *et al*. (2015) found that the permeability of pre-cracked concrete specimens incorporating a crystalline admixture decreased significantly when specimens were fully submerged in water in comparison to pre-cracked specimens exposed to constant RH (either 40% or 95 $\pm$ 5%). Another study by Wang *et al*. (2014) (a) investigated self-healing using microencapsulated bacteria spores in concrete. Their results showed that specimens with bio-microcapsules had decreased water permeability by about 10 times compared to that for specimens with no bacteria spores, but only when specimens were

exposed to liquid water. However, both specimens with and without bacteria indicated no self-healing when exposed to up to 95% RH. Therefore, the presence of liquid water appears to be essential to promoting self-healing in cement-based materials.

2.3.5 SEM and EDX Analyses

Figure 2.21 shows typical SEM image and EDX analysis for the healing product formed in surface cracks. SEM and EDX analyses were used to explore the microstructure and analyze the composition of self-healing products. The initial crack opening of the healed crack shown was 50 ± 10 µm. It can be observed that the self-healing product had multiple-shaped and irregular crystals including trigonal, cubical, and rectangular shapes. Energy-dispersive X-ray spectroscopy revealed that the healing products at the crack surface were mainly composed of calcium with some carbon and oxygen, indicating that it consists mainly of $CaCO_3$. Formation of $CaCO_3$ as a healing product is mainly due to the leaching and re-deposition of calcium ions Ca^{2+} from the cementitious matrix and diffusion of carbonates into cracks (e.g. Jiang *et al*., 2015; Sisomphon *et al*., 2012).
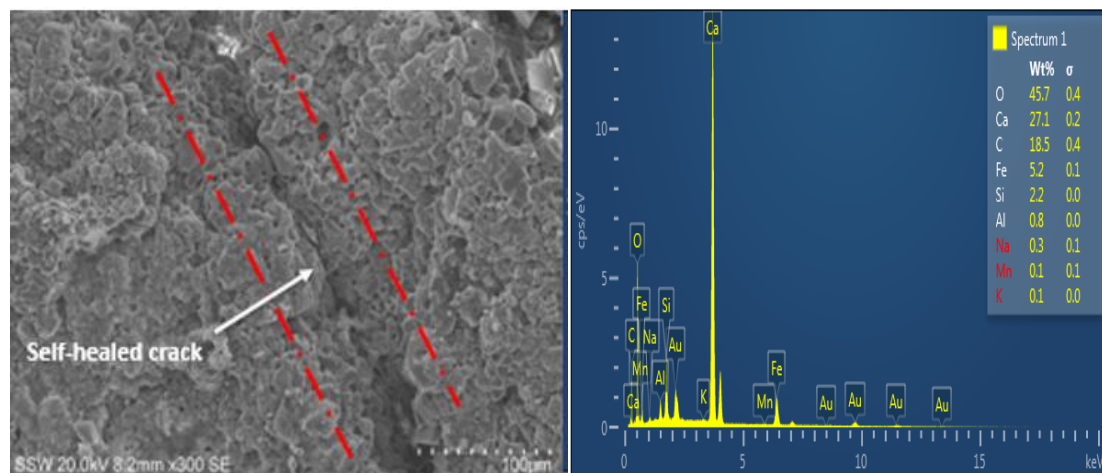
Figure 2.21 SEM micrograph with EDX pattern of products in self-healed cracks.

2.3.6 X-ray Computed Tomography

Figure 2.22 shows X-ray tomography images of specimens after 3 months of healing. Only specimens submerged in water with crack width in the range (150 – 300 µm) were selected for X-ray µCt analysis since they exhibited visible crack healing in optical microscopy analysis.
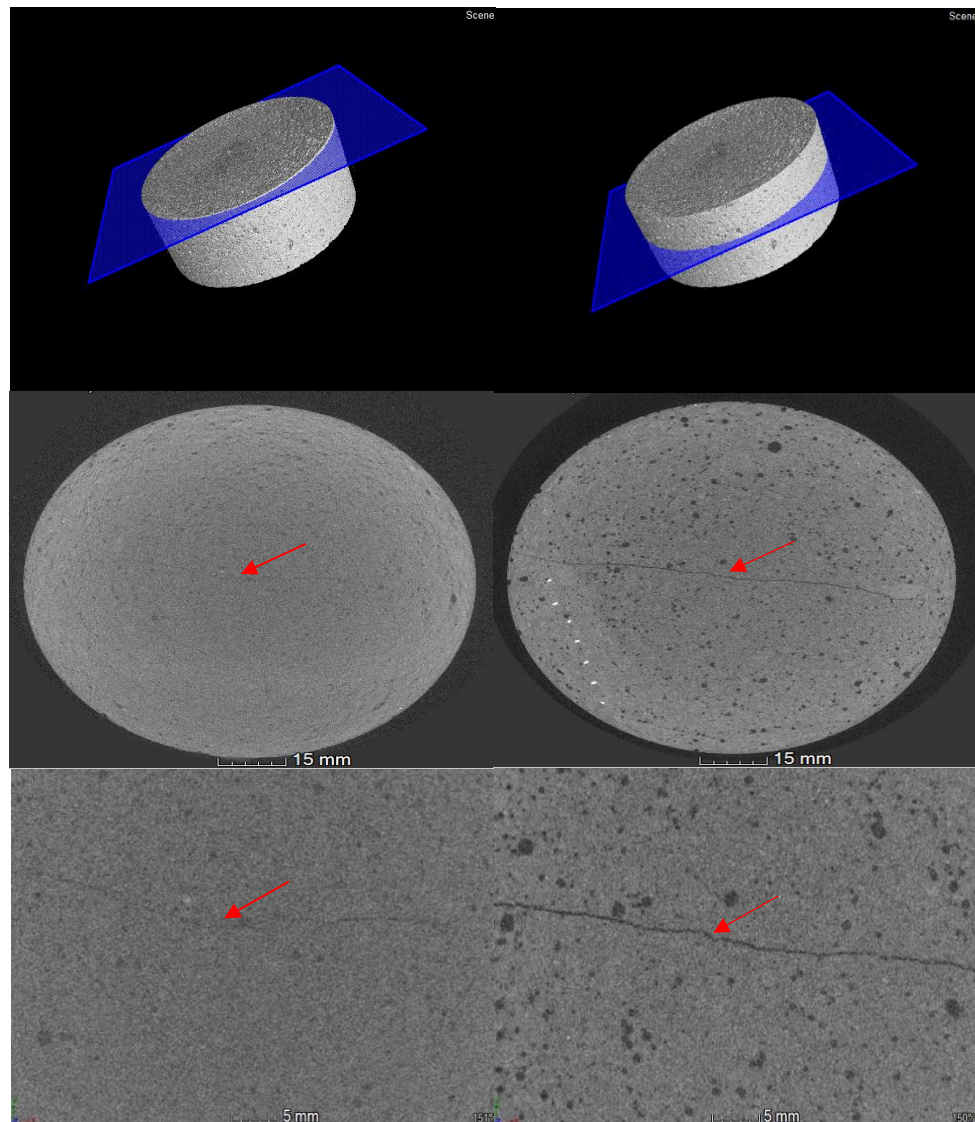
Figure 2.22 X-ray µCT scan images show cracks at (a) surface, and (b) inside at the middle of the healed specimen.

It can be observed that images from the surface of specimens had higher density in the crack region, indicating complete healing of surface cracks. CT scan images showed that the maximum crack depth which exhibited self-healing was 340 ± 30 µm from the surface of the cracked specimens. Images from deeper inside the specimens indicated low density (dark color in the crack region), suggesting that no significant healing occurred. The long-term change in interior crack width owing to self-healing was also investigated. Specimens were re-immersed in water for 9 months and then scanned

using X-ray µCt. Images from X-ray µCt scans indicate that the crack width at the interior of specimens remained unchanged, as shown in **Figure 2.23**.
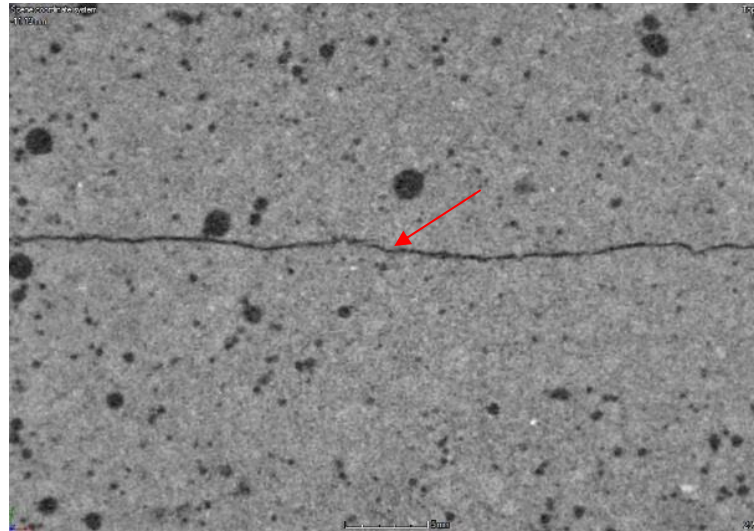
Figure 2.23 X-ray µCT scanning images show internal cracks at 400 µm depth below the surface of the self-healed specimen after 9 months of water submersion.

This suggests that complete self-healing was mostly localized at the top surface of cracked specimens. Sealing of cracks by healing products could be responsible for halting the self-healing mechanism from reaching deeper inside healed cracks. Similar results were found by Wang *et al*. (2014) (b) in bacterial-based self-healing of concrete. In their study, X-ray µCt analysis showed that the healing product was mostly distributed in the surface layer and had a sharp decrease in the subsurface layer deeper inside samples. According to Sisomphon *et al*. (2012), locations near the surface of a cracked cement-based material contained significant amounts of both calcium and carbonate ions that formed calcium carbonate ($CaCO_3$) as a healing product. Accordingly, large amounts of $CaCO_3$ can form and heal surface cracks.

2.3.7 Environmental Exposure and Self-healing

Optical microscopy and SEM observations showed evidence of self-healing of surface cracks in specimens fully submerged in water. However, no crack healing was observed in identical specimens exposed to cyclic T and RH. This suggests that autogenous or improved autogenous self-healing of a cementitious material primarily depends on the surrounding environment. For instance, previous study by Roig-flores *et al*. (2015)

showed that specimens with a similar composition (i.e. concrete incorporating crystalline admixture) exhibited different self-healing tendencies when exposed to different environmental conditions including water immersion, water contact, and a humidity chamber at constant T = 20 °C and RH = 95 ± 5%. In addition, they found that no self-healing occurred for all specimens exposed to constant T and RH. Özbay *et al*. (2013) also found that no crack width change occurred for engineered cementitious composites (ECC) exposed to continuous air in comparison to similar specimens exposed to either continuous submersion in water or cyclic submersion and drying. Similarly, studies by Luo *et al*. (2015) and Wang *et al*. (2014) (a) reported that the self-healing efficiency of cracks in a bacteria-based concrete depended solely on the surrounding environment since, for both studies, no self-healing was found in specimens exposed to constant RH. Therefore, in the current study, cracked specimens exposed to cyclic T and RH showed no self-healing, which further reinforces the fact that the presence of water in a liquid state in cracks is an essential factor for promoting self-healing in cementitious materials.

2.3.8 Microstructural Densification and Self-healing

In the present study, MIP analysis demonstrated that submerged specimens exhibited considerable reduction in porosity. Decrease in porosity occurred primarily due to the presence of capillary liquid water, which promotes further hydration, leading to microstructural densification. However, combining results of X-ray µCt, SEM/EDX, and MIP analysis indicates that further hydration and pozzolanic reactions may play insignificant role in crack closing. For instance, although MIP results underlined continuous reduction in porosity as cement hydration reactions proceeded from 28-d to 1 year, X-ray µCt images revealed that interior crack widths remained unchanged. SEM/EDX analysis confirmed that carbonation was a primary healing mechanism at the surface of cracked specimens. Hence, reduction in porosity due to hydration and/or pozzolanic reactions primarily designates microstructural densification of the original space of un-hydrated cement. These findings agree with previous study by Huang *et al.* (2013) who investigated the self-healing of microcracks via further hydration of un-hydrated cement paste and found that the percentage of calcium hydroxide (CH) forming in cracks was much higher than calcium silicate hydrate (C-S-H). According to Huang *et al.* (2013), on crack surfaces, un-hydrated cement particles exposed to water form inner hydrated products that occupy the original space of the un-hydrate

cement particles and has negligible contribution in filling cracks. Accordingly, further cement hydration and continuous pozzolanic reactions had little contribution to self-healing of cracks.

2.4 Conclusions

In the present study, the self-healing of surface and interior cracks in a cement mortar exposed to different environmental curing conditions was investigated. Based on the experimental findings, the following conclusions can be drawn:

- No self-healing could be demonstrated for specimens exposed to cyclic T and RH.
- Cracks in a cement-based material exhibited self-healing primarily when the curing environment was conducive to contact with liquid water.
- X-ray computed tomography showed that self-healing was mainly restricted to surface cracks. The maximum crack depth that exhibited self-healing was 340 $\pm$ 30 µm from the surface of the cracked specimens. The maximum crack width healed in the tested specimens submerged in deionized water in this study was only 300 µm for the tested one year period.
- The main healing product formed in surface crack was $CaCO_3$.
- Both further cement hydration and pozzolanic reactions had negligible contribution to filling cracks and crack healing.
- There is strong indication that the effectiveness of autogenous self-healing of cracks in cement-based materials significantly depends on the surrounding environment.

2.5   References

E. Tsangouri, G. Karaiskos, A. Deraemaeker, D. Van Hemelrijck. D. Aggelisa (2016) "Assessment of Acoustic Emission localization accuracy on damaged and healed concrete" *Construction and Building Materials*, 129: 163-171.

E. Özbay, M. Şahmaran, M. Lachemi, and H. E. Yücel (2013) "Self-Healing of microcracks in high-volume fly-ash-incorporated engineered cementitious composites", *ACI Materials Journal*, 110 (1): 33-43.

H. Huang, G. Ye, and D. Damidot (2013) "Characterization and quantification of self-healing behaviors of microcracks due to further hydration in cement paste", *Cement and Concrete Research*, 52: 71-81.

J. Wang, J. Dewanckele, V. Cnudde, S. Van Vlierberghe, W. Verstraete, N. De Belie (2014) (b) "X-ray computed tomography proof of bacterial-based self-healing in concrete" *Cement and Concrete Composites*, 53: 289-304.

J.Y. Wang, H. Soens, W. Verstraete, and N. De Belie (2014) (a) "Self-healing concrete by use of microencapsulated bacterial spores", *Cement and Concrete Research*, 56: 139-152.

K. Sisomphon, O. Copuroglu, and E.A.B. Koenders(2012) "Self-healing of surface cracks in mortars with expansive additive and crystalline additive", *Cement and Concrete Composites*, 34(4): 566-574.

K. Van Tittelboom, N. De Belie, W. De Muynck, and W. Verstraete (2010) "Use of bacteria to repair cracks in concrete", *Cement and Concrete Research*, 40(1): 157-166.

L. Ferrara, V. Krelani, and M. Carsana (2014) "A ''fracture testing'' based approach to assess crack healing of concrete with and without crystalline admixtures", *Construction and Building Materials*, 68(15): 535-551.

L. Ferrara, V. Krelani and F. Moretti (2016) "On the use of crystalline admixtures in cement based construction materials: from porosity reducers to promoters of self healing", *Smart Materials and Structures*, 25: 17 p.

L. Ferrara, V. Krelani, F. Moretti, M. Roig Flores, P. S. Rosb (2017) "Effects of autogenous healing on the recovery of mechanical performance of High Performance Fibre Reinforced Cementitious Composites (HPFRCCs): Part 1", *Cement and Concrete Composites*, 83: 76-100.

M. Roig-Flores, S. Moscato, P. Serna, and L. Ferrara (2015) "Self-healing capability of concrete with crystalline admixtures in different environments", *Constr. & Building Materials*, 86: 1-11.

M. Luo, C. Qian, and R. Li (2015) "Factors affecting crack repairing capacity of bacteria-based self-healing concrete", *Construction and Building Materials*, 87: 1-7.

R. Borg, E. Cuenca, E. Brac and L. Ferrara (2018) "Crack sealing capacity in chloride-rich environments of mortars containing different cement substitutes and crystalline admixtures", *Journal of Sustainable Cement-Based Materials*, 7(3): 141-159.

S. Liu, Z. B. Bundur, J. Zhu, R. D. Ferron (2016) "Evaluation of self-healing of internal cracks in biomimetic mortar using coda wave interferometry" *Cement and Concrete Research*, 83: 70-78.

Test Method No. II.4 (2006) "Water Absorption Tube Test", *RILEM: Paris, France*.

Z. Jiang, W. Li and Z. Yuan (2015) "Influence of mineral additives and environmental conditions on the self-healing capabilities of cementitious materials", *Cement and Concrete Composites*, 57: 116-127.

<div align="right">

CHAPTER THREE

</div>

Visualization and Quantification of Crack Self-Healing in Cement-Based Materials Incorporating Different Minerals*

3.1   Introduction

In this chapter, multiple test methods were used to investigate self-healing of cracks in cement mortar incorporating metakaolin, bentonite, and calcium carbonate microfiller in different environmental exposure. Change in crack width was monitored using optical microscopy. Backscattered electron microscopy coupled with energy disperse X-ray analysis was used to identify healing compounds. Mercury intrusion porosimetry and water absorption were employed to assess porosity. X-ray computed micro-tomography (X-ray μCT) with 3-dimensional image processing was used to segment and quantify cracks before and after healing.

3.2   Experimental Program

3.2.1 Materials and Specimen Preparation

Mortar specimens were made with ordinary portland cement (OPC) compliant with requirements of CSA A3001 and ASTM C150. Water-to-cementitious materials ratio (w/cm) of 0.35 and sand-to-cementitious materials mass ratio (s/c) of 2 were used. Three different mineral additions including high-reactivity metakaolin (MK) as a silica-based material, granular bentonite (BN) as a swelling agent, and fine calcium carbonate powder (CC) as a carbonate mineral were used. Physical and chemical properties of the OPC, MK, BN, and CC are summarized in **Table 3.1**. The mixture design of mortars is reported in **Table 3.2**. A polycarboxylate-based high-range water reducing admixture (HRWRA) as per ASTM C494 was used to adjust workability. PVA fiber at a dosage of 1% by volume fraction was added to the mortar mixtures. Disk specimens (50 mm

diameter and 25 mm height) were prepared for acquiring high resolution X-ray μCT images. All specimens were cured for 28-d in a moist room at RH ≥ 95% and T = 21 ± 1°C as per ASTM C511 (Standard Specification for Mixing Rooms, Moist Cabinets, Moist Rooms, and Water Storage Tanks Used in the Testing of Hydraulic Cements and Concretes).

Table 3.1: Physical and chemical properties of materials used

Components /Property	MK	BN	CC
Assay percent range (%)	-	-	>99
Montmorillonite (%)	-	85.0	-
Quartz (%)	-	5.0	-
Calcium oxide (CaO) (%)	0.20	-	-
Calcium	-	1	-
Fledspars (%)	-	5.0	-
Silicon oxide (SiO_2) (%)	53.50	-	-
Cristobalite (%)	-	2.0	-
Aluminum oxide (Al_2O_3) (%)	42.50	-	-
Ferric oxide (Fe_2O_3) (%)	1.90	-	-
Sulfur trioxide (SO_3) (%)	0.05	-	-
Loss on ignition (%)	0.50	-	-
Specific gravity	2.60	2.50	2.70
Surface area (m^2/kg)	15000	-	-
Time of setting (min) Vicat Initial	-	-	-

Table 3.2: Mixture design of mortars by mass ratio

Mix	Description	OPC	MK	BN	CC	Sand	Water
1	OPC	100	-	-	-	200	35
2	MK15	85	15	-	-	200	35
3	BN8	92	-	8	-	200	35
4	CC8	92	-	-	8	200	35

Crack was created at the age of 28 days using a screw jack as shown in the (**Fig. 3.1**). The crack width was controlled during the screwing process via a calibration ruler. For each environmental exposure, three groups of specimens with three different values of crack width were tested. The first group consisted of three specimens with an average crack width in the range of 50 – 150 µm. For the second and third groups, the average crack widths were 150 – 300 µm and 300 – 500 µm, respectively.

Figure 3.1 Cracking of specimens using screw jack.

3.2.2 Inductively coupled plasma atomic emission spectroscopy (ICP-AES)

Ions leached out from the pre-cracked mortar specimens were analysed using a Varain Vista Pro apparatus, as shown in (**3.2**). The wavelength range was 167-785 nanometer with Peltier cooled CCD detection. Before the test, pre-cracked mortar specimens were immersed into de-ionized water to allow the ions to leach out of the specimens.

Figure 3.2 ICP-AES system.

3.3 Experimental Results and Discussion

3.3.1 Self-healing of Surface cracks

Surface cracks of mortar specimens prior to and after the self-healing process were investigated using optical microscopy at 40x magnification. For specimens exposed to cyclic T and RH, no self-healing was observed (**Fig. 3.3**). However, for identical cracked specimens exposed to continuous water submersion (**Figs. 3.4** to **3.7**), surface cracks having different widths were filled with self-healing products. This suggests that self-healing of a cementitious material primarily depends on both the original crack width and surrounding environment. For instance, previous study by Jiang *et al.* (2015) found that mortar specimens exposed to still water curing exhibited a larger decrease in crack width compared to that of identical specimens cured in flowing water. Wang *et al.* (2014) reported that the self-healing efficiency of cracks in a bacteria-based concrete depended primarily on the surrounding environment. Other studies by Sahmaran *et al.* (2013), Zhang and Zhang (2017), Zhu *et al.* (2012), and Qian *et al.* (2010) showed that the self-healing ability of engineered cementitious composites (ECC) highly depended on the exposed environment. Accordingly, in the current study, cracked specimens exposed to cyclic T and RH exhibited no self-healing, which further reinforces the argument that the presence of water in a liquid state in cracks is an essential factor for promoting self-healing of cement-based materials.

Results also showed that CC8 specimens exhibited best healing potential where the surface crack up to about 330 µm was completely sealed. In comparison, MK15 specimens showed the least self-healing in terms of crack closing. The maximum crack width healed in MK15 specimens was 240 µm. For OPC and BN8 specimens, the maximum crack width healed was 290 µm and 260 µm, respectively. Hence, the ability of crack healing was in the order of CC8 > OPC >BN8 >MK15. **Figure 3.8** illustrates the crack sealing index of specimens after on year of water submersion. The results are plotted in terms of evolution of the crack sealing index over time. The self-healing behaviour of each specimen can be explained from the ICP-AES results. As observed in **Table 3.3**, the higher Ca^{2+} ions released from specimens, the higher was the self-healing ability. According to Sisomphon *et al.* (2012) and Jiang *et al.* (2015), more

Ca^{2+} ions released from cracked specimens would promote self-healing due to precipitation of calcium carbonate on the surface cracks.

Table 3.3: Duration of each temperature/humidity cycle

Specimen	*Ca^{2+} concentration (mg/l)*
OPC	9.2010
MK15	1.2118
BN8	2.6820
CC8	10.7705
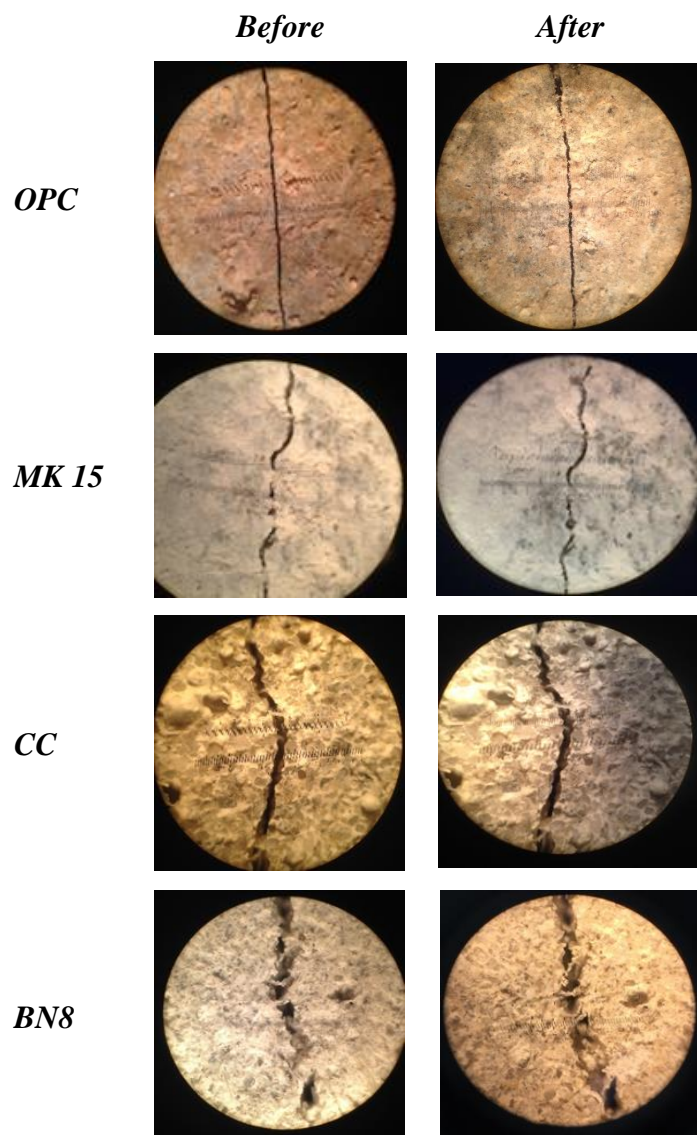
Figure 3.3 Surface cracks before and after exposure to cyclic T and RH showing no self-healing.
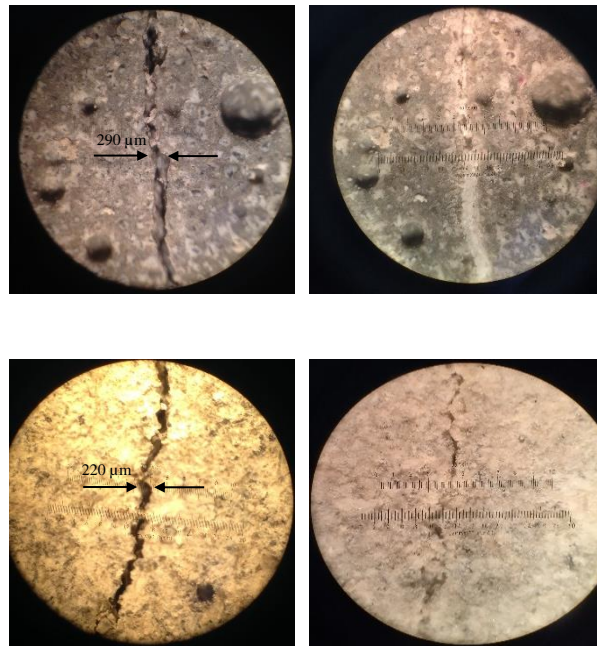
Figure 3.4 Surface cracks in OPC specimens before and after water submersion showing self-healing.
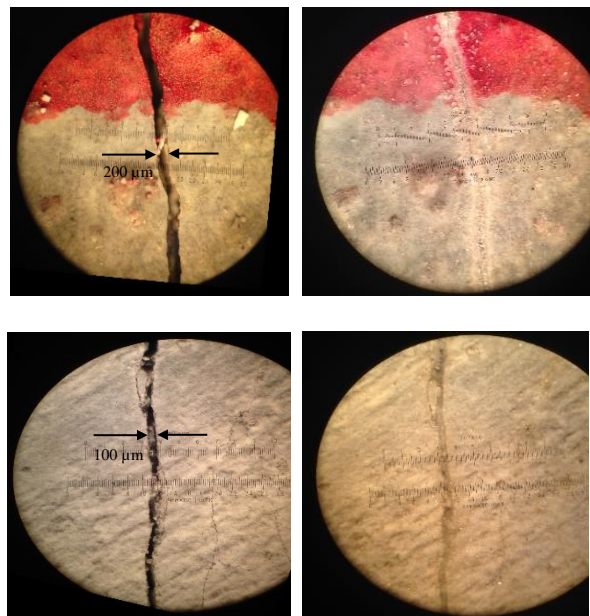
Figure 3.5 Surface cracks in MK15 specimens before and after water submersion showing self-healing.
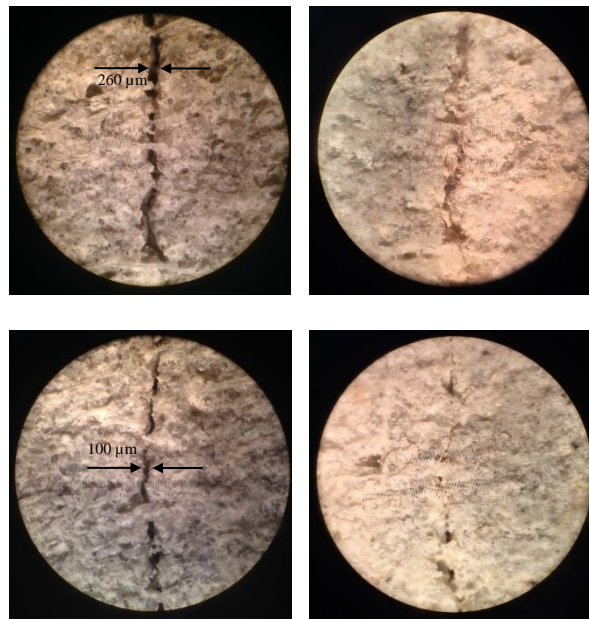
Figure 3.6 Surface cracks in BN8 specimens before and after water submersion showing self-healing.
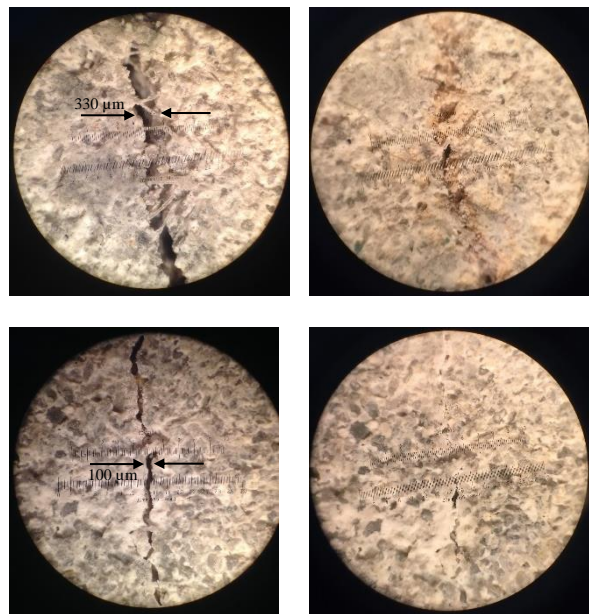
Figure 3.7 Surface cracks in CC8 specimens before and after water submersion showing self-healing.
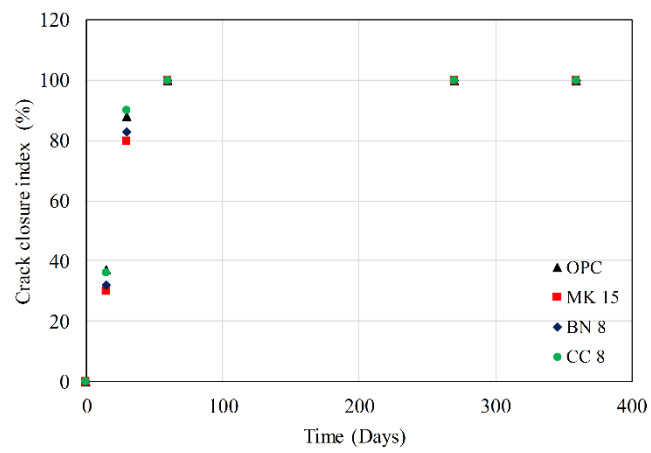
(a)
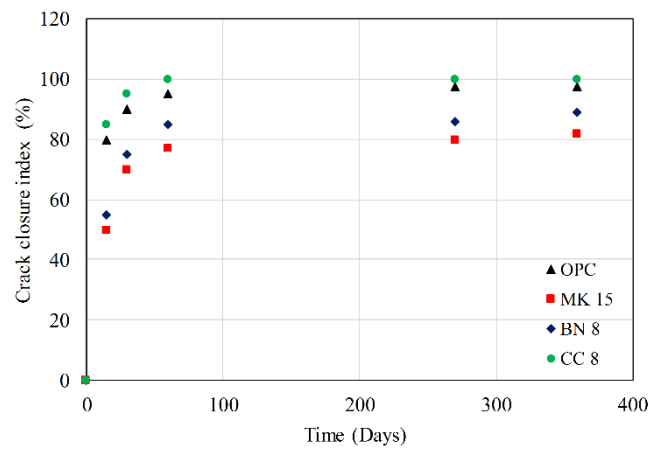
(b)
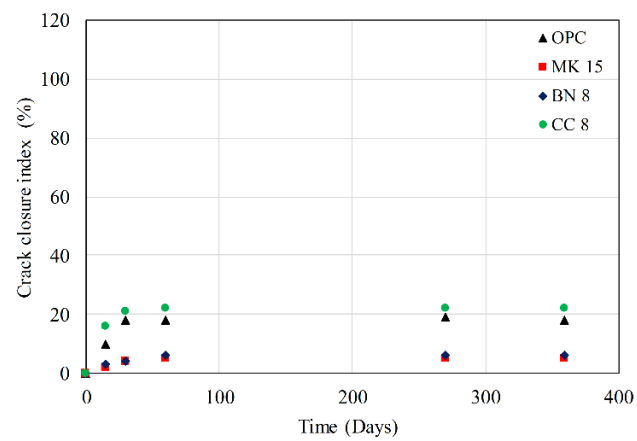
(c)

Figure 3.8 Change in surface crack width of specimens submerged in water with initial crack width (a) 50-150 μm; (b) 150-300 μm; and (c) 300-500 μm.

3.3.2 Pore and Microstructure Change

The evolution of pore structure with time was investigated using MIP. Only specimens that exhibited self-healing were tested. **Figure 3.9** displays the cumulative mercury intrusion curves as a function of the pore diameter for cracked mortar specimens before and after water submersion.

(a)

(b)
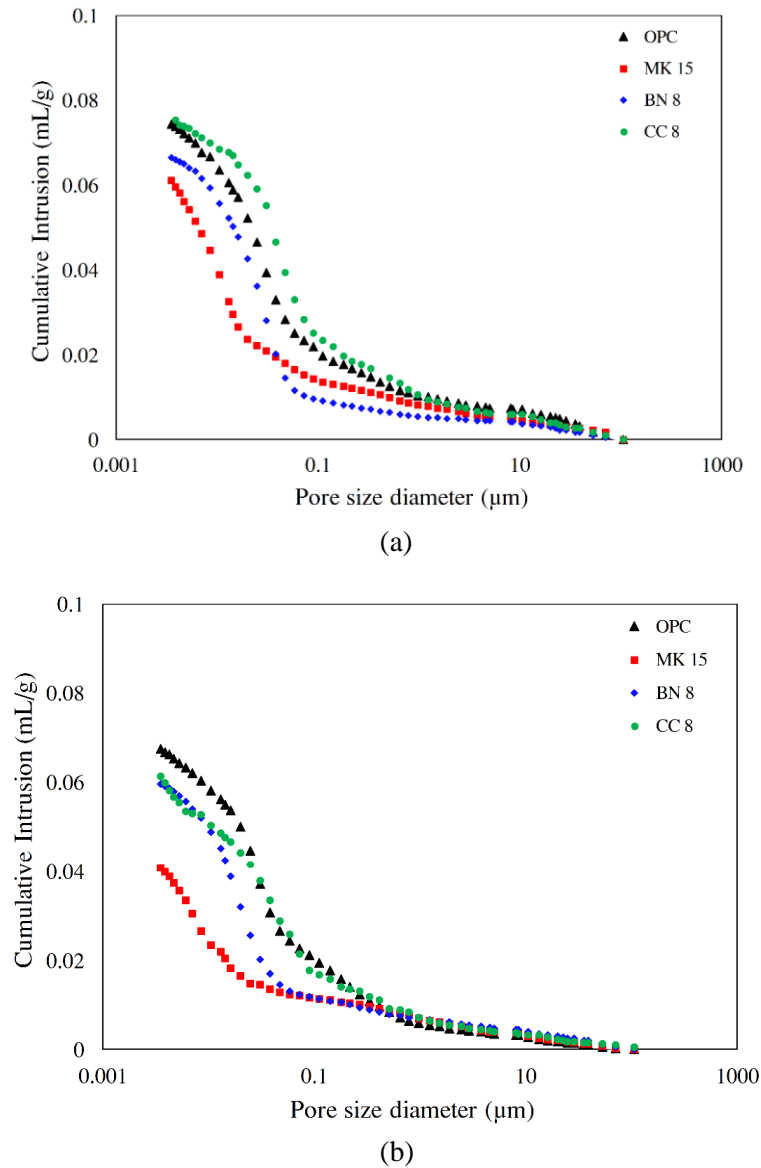
Figure 3.9 Cumulative intruded pore volume vs. pore diameter for cracked specimens (a) at 28 days, and (b) one year after water submersion.

All cracked specimens exhibited reduction in and refinement of pore size after one year. It can be observed that although the MK15 specimens showed the least crack self-healing after one year of water submersion, they exhibited the highest reduction in porosity compared to that of other specimens, even those that exhibited better crack self-healing. This is likely due to the ongoing pozzolanic reaction of metakaolin. Results from ICP-AES analysis showed that the concentration of Ca^{2+} in the water used to cure MK15 specimens was less than that in water used to cure CC8, OPC, and BN8 specimens. Ca^{2+} ions released from specimens would promote the precipitation of calcium carbonate, which was identified as the primary self-healing compound. Therefore, ongoing pozzolanic reactions seem to play insignificant role in crack closing, while they appear to be predominant in pore reduction and refinement. Previous study by Huang *et al*. (2013) reported that the percentage of calcium hydroxide (CH) forming in cracks was much higher than calcium silicate hydrate (C-S-H). Similarly, Sisomphon *et al*. (2012) and Jiang *et al*. (2015) showed that the more Ca^{2+} released from cracked specimens, the more self-healing occurs. Therefore, further cement hydration or continuous pozzolanic reactions seem to have little or negligible contribution to self-healing of cracks.

3.3.3 SEM and EDX Analyses

Figure 3.10 shows typical SEM-BSE images and EDX analyses for healing products formed within surface cracks. Elemental EDX analysis at different locations revealed that the healing products at crack surfaces in all specimens were mainly composed of calcium with some carbon and oxygen, indicating that it primarily consists of $CaCO_3$. Only small amounts of Si were found at the crack surfaces, suggesting limited formation of calcium silicate hydrate (C-S-H) gel as a healing product. Several previous studies have also shown that $CaCO_3$ was the main healing product filling cracks in concrete incorporating different additives (e.g. Sahmaran *et al*., 2013; Jiang *et al*., 2015; Sisomphon *et al*., 2012; Roig-Flores *et al.,* 2015; Wang *et al*., 2014; Wiktor and Jonkers, 2011). For example, Jiang *et al*. (2015) investigated the effect of four types of mineral additives including silica-based components, chemical expansive agents, swelling minerals and crystalline materials on the self-healing of concrete.
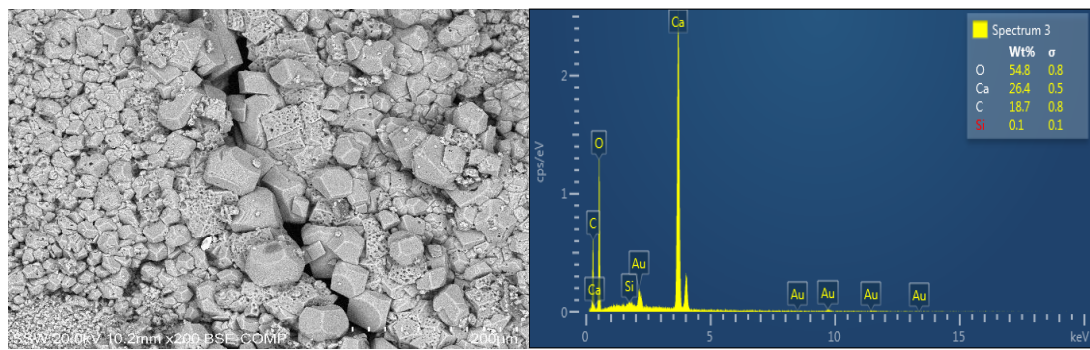
(a)
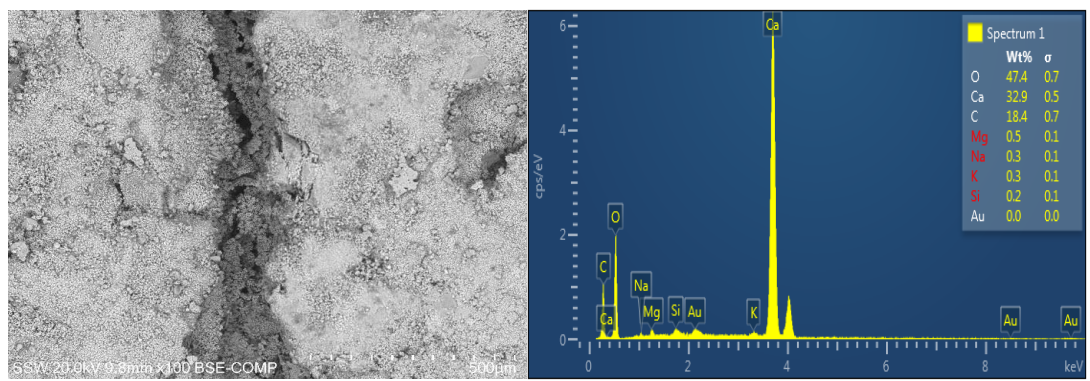
(b)
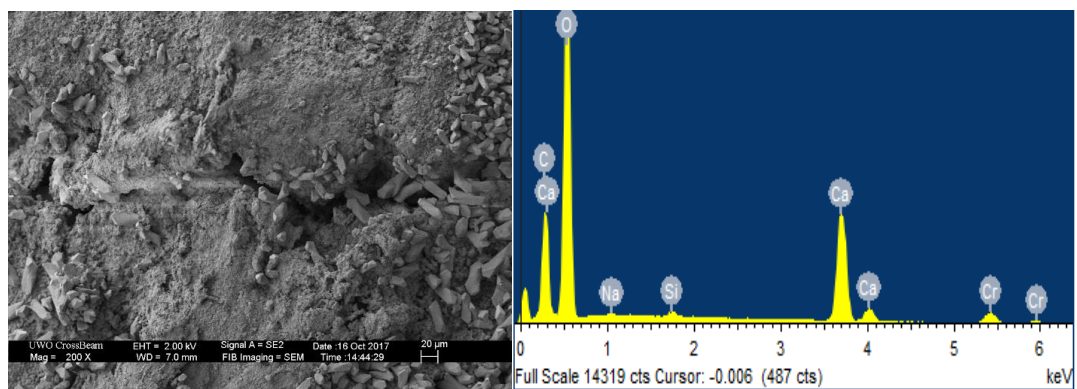
(c)

Figure 3.10 SEM-BSE micrograph with EDX pattern of products in self-healed cracks of specimens (a) MK15; (b) BN8; and (c) CC8.

Their results showed that $CaCO_3$ was the main healing product formed in surface cracks. Similarly, Wang *et al*. (2014) found that $CaCO_3$ was the main healing product formed in cracks for concrete with hydrogel encapsulated bacterial spores. Formation of $CaCO_3$ as a healing product is mainly due to the leaching and re-deposition of calcium ions Ca^{2+} from the cementitious matrix and diffusion of carbonates into cracks (e.g. Jiang *et al*., 2015; Sisomphon *et al*., 2012). Therefore, the main self-healing product in the present study was calcium carbonate, in agreement with previous research.
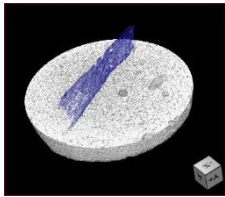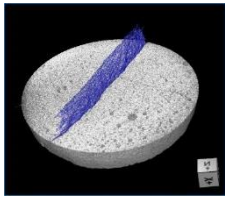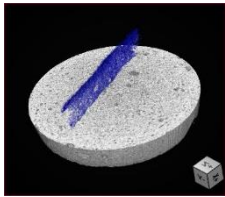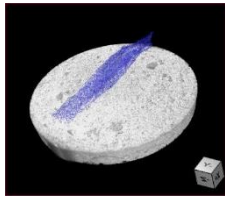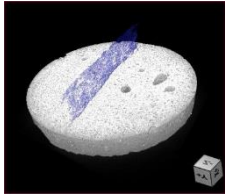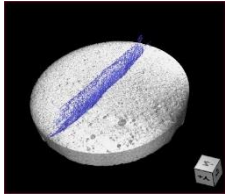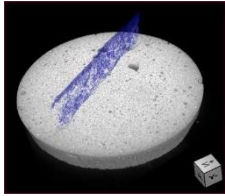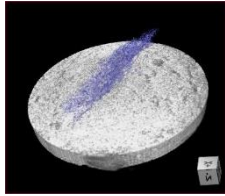
3.3.4 Crack Quantification Using X-ray Computed Tomography

X-ray computed tomography is an imaging technique where digital geometry processing can be used to generate 3D-images of scanned specimens. In the present study, only specimens submerged in water with crack width in the range of 150 to 300 µm were selected for X-ray µCT analysis since they exhibited visible crack healing in optical microscopy analysis. The selected specimens were scanned before and after water submersion. To quantify the change in crack volume owing to self-healing, two datasets representing the condition before and after self-healing were input into a 3D rendering software (Dragonfly 3.5), which is an application used for 3D data visualization and image processing analysis. The software can import data of different types, sizes, and scales to measure and quantify objects within multi-region of interests, such as fibers, pores, and vesicles.

Figure 3.11 displays 3D-images of a typical crack profile (in blue color) before and after self-healing. For the same specimen, the crack was segmented and its total volume was measured. Accordingly, the amount of healing product can be quantified by subtracting the volume of crack before and after self-healing. **Table 3.4** reports the results of segmentation and quantification analysis of cracks before and after self-healing. Results show that the healing efficiency was 32.26%, 27.27%, 25.6%, and 24.1% for the CC8, OPC, BN8, and MK15 specimens, respectively. The self-healing efficiency improved with the increase of Ca^{2+} released from the cracked specimens. In addition, images from X-ray µCT scans indicate that complete self-healing was mostly concentrated at the surface of the mortar specimens. Sealing of cracks against liquid water by healing products could be the reason for stopping the self-healing mechanism

from reaching deeper inside the specimen. Recent studies have shown similar results in concrete with a different binder. For instance, Snoeck *et al*. (2016) investigated the self-healing of cementitious materials promoted by superabsorbent polymers. Their results showed that most of the healing product was formed at the surface of cracks, while fewer healing products were found deeper in the interior of the tested samples. Similar findings were reported by Wang *et al*. (2014) when they studied the self-healing behaviour of concrete specimens incorporating bio-hydrogels (hydrogel encapsulated bacterial spores). Although specimens incorporating bio-hydrogels distinctly improved the self-healing efficiency compared to that of the reference specimens, complete self-healing was mainly restricted to surface cracks. This is likely because locations near the surface of cracked cement-based materials contain significant amounts of both calcium and carbonate ions that can form calcium carbonate ($CaCO_3$) as a healing product (Sisomphon *et al*., 2012).

Table 3.4: Segmentation and quantification of cracks before and after self-healing

	OPC	*MK15*	*BN8*	*CC8*
Before Healing	V = 167,195,668,403.68 (μm^3)	V = 160,304,407,584.47 (μm^3)	V =144,004,409,504.02 (μm^3)	V = 165,091,401,765.79 (μm^3)
After Healing	V = 120,857,968,631.44 (μm^3)	V = 121,681,452,585.80 (μm^3)	V = 106,823,819,309.56 (μm^3)	V = 111,816,441,002.71 (μm^3)
Healing Efficiency	*27.7%*	*24.1%*	*25.6%*	*32.2 %*

(a)   (b)
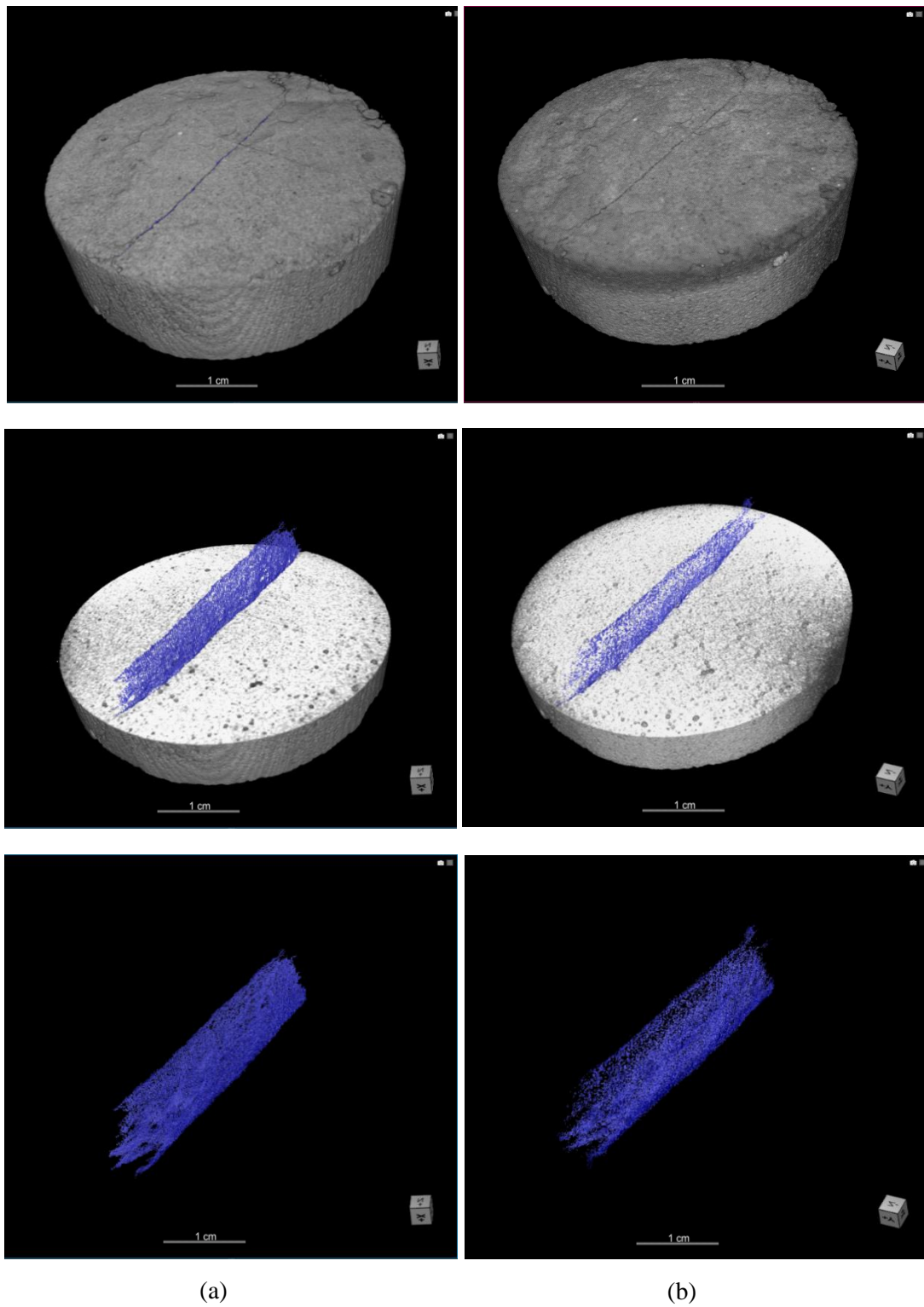
Figure 3.11 X-ray µCT scan images showing (a) before self-healing, and (b) after self-healing.

3.4   Conclusions

In this chapter, the self-healing of cracks in cement-based materials incorporating various minerals (i.e., metakaolin as a pozzolanic material, bentonite as a swelling agent, and limestone microfiller as a carbonate mineral) was explored using a portfolio of test methods. Based on the experimental findings, the following conclusions can be drawn:

- Self-healing of cement-based materials depends, to a large extent, on the moisture conditions prevailing around the tested specimens. While no significant self-healing could be identified in cement-based mortar specimens exposed to cyclic T and RH, cracks in identical specimens exhibited self-healing primarily when the curing environment was conducive to direct contact with liquid water.

- Mobilizing multiple test methods such as MIP, optical microscopy, SEM-EDX and X-ray µCT can yield synergistic information that better illustrates the existence, extent and quantity of self-healing in cement-based materials.

- X-ray µCT coupled with powerful 3-dimentional image analysis and processing can offer an effective tool for quantifying self-healing in cracked cement-based materials.

- X-ray µCT showed that self-healing was restricted to cracks near the surface of specimens. Thus, concreted research efforts are needed to better dissociate self-healing as a mechanism for sealing the surface of cement-based materials to enhance its durability, from that intended to fully close cracks aiming to re-establish structural integrity and mechanical performance.

- The maximum crack width healed for specimens submerged in deionized water over the one-year test period in the present study was about 330 µm, 290 µm, 260 µm, and 240 µm for specimens incorporating limestone microfiller, ordinary portland cement, bentonite, and metakaolin, respectively. Longer term testing is needed to define whether this behaviour can change further over time.

- The main crack healing product formed in cement mortar specimens was $CaCO_3$.

- Based on the quantification analysis, the healing efficiency was 32.26%, 27.27%, 25.6%, and 24.1% for specimens with limestone microfiller, ordinary portland cement, bentonite, and metakaolin, respectively.

3.5   References

D. Snoeck, J. Dewanckele, V. Cnudde, and N. De Belie (2016) "X-ray computed microtomography to study autogenous healing of cementitious materials promoted by superabsorbent polymers", *Cement and Concrete Composites*, 65: 83-93.

H. Huang, G. Ye, and D. Damidot (2013) "Characterization and quantification of self-healing behaviors of microcracks due to further hydration in cement paste", *Cement and Concrete Research*, 52: 71-81.

J. Wang, J. Dewanckele, V. Cnudde, S. Van Vlierberghe, W. Verstraete, N. De Belie (2014) "X-ray computed tomography proof of bacterial-based self-healing in concrete" *Cement and Concrete Composites*, 53: 289-304.

K. Sisomphon, O. Copuroglu, and E.A.B. Koenders (2012) "Self-healing of surface cracks in mortars with expansive additive and crystalline additive", *Cement and Concrete Composites*, 34(4): 566-574.

M. Sahmaran, G. Yildirim, and T. K. Erdem (2013) "Self-healing capability of cementitious composites incorporating different supplementary cementitious materials" *Cement and Concrete Composites*, 35 (10): 89-101.

M. Roig-Flores, S. Moscato, P. Serna, and L. Ferrara (2015) "Self-healing capability of concrete with crystalline admixtures in different environments", *Construction Building Materials*, 86: 1-11.

S.Z. Qian, J. Zhou, and E. Schlangen (2010) "Influence of curing condition and precracking time on the self-healing behavior of Engineered Cementitious Composites" *Cement and Concrete Composites*, 32: 686-693.

V. Wiktor and H. M. Jonkers (2011) "Quantification of crack-healing in novel bacteria-based self-healing concrete", *Cement and Concrete Composites*, 33(7): 763-770.

Y. Zhu, Y. Yang, and Y. Yao (2012) "Autogenous self-healing of engineered cementitious composites under freeze–thaw cycles" *Construction and Building Materials*, 34:522-530.

Z. Jiang, W. Li and Z. Yuan (2015) "Influence of mineral additives and environmental conditions on the self-healing capabilities of cementitious materials", *Cement and Concrete Composites*, 57: 116-127.

Z. Zhang and Q. Zhang (2017) "Self-healing ability of Engineered Cementitious Composites (ECC) under different exposure environments" *Construction and Building Materials*, 156:142-151.

CHAPTER FOUR

Exploring Mechanical Strength Recovery of Cement-Based Materials Induced by Self-healing Using Shear Wave Velocity

4.1 Introduction

Portland cement, the main ingredient of concrete, is the most consumed commodity on earth after water, and its production continues to grow. According to the U.S. Geological Survey (2018), the United States produced 86.3 million metric tons of cement in 2017 in comparison to only 67.2 (MT) in 2010. China's cement production in 2017 amounted to 2.4 billion metric tons, nearly half the total world's production. According to Cao *et al*. (2016), from 1978 to 2010, China's cement consumption and cement related CO_2 emissions have increased from 65.24 to 1879.19 Mt and from 8.87 to 255.68 Mt, respectively. By 2030, the global cement production is expected to reach 5 billion metric tons. Since cement production involves the consumption of large amounts of energy and raw materials, its environmental footprint is colossal.

Likewise, concrete structures continue to deteriorate prematurely around the world, inflicting enormous economic loss and environmental damage. Concrete structures are vulnerable to cracking due to mechanical loading and environmental exposure. Hence, deleterious substances can easily ingress through cracks, leading to corrosion of the steel reinforcement and degradation of the cementitious matrix (e.g. Aldea *et al.*, 1999; Basheer *et al.*, 2001; Wang *et al.*, 1997). In Canada, for example, the current infrastructure deficit has been valued at more than $US 570 billion. In most parts of the world, existing civil infrastructure continues to age and deteriorate, leading to overwhelming financial crises that threaten to stifle economic prosperity.

To mitigate infrastructure deterioration, researchers around the world have been recently investigating the development of self-healing cement-based materials. These can preserve this infrastructural maintenance and repair budgets, reduce carbon dioxide emissions, and produce more sustainable structures. Accordingly, different techniques have been used to evaluate the efficiency of self-healing in cement-based materials (e.g. Van Tittelboom and De Belie, 2013; Şahmaran *et al*., 2008; Tang *et al*., 2015; Wu *et al*., 2012; Snoeck and De Belie, 2015; Ferrara *et al*., 2014; Kempl and Çopuro, 2016; Huang *et al*., 2013 & 2014; Jonkers *et al*., 2010; Wiktor and Jonkers, 2011; Van Tittelboom *et al*., 2012; Wang *et al*., 2014; Borg *et al.,* 2018; Cuenca *et al.,* 2018).

For instance, Gagné and Argouges (2012) evaluated the autogenous self-healing of cement mortars using air-flow measurements and scanning electron microscopy (SEM). Both techniques showed evidence of self-healing of surface cracks in cement mortars exposed to a high humidity environment. Wang *et al*. (2014) used a high-resolution X-ray computed microtomography (X-ray µCT) to investigate the self-healing behaviour of concrete specimens incorporating bio-hydrogels (hydrogel encapsulated bacterial spores). Their results showed that incorporating bio-hydrogels into cement mortars improved the healing efficiency in terms of crack closure behavior. Termkhajornkit *et al*. (2009) indirectly investigated the self-healing performance of cement pastes incorporating fly Ash. They reported that the self-healing ability of cement pastes increased as the rate of fly ash replacement for cement increased. Sahmaran *et al*. (2013) used optical microscopy and rapid chloride penetrability testing (RCPT) and found that the self-healing efficiency of cementitious composites could differ depending on the type of fly ash used. Another study by Jiang *et al*. (2015) used permeability and water absorption testing to indicate that the self-healing efficiency can be improved using combination of minerals.

An extensive survey of pertinent studies in the open literature shows that self-healing in cement-based materials has been mainly investigated from a durability prospective, particularly considering crack closure behavior, chloride ions diffusion, and recovery of liquid and gas tightness. On the other hand, mechanical strength recovery due to self-healing has received less attention (Ferrara *et al*., 2014; Li *et al*., 2017). According to Li *et al*. (2017), mechanical strength recovery due to self-healing can hardly be captured through conventional destructive testing methods since the healing mechanisms are

normally local and on microscale level. Therefore, it requires a non-destructive technique that is sufficiently sensitive to measure strength recovery due to self-healing.

The shear wave velocity technique (SWV) is a non-destructive technique that has been employed in several fields including the geotechnical, structural, and medical science fields. For example, Mehta and Antich (1997) assessed the biomechanical competence of bone using SWV techniques. Cortez *et al*. (2016) used SWV measurements to detect musculoskeletal abnormalities. Liu *et al*. (2014), Birgül (2009), An *et al*. (2009), Soliman *et al*. (2015), and Zhu *et al*. (2011) evaluated different properties of concrete using SWV testing. Other studies used SWV to investigate the properties of different soils and rocks (e.g. L'Heureux and Long 2017; Rajabi and Sharifipour 2017; Karray *et al*., 2015; Liu *et al*., 2016; El Takch *et al*., 2016).Therefore, in the present chapter, mechanical strength recovery of cement-based materials was investigated via the SWV technique.

4.2   Experimental Program

4.2.1 Materials and Specimen Preparation

Mortar specimens were made with ordinary portland cement (OPC) compliant with requirements of CSA A3001 and ASTM C150. Water-to-cementitious materials ratio (w/cm) of 0.35 and sand-to-cementitious materials mass ratio (s/c) of 2 were used. Four different mineral additions including granular bentonite (BN) as a swelling agent, fine calcium carbonate powder (CC) as a carbonate mineral, and high-reactivity metakaolin (MK) and fly ash (FA) as silica-based materials were used. A polycarboxylate-based high-range water reducing admixture (HRWRA) as per ASTM C494 was used to adjust workability. PVA fiber at a dosage of 1% by volume fraction was added to the mortar mixtures. To determine shear wave velocity, 50 mm cubic specimens were prepared for each mixture according to ASTM C109 (Standard Test Method for Compressive Strength of Hydraulic Cement Mortars). After demolding at 1-d, specimens were cured for 28-d in a moist room at RH $\geq$ 95% and T = 21 $\pm$ 1°C. The curing was carried out according to ASTM C511 (Standard Specification for Mixing Rooms, Moist Cabinets, Moist Rooms, and Water Storage Tanks Used in the Testing of Hydraulic Cements and Concretes). At the age of 28-d, specimens were removed from the moist room and cracks were induced as displayed in **Fig. 4.1**. The maximum applied load on the

specimens was set as the first crack value according to the method described by Pang *et al*. (2016). The cracked specimens were then placed in different environmental conditions.

Figure 4.1 Cracking of specimens using MTS machine.

4.2.2 Shear Wave Velocity

A piezoelectric ring actuator (PRA) technique was used for measuring the shear wave velocity of the tested specimens. This technique was originally developed at the University of Sherbrooke (Gamal El-Dean, 2007) and further developed at Western University (Ahmed *et al*., 2016). Two piezoelectric ring-shaped transducers were mounted on tow opposite surfaces of the tested specimens to evaluate shear wave velocity, as shown in **Fig. 4.2**. A data acquisition system was used to receive and record the resulting signals. During the test, a high voltage sinusoidal wave was generated through the specimen with different input excitation frequencies. **Figure 4.3** shows a typical signal with clear shear wave arrival. The arrival point of the shear wave signal was taken as the first significant excursion in the signal with positive polarity as described by Mneina *et al*. (2018). The variation in SWV before and after cracking and healing was periodically investigated.
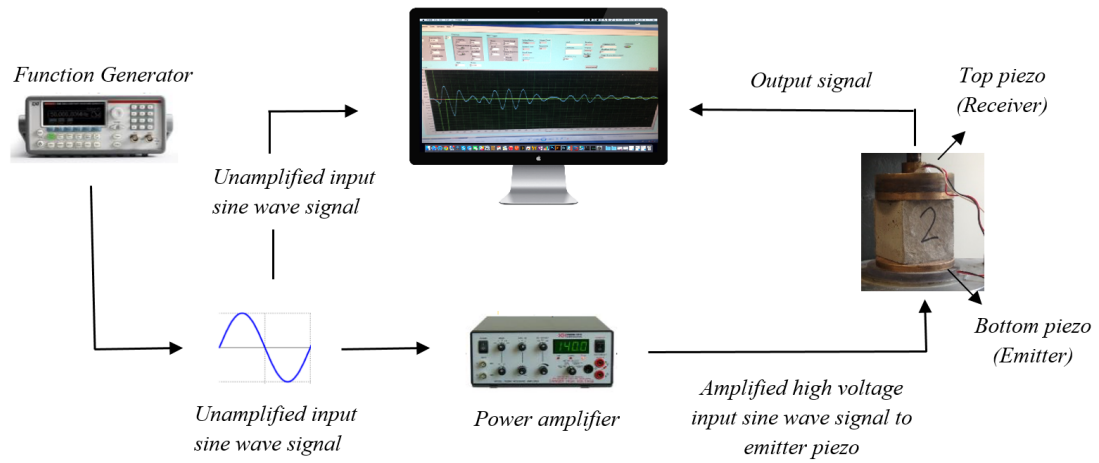
Figure 4.2 Schematic representation of PRA test set-up.
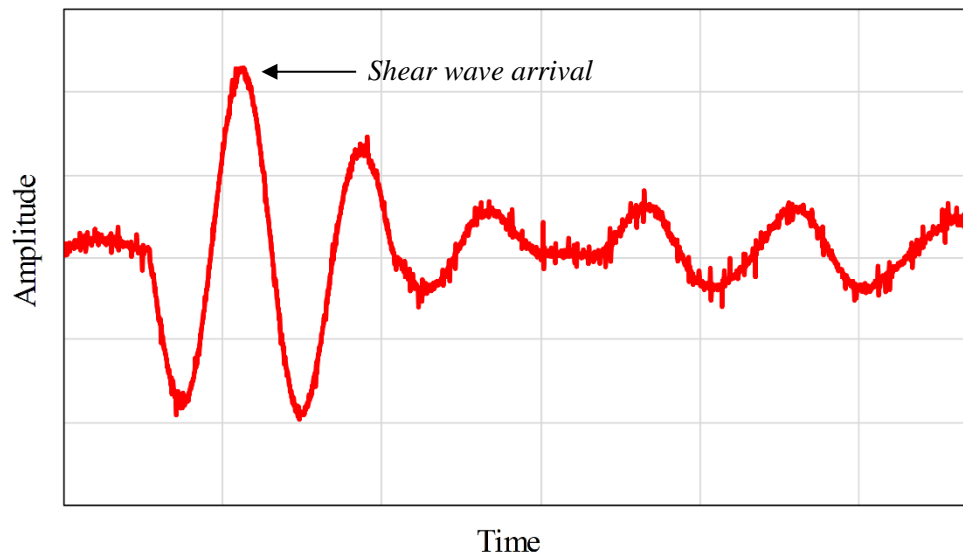
Figure 4.3 Typical output signal with clear shear wave arrival.

4.3 Experimental Results and Discussion

4.3.1 Shear Wave Velocity and Mechanical Strength Recovery

Figures 4.4 and **4.5** show the compressive strength of the pre-cracked specimens exposed to different environmental exposures. After one year, the cracked and cured specimens were re-cracked to the maximum load. Based on the results, self-strength recovery can hardly be interpreted using a destructive technique such as compression testing. Several studies have previously investigated various properties of concrete using ultrasonic measurements. For instance, Liu *et al*. (2014) monitored the setting and hardening process of mortar and concrete using ultrasonic shear waves. Their results showed that shear wave velocity can be a sensitive measurement to detect the setting and hardening process of cementitious materials. Similarly, Soliman *et al*. (2015) reported that early-age properties of concrete can be monitored using the shear-wave velocity technique. Another study by Naji *et al*. (2017) evaluated the potential segregation of self-consolidating concrete through monitoring the changes in shear waves using a piezoelectric ring actuator technique. They found that static stability of SCC concrete can be assessed using such a technique. An *et al*. (2009) showed that shear wave velocity can be used to characterize the compressive strength development of concrete under various curing regimes. In the current study, the development of strength recovery due to self-healing in cement-based materials was investigated using shear wave velocity measurements.

Tables 4.1 and **4.2** report the shear wave velocity, SWV evolution of the self-healed specimens exposed to different environments. Several measurements of SWV were taken over a period of year. The test results have been normalized with respect to the original value before cracking. For specimens exposed to water submersion, results showed that FA20 specimens exhibited significant strength recovery. In comparison, BN8 specimens showed the least self-healing in terms of strength recovery. For FA20 specimens, strength recovery can be related to the progress of hydration reactions and further formation of calcium silicate hydrate C-S-H due to pozzolanic reactions. For MK15 specimens, although metakaolin undergoes pozzolanic reaction and refines the microstructure of the hydrated cement paste, it reacts quicker than fly ash due to its smaller particle size and higher surface area.
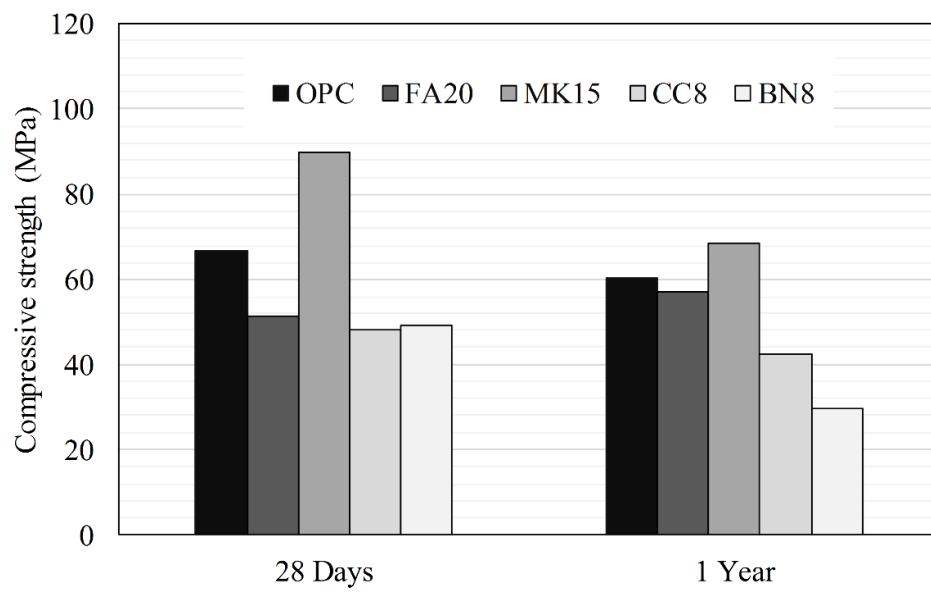
Figure 4.4 Compressive strength of pre-cracked specimens submerged in water.
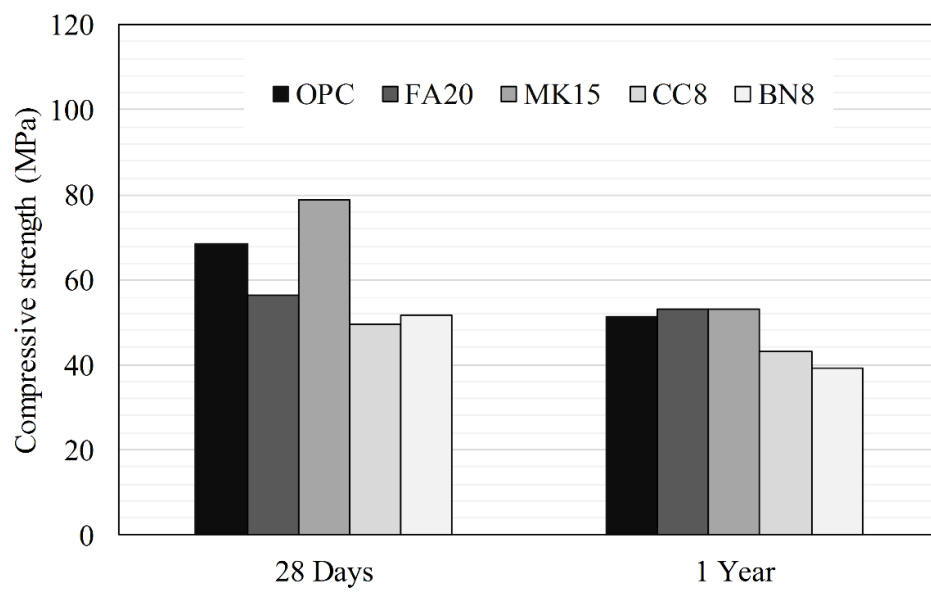
Figure 4.5 Compressive strength of pre-cracked specimens exposed to cyclic T and RH.

Table 4.1: Shear wave velocity evolution of specimens submerged in water

	Normalized SWV				
	Uncracked	Cracked	3 months	6 months	1 year
OPC	1	0.55	0.64	0.77	0.79
FA 20	1	0.59	0.68	0.78	1.12
MK 15	1	0.51	0.64	0.74	0.81
BN 8	1	0.56	0.71	0.72	0.75
CC 8	1	0.53	0.70	0.72	0.77

Table 4.2: Shear wave velocity evolution of specimens exposed to cyclic T and RH

	Normalized SWV				
	Uncracked	Cracked	3 months	6 months	1 year
OPC	1	0.58	0.61	0.64	0.65
F20	1	0.52	0.62	0.66	0.69
MK15	1	0.53	0.59	0.65	0.66
BN8	1	0.58	0.59	0.64	0.65
CC8	1	0.54	0.57	0.59	0.61

On the other hand, bentonite in the BN8 specimens contains montmorillonite, which is a crystalline material that has less contribution to the C-S-H formation, resulting in less strength recovery. Similarly, CC8 specimens did also exhibit low strength recovery. According to Kenai *et al*. (2004) incorporating fine calcium carbonate powder may reduce the long-term compressive strength. This reduction in compressive strength may be explained by the cement hydration dilution effect of fine calcium carbonate powder (Cao *et al*., 2019). Therefore, in the current study, the ability of self-strength recovery was in the order of FA20 > MK15 > OPC > CC8 > BN8.

For specimens exposed to cyclic T and RH (**Table 4.2**), the self-strength recovery was considerably lower than that of specimens exposed to continuous water submersion. This may be attributed to the fact that further hydration of specimens exposed to cyclic T and RH is significantly diminished. For example, previous study by Özbay *et al.* (2013) showed that mechanical recovery of pre-cracked engineered cementitious

materials cured in continuous air was significantly reduced in comparison with identical specimens cured in continuous water. Similar results were also reported by Sisomphon *et al.* (2013) when they investigated strain hardening cementitious composites incorporating calcium-sulfo-aluminate based expansive additive and crystalline additive. Their results also showed that all specimens exposed to ambient air had minimal mechanical recovery in compassion to specimens exposed to damp environments. This suggests that self-strength recovery of a cementitious material primarily depends on the surrounding environment. Therefore, further hydration of cementitious materials, which requires the presence of water, appears to be the main mechanism for mechanical strength recovery in the cement-based materials.

4.3.2 Crack Self-healing and Mechanical Strength Recovery

Figure 4.6 illustrates the crack sealing index of specimens after 400 days of water submersion. The results are plotted in terms of evolution of the crack sealing index over time. It can be observed that surface cracks having different widths exhibited self-healing **(Fig. 4.7)**. Accordingly, the ability of a surface crack to self-heal was in the order of CC8 > FA20 > OPC > BN8 > MK15. On the other hand, cracks in all specimens exposed to cyclic T and RH showed no self-healing. For crack self-healing to occur, water and carbon dioxide need to be present inside the crack. As the cracked specimen starts to release Ca^{2+} ions, calcium carbonate ($CaCO_3$) will precipitate and fill the crack, leading to crack self-healing as per the following reaction:

$$Ca(OH)_2 + CO_2 \rightarrow CaCO_3 + H_2O$$
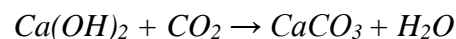
Several studies have reported precipitation or crystallisation of $CaCO_3$ as the main healing mechanism of surface cracks (Zhu *et al*., 2012; Wang *et al*., 2014; Van Tittelboom *et al*., 2012; Sisomphon *et al.*, 2012; Huang *et al*., 2013; Jiang *et al*., 2015; Snoeck *et al*., 2016; Tomczak and Jakubowski. 2018; Wang *et al*., 2018; Zha *et al*., 2018). For instance, Zhu *et al*. (2012) investigated the self-healing of engineered cementitious composites exposed to two different cyclic freeze/thaw regimes. They found that, for both exposures, $CaCO_3$ was formed and sealed the cracks. Tomczak and Jakubowski (2018) studied the self-healing process in high-cement content and low w/c ratio composites. Their results also showed that $CaCO_3$ was the main healing product

formed in surface cracks. Similarly, Wang *et al*. (2014) reported that $CaCO_3$ was the main healing product formed in cracks for concrete with hydrogel encapsulated bacterial spores.
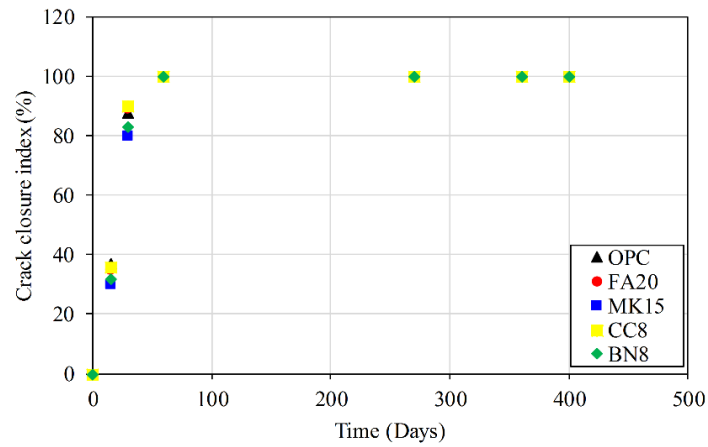
(a)
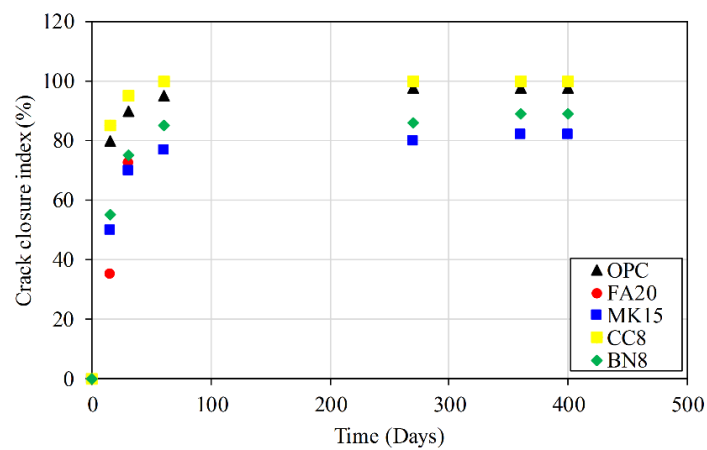
(b)
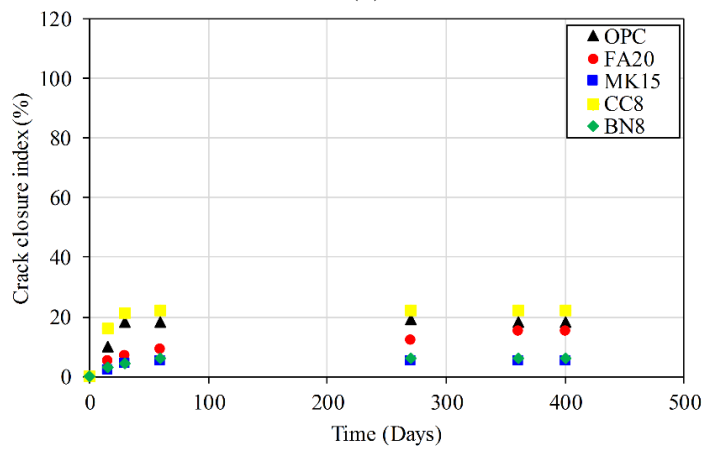
(c)

Figure 4.6 Change in surface crack width of specimens submerged in water with initial crack width (a) 50-150 μm; (b) 150-300 μm; and (c) 300-500 μm.

In the present study, mortar specimens incorporating fine calcium carbonate powder achieved the best self-healing performance in terms of surface crack closing. **Figure 4.8** shows typical SEM images and EDX analyses for healing products formed within surface cracks of CC8 specimens. Elemental EDX analysis revealed that the healing products at crack surfaces were mainly composed of calcium with some carbon and oxygen, indicating that it primarily consists of $CaCO_3$. However, in terms of strength recovery, CC8 specimens did not achieve an appreciable improvement in comparison with FA20 specimens. For the FA20 specimens, SEM images and EDX analysis also showed that the healing products at crack surfaces were mainly composed of calcium with some carbon and oxygen, indicating that it primarily consists of $CaCO_3$ (**Fig. 4.9**). Only small amounts of Si were found at the crack surfaces, suggesting limited formation, if any, of C-S-H as a healing product.

To quantify the change in crack volume owing to self-healing, X-ray computed microtomography was performed. Two datasets representing the condition before and after self-healing were input into a 3D rendering software (Dragonfly 3.5). **Figure 4.10** shows 3D-images of a typical crack profile (in red color) for a FA20 specimen before and after self-healing. For the same specimen, the crack was segmented, and its total volume was measured. Accordingly, the amount of healing product can be quantified by subtracting the volume of crack before and after self-healing. Results show that the healing efficiency was 26.95% for the FA20 specimen. In the previous chapter, the healing efficiency for CC8, OPC, BN8, and MK15 was 32.26%, 27.27%, 25.6%, and 24.1%, respectively. The results indicated that FA20 specimens showed less crack healing than that of both the CC8 and OPC specimens. This finding could suggest that crack self-healing may have little or negligible contribution to mechanical strength recovery of cement-based materials. Previous study by Yang *et al*. (2009) investigated the autogenous healing of engineered cementitious composites under wet-dry cycles. In their study, specimens were subjected to tensile loading after undergoing self-healing. They found that most cracks formed tended to follow the previous crack lines. Similar observation was also reported by Zhu *et al*. (2012). According to Yang *et al*. (2009), the healing products, which are mainly $CaCO_3$ crystals formed in cracks, have weak bonding forces and are relatively weaker than the hydrated cementitious matrix. Therefore, it can be hypothesized that strength recovery

of cementitious materials can be primarily attributed to the ongoing hydration of the un-cracked portion of the matrix.

	Before	*After*
FA20		
MK15		
CC8		
BN8		
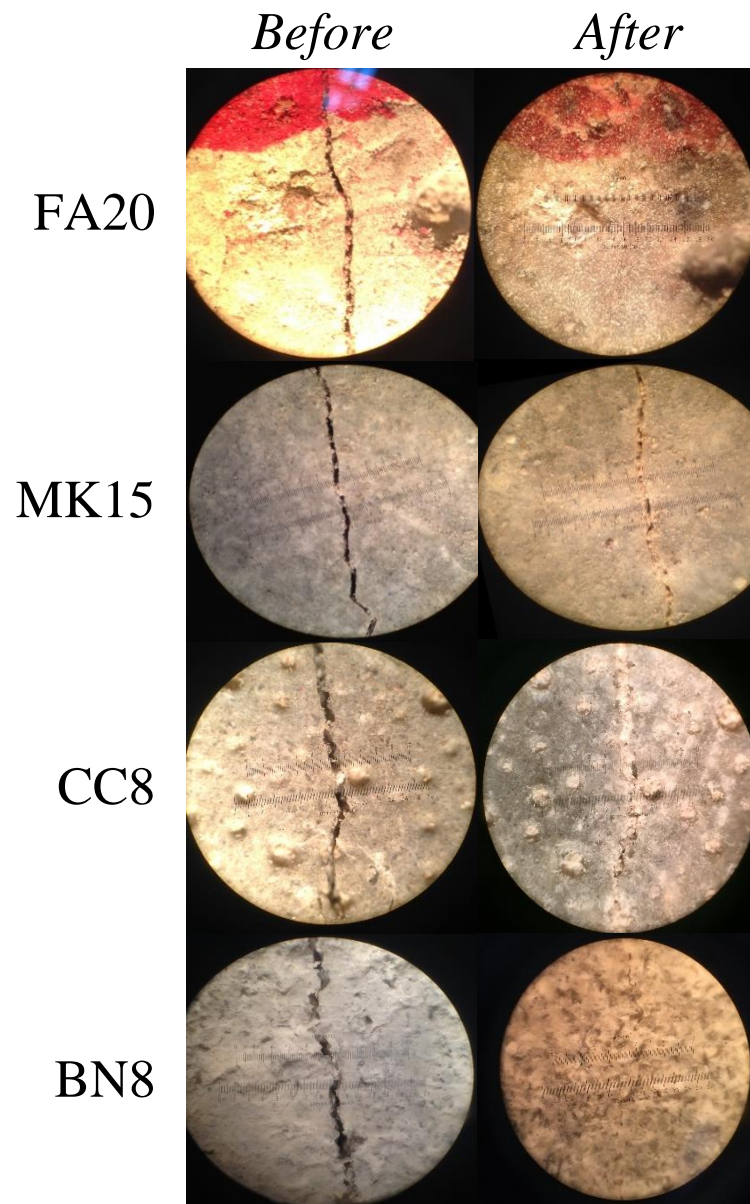
Figure 4.7 Surface cracks before and after water submersion showing self-healing.
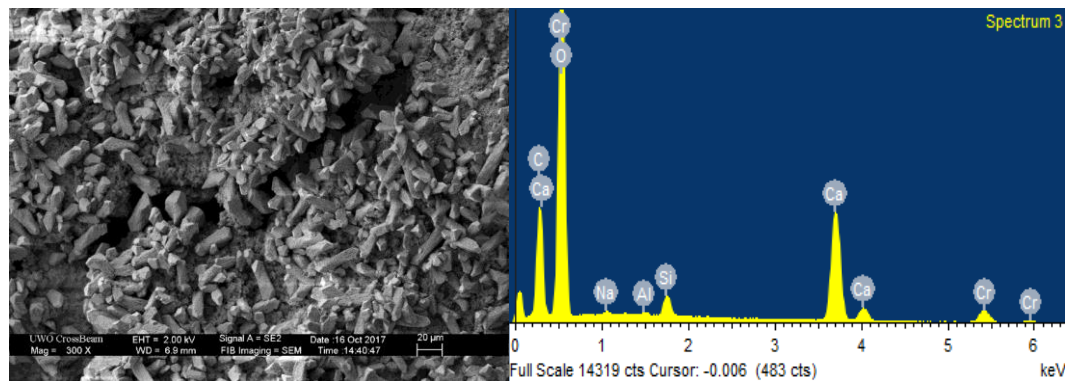
Figure 4.8 SEM micrograph with EDX pattern of products in self-healed cracks of CC8 specimens.
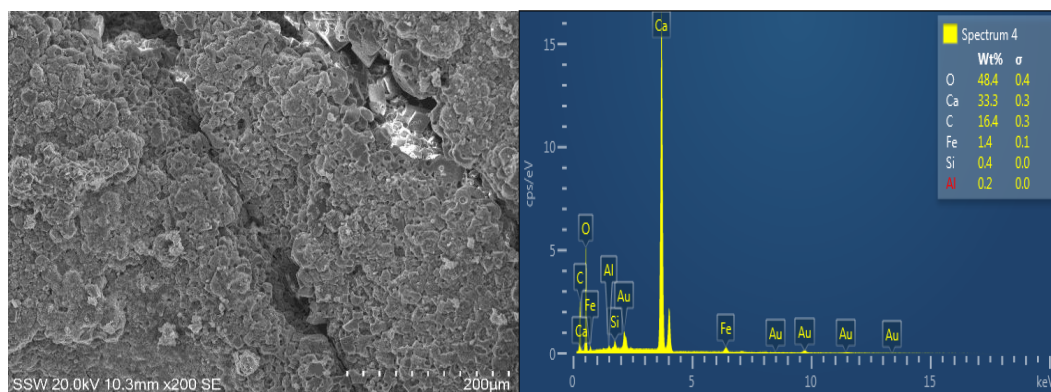
Figure 4.9 SEM micrograph with EDX pattern of products in self-healed cracks of FA20 specimens.

(a)   (b)
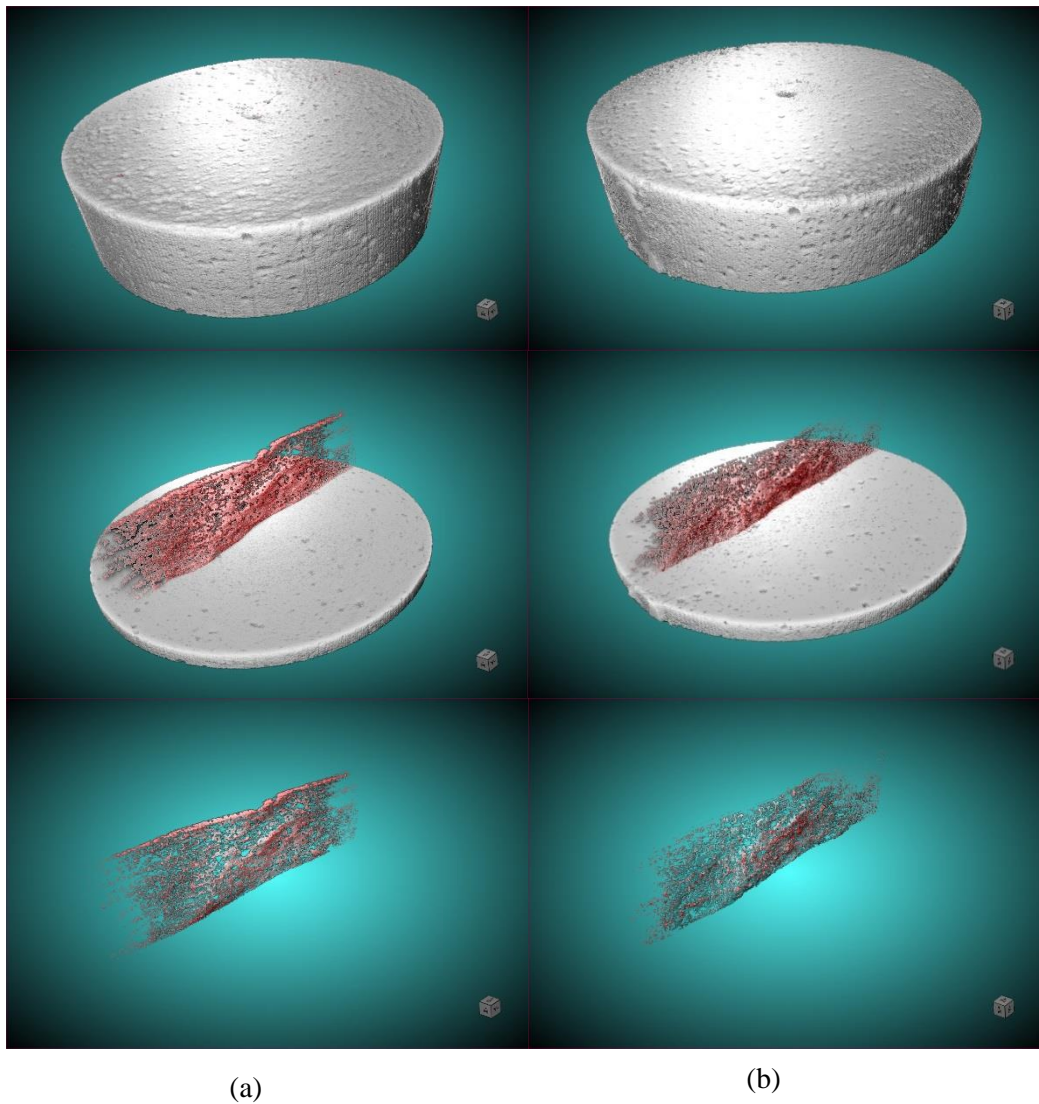
Figure 4.10 X-ray μCT scan images for FA20 specimen submerged in water showing (a) before self-healing, and (b) after self-healing.

4.3.3 Microstructural Densification and Mechanical Strength Recovery

Figure 4.11 displays the cumulative mercury intrusion curves as a function of the pore diameter for cracked mortar specimens exposed to different environments. Results showed that submerged specimens (particularly FA20) exhibited considerable reduction in porosity in comparison to that of specimens exposed to cyclic T and RH. Reduction in porosity occurred primarily due to the presence of capillary liquid water and progress of pozzolanic reactions, which promoted microstructural densification, resulting in mechanical strength enhancement. This may indicate that the strength recovery exhibited by FA20 specimens was primarily achieved by delayed hydration and pozzolanic reactions, rather than by crystallisation or precipitation of $CaCO_3$ in healed cracks. In a previous study, Ferrara *et al*. (2014) investigated the effects of self-healing on the recovery of mechanical properties of normal strength concrete exposed to different environments, with and without crystalline admixtures. They found that the mechanical recovery was attributed to further hydration reactions, rather than to transformation of calcium hydroxide, $Ca(OH)_2$ into calcium carbonate, $CaCO_3$. Sisomphon *et al*. (2013) studied the self-healing potential of strain hardening cementitious composites (SHCC) incorporating various cementitious materials. Their results showed that although formation of $CaCO_3$ is preferable in term of water tightness, it may decrease the recovery of mechanical properties of cementitious materials. According to Qian *et al*. (2010), healing products formed in cracks, including $CaCO_3$ and $Ca(OH)_2$, are typically weaker than C-S-H gel. In addition, even if the main healing product in cracks was C-S-H formed due to rehydration of cement particles, the bond strength between the crack surface and the newly formed C-S-H remains mostly weak in comparison with the tensile strength of the uncracked matrix. In the current study, although FA20 specimens showed slightly less crack volume change due to self-healing compared with the CC8 and OPC specimens, their strength recovery was significantly higher. This could be attributed to the progress of hydration and pozzolanic reactions, which related to strength enhancement of the uncracked matrix, rather than the healing of cracks. Hence, it appears at this stage that surface crack healing via deposition of calcium carbonate and hydrated lime may play a more important role in regaining durability features, such as gas and fluid tightness. However,

its contribution to mechanical strength recovery seems questionable based on the findings of the present study.
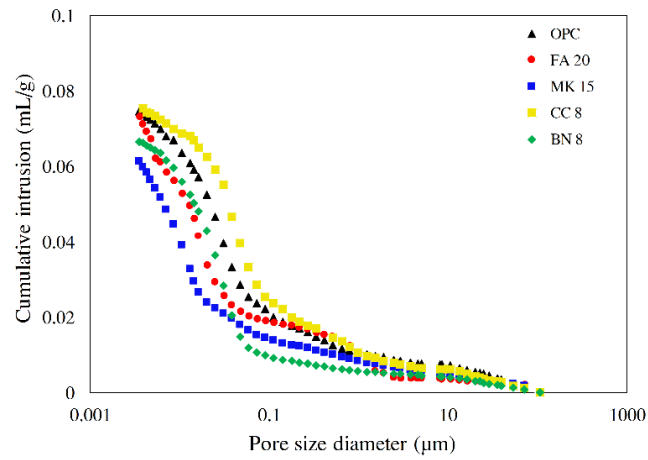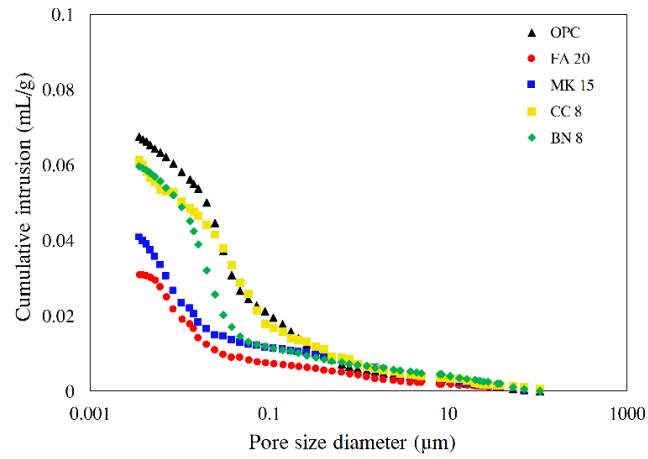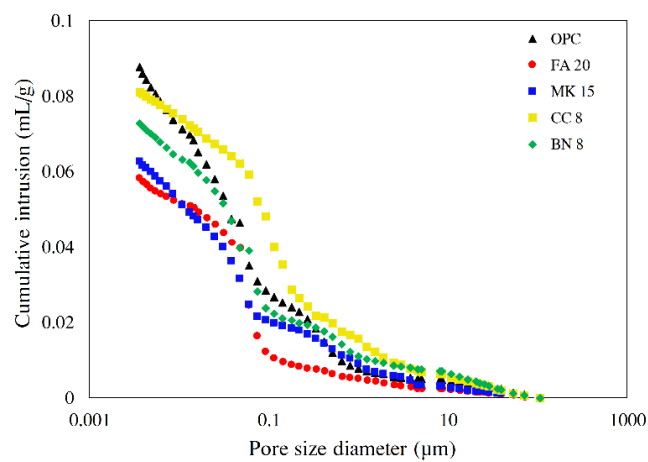
Figure 4.11 Cumulative intruded pore volume vs. pore diameter for cracked specimens (a) at 28 days, (b) one year after water submersion, and (c) one year after cyclic T and RH.

4.4 Conclusions

In this chapter, mechanical strength recovery of pre-cracked cement mortars was investigated using a shear wave velocity technique. In addition, the effects of diverse additions, such as silica-based materials, swelling agents, and carbonating minerals, on mechanical strength recovery under different environmental exposure, were also explored. Based on the experimental findings, the following conclusions can be drawn:

- The exposure condition plays an important role in the strength recovery process of cement based-materials. The water submersion condition achieved best strength recovery, particularly for the specimens incorporating fly ash.

- Further or delayed cement hydration and pozzolanic reactions appear to be the main mechanism for mechanical strength recovery in cement-based materials.

- For all specimens, the main healing product formed on the crack surface was $CaCO_3$.

- Specimens incorporating limestone micro-filler showed the best healing ability in terms of crack filling and closing.

- In terms of mechanical strength recovery, specimens incorporating fly ash showed best performance.

- Based on shear wave velocity measurements, the ability of mechanical strength recovery was in the order of FA20 > MK15 > OPC > CC8 > BN8.

- Based on the computed microtomography and 3-D image analysis, the ability of crack healing was in the order CC8 > OPC > FA20 > BN8 > MK15.

- Further hydration and pozzolanic reactions of the un-cracked cementitious matrix play a major role in mechanical strength recovery of cement-based materials. So long as this mechanism is not quantitatively dissociated from the self-healing effect, reported results of the effect of crack self-healing on mechanical strength recovery seem to be questionable.

4.5   References

A. El Takch, A. Sadrekarimi, and H. El Naggar (2016) "Cyclic resistance and liquefaction behavior of silt and sand silt soils", *Soil Dynamics and Earthquake Engineering*, 83: 98-109.

A. Mneina, A. Ahmed, and H. El Naggar (2018) "Dynamic properties of controlled low-strength materials with treated oil sand waste" *Journal of Materials in Civil Engineering*, 30(9): 10p.

B. Pang, Z. Zhou, P. Hou, P. Du, L. Zhang, and H. Xu (2016) "Autogenous and engineered healing mechanism of carbonated steel slag aggregate in concrete", *Construction and Building Materials*, 107: 191-202.

C.D. Cortez, L. Hermitte, A. Ramain, C. Mesmann, T. Lefort, J.B. Pialat (2016) "Ultrasound shear wave velocity in skeletal muscle: A reproducibility study" *Diagnostic and Interventional Imaging*, 97: 71-79.

C.-M. Aldea, S. P. Shah, and A. Karr (1999) ''Permeability of cracked concrete.'' *Materials and Structures*, 32: 370–376.

D. Gamal El-Dean (2007) "Development of a new piezo-electric pulse testing device and soil characterization using shear waves", *Ph.D. dissertation*, Université de Sherbrooke/Canada.

D. Snoeck and N. De Belie (2015) "From straw in bricks to modern use of microfibers in cementitious composites for improved autogenous healing – A review", *Construction and Building Materials*, 95(1): 774-787.

D. Snoeck, J. Dewanckele, V. Cnudde, and N. De Belie (2016) "X-ray computed microtomography to study autogenous healing of cementitious materials promoted by superabsorbent polymers", *Cement and Concrete Composites*, 65: 83-93.

E. Cuenca, A. Tejedor, L. Ferrara (2018) "A methodology to assess crack-sealing effectiveness of crystalline admixtures under repeated cracking-healing cycles" *Construction and Building Materials*, 179: 619–632

E. Özbay, M. Şahmaran, M. Lachemi, and H. E. Yücel (2013) "Self-Healing of microcracks in high-volume fly-ash-incorporated engineered cementitious composites", *ACI Materials Journal*, 110 (1): 33-43.

H. M. Jonkers, A. Thijssena, G. Muyzerb, O. Copuroglua, E. Schlangena (2010) "Application of bacteria as self-healing agent for the development of sustainable concrete", *Ecological Engineering*, 36(2): 230-235.

H. Huang, G. Ye, and D. Damidot (2013) "Characterization and quantification of self-healing behaviors of microcracks due to further hydration in cement paste", *Cement and Concrete Research*, 52: 71-81.

H. Huang, G. Ye, and D. Damidot (2014) "Effect of blast furnace slag on self-healing of microcracks in cementitious materials", *Cement and Concrete Research*, 60: 68-82.

H. Rajabi and M. Sharifipour (2017) "An Experimental Characterization of Shear Wave Velocity (Vs) in Clean and Hydrocarbon-Contaminated Sand", *Geotech Geol Eng*, 35: 2727-2745.

J. An, J. Nam, S. Kwon, and S. Joh (2009) "Estimation of the Compressive Strength of Concrete Using Shear Wave Velocity", *New Technologies in Construction and Rehabilitation of Portland Cement Concrete Pavement and Bridge Deck Pavement/ GeoHunan International Conference/ ASCE,* 154-164.

J. Kempl and O. Çopuroğlu (2016) "EH-pH- and main element analyses of blast furnace slag cement paste pore solutions activated with sodium monofluorophosphate - Implications for carbonation and self-healing", *Cement and Concrete Composites*, 71: 63-76.

J. L'Heureux and M. Long (2017) "Relationship between Shear-Wave Velocity and Geotechnical Parameters for Norwegian Clays", *J. Geotech. Geoenviron. Eng*, 143(6): 20p.

J. Wang, J. Dewanckele, V. Cnudde, S. Van Vlierberghe, W. Verstraete, N. De Belie (2014) "X-ray computed tomography proof of bacterial-based self-healing in concrete" *Cement and Concrete Composites*, 53: 289-304.

J. Zhu, S. Kee, D. Han, and Y. Tsai (2011) "Effects of air voids on ultrasonic wave propagation in early age cement pastes", *Cement and Concrete Research*, 41: 872-881.

K. Sisomphon, O. Copuroglu, and E.A.B. Koenders (2012) "Self-healing of surface cracks in mortars with expansive additive and crystalline additive", *Cement and Concrete Composites*, 34(4): 566-574.

K. Sisomphon, O. Copuroglu, and E.A.B. Koenders (2013) "Effect of exposure conditions on self healing behavior of strain hardening cementitious composites incorporating various cementitious materials", *Construction and Building Materials*, 42(4): 2017-224.

K. Tomczak and J. Jakubowski (2018) "The effects of age, cement content, and healing time on the self-healing ability of high-strength concrete" *Construction and Building Materials*, 187:149-159.

K. Van Tittelboom, E. Gruyaert, H. Rahier, and N. De Belie (2012) "Influence of mix composition on the extent of autogenous crack healing by continued hydration or calcium carbonate formation", *Construction and Building Materials*, 37: 349-359.

K. Van Tittelboom and N. De Belie (2013) "Self-healing in cementitious materials - A review". *Materials*, 6: 2182-2217

K. Wang, D. C. Jansen, and S. P. Shah (1997) "Permeability study of cracked concrete", *Cement and Concrete Research*, 27 (3): 381-393.

L. Basheer, J. Kropp, and D. J. Clelandc (2001) ''Assessment of the durability of concrete from its permeation and properties: a review'', *Construction and Building Materials*, 15(1): 93-103.

L. Ferrara, V. Krelani, and M. Carsana (2014) "A ''fracture testing'' based approach to assess crack healing of concrete with and without crystalline admixtures", *Construction and Building Materials*, 68(15): 535-551.

M. Cao, X. Ming, K. He, L. Li, and S. Shen (2019) "Effect of Macro-, Micro- and Nano-Calcium Carbonate on Properties of Cementitious Composites—A Review" *Materials*, 12,781: 20p.

M. Karray, M. B. Romdhan, M. N. Hussien, and Y. Éthier (2015) "Measuring shear wave velocity of granular material using the piezoelectric ring-actuator technique (P-RAT)", *Can. Geotech. J.*, 52: 1302-1317.

M. Şahmaran, S. B. Keskin, G. Ozerkan, and I. O. Yaman (2008) "Self-healing of mechanically-loaded self consolidating concrete with high volumes of fly ash", *Cement and Concrete Composites*, 30 (10): 872-879.

M. Sahmaran, G Yildirim and T. K. Erdem (2013) "Self-healing capability of cementitious composites incorporating different supplementary cementitious materials" *Cement and Concrete Composites*, 35: 89-101.

M. Wu, B. Johannesson, and M. Geiker (2012) "A review: Self-healing in cementitious materials and engineered cementitious composite as a self-healing material", *Construction and Building Materials*, 28: 571-583.

N.A. Soliman, K.H. Khayat, M. Karray, and A.F. Omran (2015) "Effects of air voids on ultrasonic wave propagation in early age cement pastes", *Cement and Concrete Composites*, 63: 84-95.

P. Termkhajornkit, T. Nawab, Y. Yamashiro, and T. Saito (2009) "Self-healing ability of fly ash–cement systems", *Cement and Concrete Composites*, 31(3): 195-203.

R. Birgül (2009) "Hilbert transformation of waveforms to determine shear wave velocity in concrete", *Cement and Concrete Research*, 39: 696-700.

R. Borg, E. Cuenca, E. Brac and L. Ferrara (2018) "Crack sealing capacity in chloride-rich environments of mortars containing different cement substitutes and

crystalline admixtures", *Journal of Sustainable Cement-Based Materials*, 7(3): 141-159.

R. Gagné and M. Argouges (2012) "A study of the natural self-healing of mortars using air-flow measurements", *Materials and Structures*, 45: 1625-1638.

S. Naji, K. H. Khayat, and M. Karray (2017) "Assessment of Static Stability of Concrete Using Shear Wave Velocity Approach", *ACI Materials Journal*, 114(1): 105-115.

S. Ahmed (2016) "Piezoelectric device for measuring shear wave velocity of soils and evaluation of low and high strain shear modulus", *Ph.D. dissertation*, Western University/Canada.

S. Liu, J. Zhu, S. Seraj, R. Cano, and M. Juenger (2014) "Monitoring setting and hardening process of mortar and concrete using ultrasonic shear waves" *Construction and Building Materials*, 72: 248-255.

S. Kenai, W. Soboyejo, and A. Soboyejo (2004) "Some engineering properties of limestone concrete" *Materials and Manufacturing Processes*, 19(5): 949-961.

S. Mehta and P. Antich (1997) "Measurement of Shear-Wave Velocity by Ultrasound Critical-Angle Reflectometry (UCR)", *Ultrasound in Med. & Biol*, 23(7): 1123-1126.

S.Z. Qian, J. Zhou, and E. Schlangen (2010) "Influence of curing condition and precracking time on the self-healing behavior of Engineered Cementitious Composites" *Cement and Concrete Composites*, 32: 686-693.

V. Wiktor and H. M. Jonkers (2011) "Quantification of crack-healing in novel bacteria-based self-healing concrete", *Cement and Concrete Composites*, 33(7): 763-770.

W. Tang, O. Kardani, and H. Cui (2015) "Robust evaluation of self-healing efficiency in cementitious materials – A review*", Construction and Building Materials*, 81(15): 233-247.

W. Li, Z. Jiang, and Z. Yang (2017) "Acoustic characterization of damage and healing of microencapsulation-based self-healing cement matrices*", Cement and Concrete Composites*, 84(15): 48-61.

X. Liu, J. Yang, G. Wang, and L.Chen (2016) "Small strain shear modulus of volcanic granular soil: An experimental investigation", *Soil Dynamics and Earthquake Engineering*, 86: 15-24.

X. Wang, C. Fang, D. Li, N. Han, and F. Xing (2018) "A self-healing cementitious composite with mineral admixtures and built-in carbonate" *Cement and Concrete Composites*, 92: 216-229.

Y. Yang, M. D. Lepech, E. Yang, and V.C. Li (2009) "Autogenous healing of engineered cementitious composites under wet–dry cycles" *Cement and Concrete Research*, 39(5): 382-390.

Y. Zha, J. Yu, R. Wang, P. He, and Z. Cao (2018) "Effect of ion chelating agent on self-healing performance of Cement-based materials" *Construction and Building Materials*, 190: 308-316.

Y. Zhu, Y. Yang, and Y. Yao (2012) "Autogenous self-healing of engineered cementitious composites under freeze–thaw cycles" *Construction and Building Materials*, 34:522-530.

Z. Cao, L. Shen, L. Liu, S. Zhong (2016) "Analysis on major drivers of cement consumption during the urbanization process in China" *Journal of Cleaner Production*, 133: 304-313.

Z. Jiang, W. Li and Z. Yuan (2015) "Influence of mineral additives and environmental conditions on the self-healing capabilities of cementitious materials", *Cement and Concrete Composites*, 57: 116-127.

Self-healing Behaviour of Cementitious Materials Incorporating Superabsorbent Polymers Under Simulated Field Conditions

5.1 Introduction

Some previous studies investigated the efficacy of self-healing concrete under different environments. For instance, Roig-Flores *et al*. (2015) studied the self-healing behaviour of concrete with crystalline admixtures exposed to different environments. They reported that self-healing of concrete incorporating crystalline admixtures exhibited different healing behaviour depending on the exposure environment. For instance, negligible self-healing was found in all specimens exposed to constant T and RH, demonstrating that the presence of liquid water is essentially for self-healing to occur. Similarly, Özbay *et al*. (2013) reported that no crack healing occurred for engineered cementitious composites (ECC) exposed to continuous air in comparison to similar specimens exposed to either continuous submersion in water or cyclic wetting and drying. Another study by Wang *et al*. (2014) found that no crack healing occurred in a bacteria-based concrete when stored at 60 % RH and 95% RH. In addition, due to the additional drying shrinkage, the final crack widths for the specimens stored at 60% were even larger than the initial widths. According to Wang *et al*. (2014), lack of water supply to the cracked specimens in both conditions was the main reason for the non-self-healing behaviour. Therefore, in this chapter, the potential of superabsorbent polymers to promote crack self-healing of cement based-materials under simulated field conditions including cold and hot temperatures, high and low humidity, wet and dry cycles, and continuous underwater environments was investigated. The results should provide qualitative and quantitative bases for the assessment of self-healing capacity of cement-based materials under simulated field conditions.

5.2   Experimental Procedures

5.2.1 Materials and Specimen Preparation

Mortar specimens were made with ordinary portland cement (OPC) compliant with requirements of CSA A3001 and ASTM C150. The mixture design of mortars is reported in **Table 5.1**. A varying dosage of superabsorbent polymers (SAPs) expressed as mass percentage of cement weight, as shown in the **Table 5.1,** were used. Physical and chemical properties of the SAPs are summarized in **Table 5.2**. PVA fiber at a dosage of 1% by volume fraction was added to the mortar mixtures. To ensure a homogeneous distribution of the SAPs in the mixture, cement, PVA, and SAPs were first dry mixed for about 1 min. The sand was then added, and dry mixing continued for another 1 min. Subsequently, water was added and a polycarboxylate-based high-range water reducing admixture (HRWRA) as per ASTM C494 was used to adjust workability. The mortar was mixed in a Hobart mixer for 2 min. Cylinder specimens (50 mm diameter and 25 mm height) were cast in order to determine the compressive and splitting tensile strength of the mortars. Disk specimens (50 mm diameter and 25 mm height) were prepared for acquiring high resolution X-ray μCT images.   All specimens were cured for 28-d in a moist room at RH ≥ 95% and T = 21 ± 1°C as per ASTM C511 (Standard Specification for Mixing Rooms, Moist Cabinets, Moist Rooms, and Water Storage Tanks Used in the Testing of Hydraulic Cements and Concretes).

Table 5.1: Proportions of tested mortar mixtures

Mix	*Description*	*OPC*	*SAP*	*Sand*	*Water*
1	0% SAP	100	-	200	35
2	0.5 SAP	99.50	0.5	200	35
3	1% SAP	99	1	200	35
4	2% SAP	98	2	200	35

Table 5.2: Properties of SAP used

Characteristics	*SAP*
Particle size distribution (μ)	1-140
Absorption deionized water (g/g)	> 180
Absorption 0.9% NaCl (g/g)	50
Apparent bulk density (g/l)	≃ 540
pH value	6 - 7

5.2.2 Inducing Crack

Crack was created at the age of 28 days using a screw jack similar to the procedure reported in **Chapter 3**.

5.2.3 Environmental Exposure

Cracked specimens were divided into three groups. Specimens of the first group were fully submerged in deionized water at a constant temperature of T = 19°C. Barnstead™ Easypure™ RoDi water purification system model was used. The second group of specimens was placed inside a walk-in environmental chamber and exposed to cyclic temperature ranging from 10°C to 40°C and relative humidity in the range of 20% to 90%. Specimens of the third group were exposed to cyclic wetting and drying at 20 ± 2°C (stored in deionized water for 4 days, and then dried in the lab for 4 days).

5.3 Results and Discussion

Previous studies used superabsorbent polymers (SAPs) as an admixture in cementitious materials to mitigate cracking due to shrinkage by providing internal curing (Jensen and Hansen, 2001 & 2002; Wang *et al*., 2009; Soliman and Nehdi, 2013; Dang *et al*., 2017). For instance, Jensen and Hansen (2002) reported that autogenous shrinkage after setting, as well as cracking due to restraining hardening in high-performance concrete, can be avoided when SAPs are used as a water entraining admixture. Similar findings were also reported by Wang *et al*. (2009) and Soliman and Nehdi (2013). Superabsorbent polymers are cross-linked polyacrylates and copolymerized that can absorb significant amount of liquid from the surrounding environment (more than 100 times of their weight) and then retain the liquid within their structure without dissolving (Jensen and Hansen, 2001). Therefore, in the current study, the effects of using SAPs

on the self-healing behaviour of cement-based materials under different environmental exposure was investigated.

5.3.1 Compressive and Tensile Strength

Figure 5.1 shows the compressive and tensile strength of the mortar specimens after 28 days. It can be observed that 0.5% SAP specimens exhibited an increase in compressive and tensile strength. This increase can be explained by the fact that SAP particles absorb some mixing water, leading to lower w/c ratio, which results in densification of the cementitious matrix. However, by increasing the amount of SAP particles in the cementitious matrix, both compressive and tensile strength decreased. The reduction in compressive and tensile strength can be attributed to the formation of macro-pores when SAP particles release the absorbed water at later stage and shrink.

5.3.2 MIP and Pore Structure

Figure 5.2 (a) displays the cumulative mercury intrusion curves as a function of the pore diameter for cracked mortar specimens at age of 28 days (before self-healing). Results show that 0.5% SAP specimens exhibited a decrease in porosity compared to the 0% SAP specimens since SAP particles absorb some mixing water, which reduces the w/c ratio and results in lower porosity. Similar findings were reported by Mönnig (2005) who found that the total measured pore volume in specimens incorporating SAPs was smaller than that in specimens without SAPs. Snoeck *et al.,* (2015-b) reported that cement pastes with SAPs and without additional water had a decrease in porosity compared to reference specimens with the same total water-to-cement-ratio.

On the other hand, MIP results showed that the total porosity of cement mortars with SAPs increased as the SAPs content increased beyond 0.5%. During hardening, SAP particles release the absorbed water and shrink, leaving behind in the cementitious matrix voids having hundreds of microns in size (Snoeck *et al.*, 2015-b); Lee *et al.*, 2016). For example, previous study by Snoeck *et al.* (2014) investigated the effect of high amounts of SAPs on the properties of cementitious materials. Their results showed that increasing the amount of SAP particles in cement mortars resulted in increasing the total amount of pores. This effect was more pronounced with smaller SAP particles, due to their higher surface area available to combine mixing water (Snoeck *et al.*, 2014).

(a)

(b)
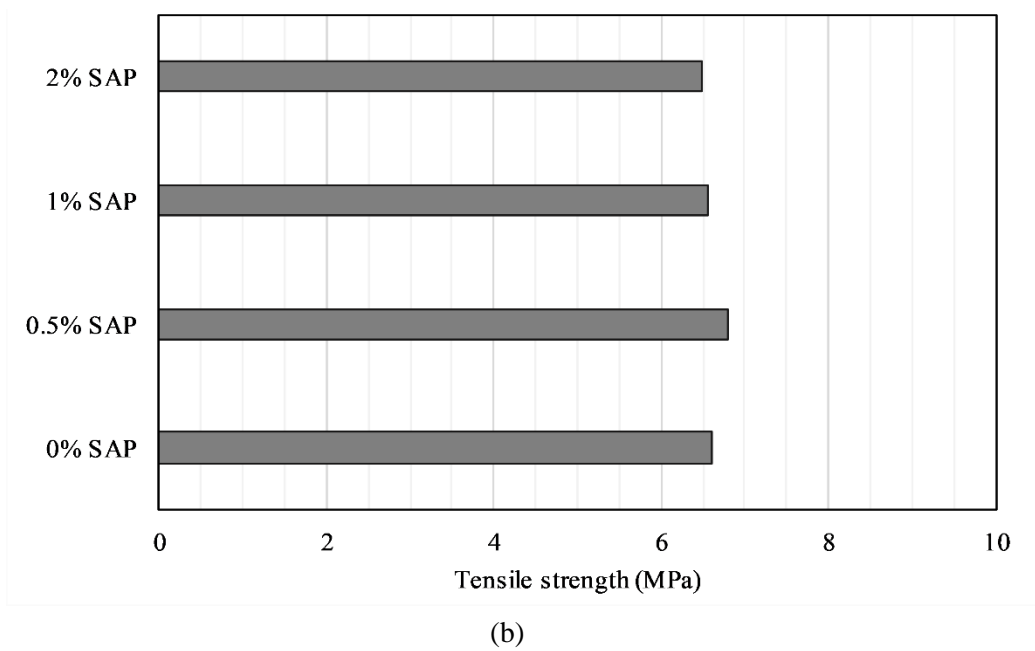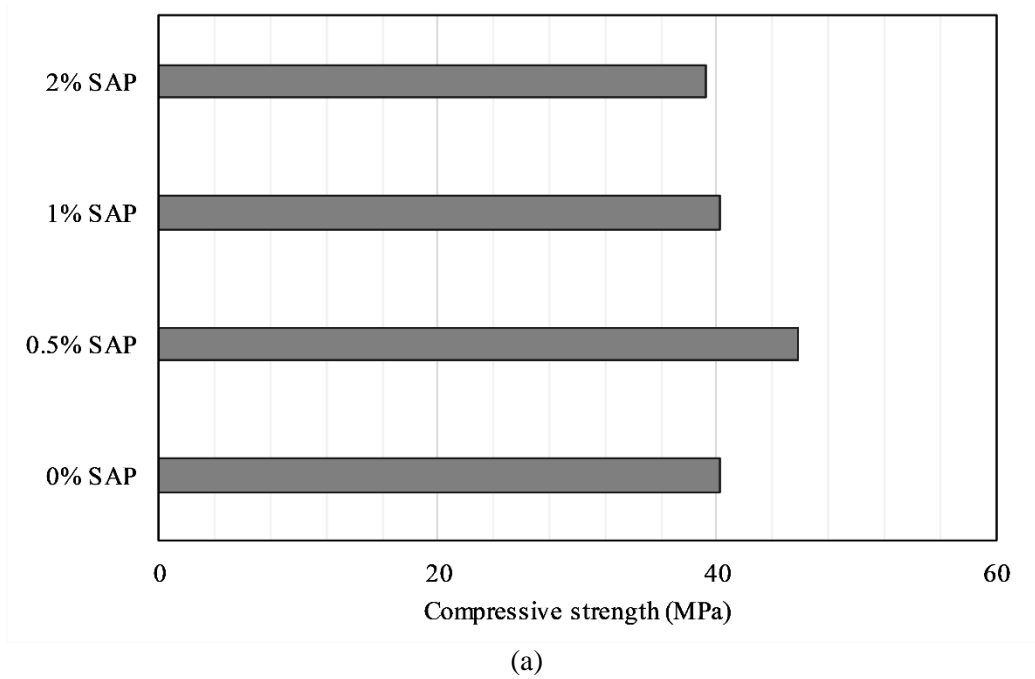
Figure 5.1 (a) Compressive, and (b) tensile strength of specimens (with and without SAPs) after 28 days.

(a)

(b)
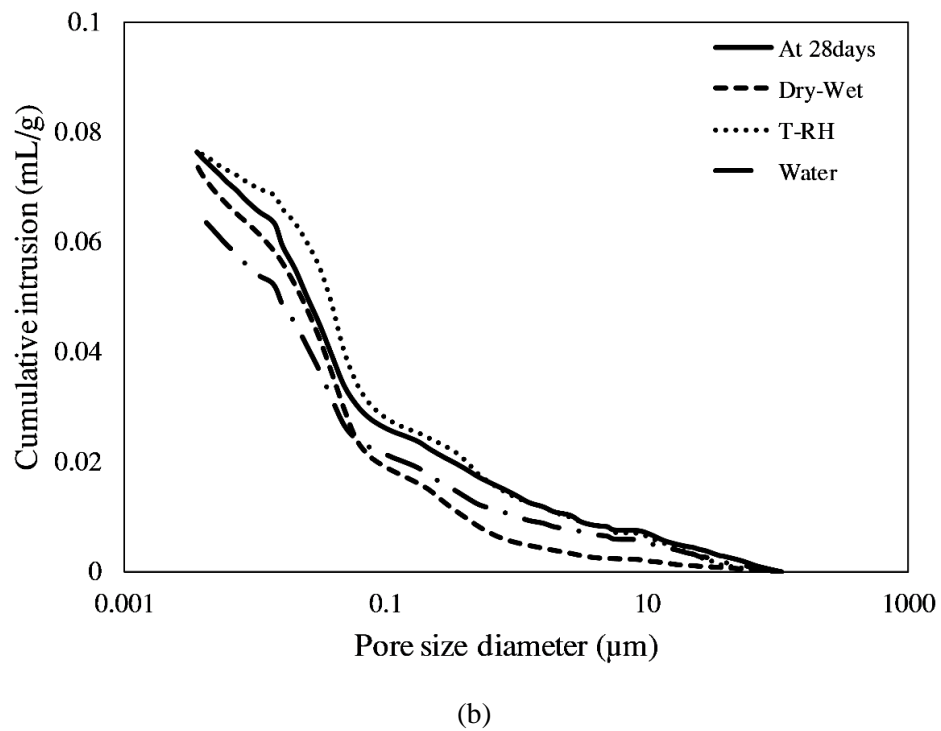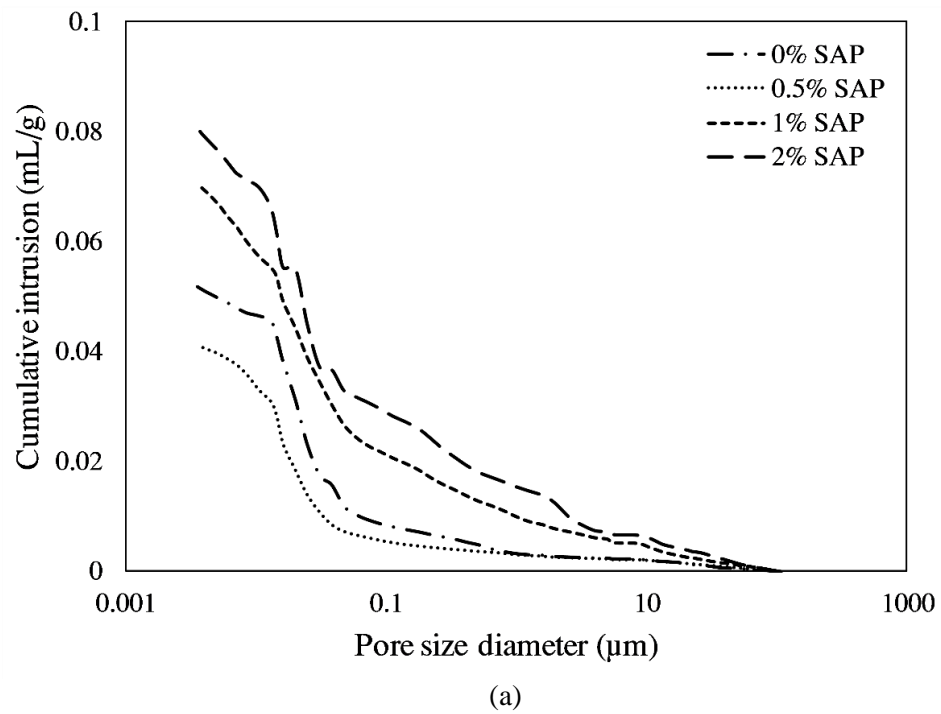
Figure 5.2 Cumulative intruded pore volume vs. pore diameter for cracked specimens (a) at 28 days, and (b) specimens with 1% SAP after five months of exposure to different environments.

Figure 5.2 (b) displays the cumulative mercury intrusion curves as a function of the pore diameter for cracked mortar specimens with 1% SAPs and exposed to different environments. Results show that submerged specimens and specimens exposed to cyclic wetting and drying achieved reduction in porosity in comparison to that of specimens exposed to cyclic T and RH. Reduction in porosity occurred primarily due to the presence of capillary liquid water, which promoted microstructural densification. Specimens exposed to cyclic T and RH had slight increase in porosity, which may be related to the formation of microcracks resulting from the cyclic exposure to different T and RH.

5.3.3 Surface Crack Healing

5.3.3.1 Underwater submersion

Surface cracks of mortar specimens prior to and after the self-healing process were monitored using optical microscopy at (40-1000×) magnification. At the beginning of the experiment, for specimens incorporating SAPs and submerged in water (4 days of water submersion), surface cracks achieved rapid self-sealing. This is likely because SAP particles absorb water and swell to form a transplant gel that fills a significant portion of the surface crack (**Fig. 5.3**). The maximum width of cracks filled with a transplant gel was 385 ± 20 µm for specimens incorporating 2% SAPs. However, specimens with 0% SAPs did not exhibit any rapid self-sealing. A similar finding was reported by others. For instance, Snoeck *et al.* (2012) studied the water penetration in cementitious materials with superabsorbent polymers by means of neutron radiography. Their results showed that capillary absorption in and water permeability through cracks are significantly reduced in specimens containing SAPs particles. Lee *et al*, (2016) showed that the ingress of water into cracks causes SAP particles to swell and expand into the crack, thereby limiting the further flow of water. However, they found that when the specimens were dried at room temperature for 24 hrs, the swollen SAPs shrunk, thus allowing the crack to be visible again. In the current study, in order to determine the permanent crack healing at the end of each exposure, all specimens were dried at room temperature for 3 days. **Figure 5.4** shows the surface crack healing of specimens after five months of water submersion.
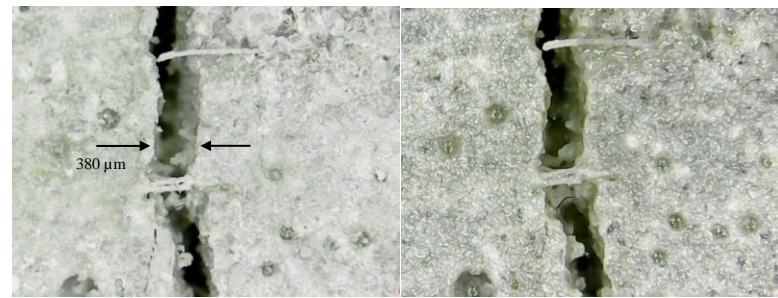
(a)
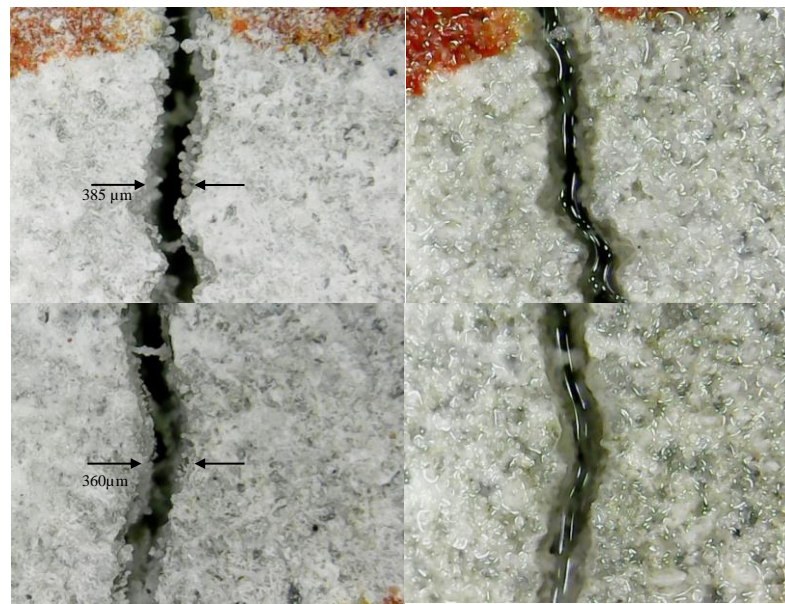
(b)

Figure 5.3 Surface cracks after 4 days of water submersion for (a) specimen without SAPs, and (b) specimens with SAPs.

For specimens (with and without SAPs) fully submerged in water, surface cracks having different widths were filled with self-healing products. It was found that the healing products, which mainly formed in the cracks, were white crystals. After five months of water submersion, only the first group of specimens with initial crack widths of 50 – 150 µm (with and without SAPs) exhibited complete surface crack healing. For the second group of specimens having initial crack widths of 150 – 300 µm, surface cracks were only able to heal partly. The maximum crack width healed for specimens submerged in deionized water over the five months test period was about 275 ± 15 µm,

260 ± 10 µm, 255 ± 10 µm, and 235 ± 5 µm for the 0% SAP, 0.5% SAP, 1% SAP, and 2% SAP specimens, respectively.
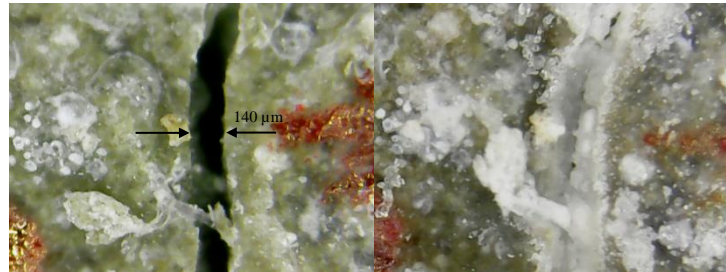
(a)
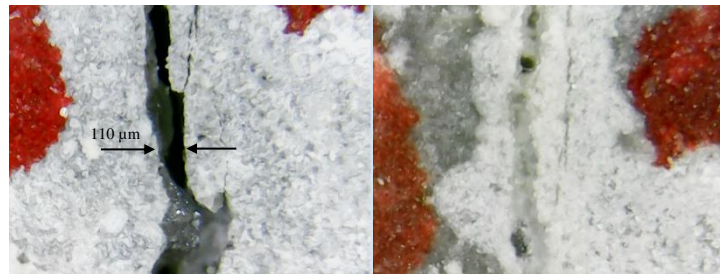
(b)
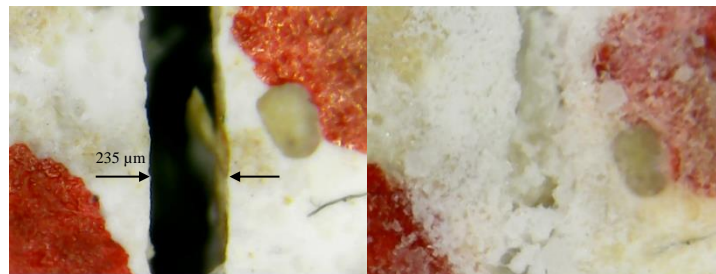
(c)
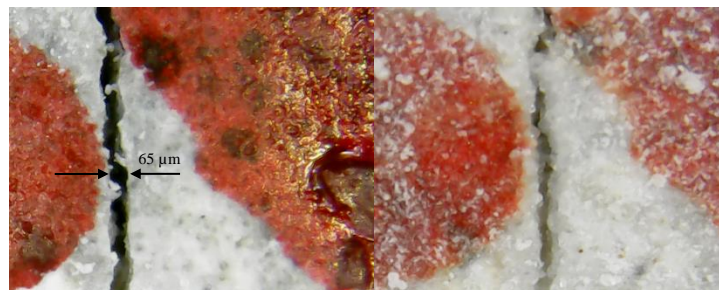
(d)

Figure 5.4 Surface cracks before and after water submersion of specimens (a) 0% SAP; (b) 0.5% SAP; (c) 1% SAP; and (d) 2% SAP.

For the third group of specimens having initial crack widths of 300 – 500 µm, surface cracks showed no or very minor self-healing. Similar results were reported by others who found that the maximum surface crack width healed due to autogenous or improved autogenous self-healing (using crystalline, expansive, or other supplementary cementitious materials) was less than 400 µm for specimens submerged in water (Van Tittelboom *et al*., 2012; Roig-Flores *et al*., 2015; Sahmaran *et al*., 2013; Sisomphon *et al*., 2012; Jiang *et al*., 2015). According to Van Tittelboom *et al*. (2012), as the crack width increased, crack self-healing became more difficult. This indicates that crack self-healing is inversely proportional to the crack width. In the current study, at the beginning of the experiment, although only the specimens incorporating SAPs exhibited rapid self-sealing, after five months of water submersion, the permeant surface crack healing for specimens (with and without SAPs) submerged in water was comparable. **Figure 5.5** shows typical SEM images and EDX analyses for healing products formed within surface cracks for specimens submerged in water. SEM was used to observe the surface morphologies of the healing products, and EDX was used for elemental analysis. It can be observed that the self-healing products had multiple-shaped and irregular crystals. EDX analysis at different locations showed that the healing products at crack surfaces in all specimens were mainly composed of three elements, namely calcium, carbon and oxygen, indicating that it primarily consists of $CaCO_3$.
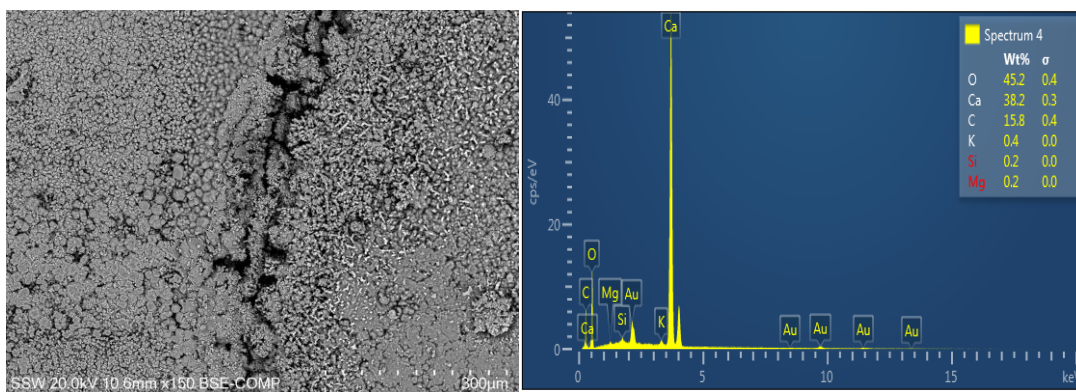
Figure 5.5 SEM micrograph with EDX pattern of products in self-healed cracks of specimens with 1% SAP after water submersion.

5.3.3.2 Cyclic Wetting and Drying

Figure 5.6 shows the surface crack healing of specimens after five months of exposure to cyclic wetting and drying.
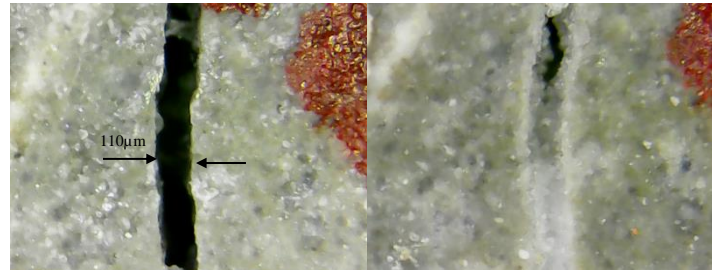
(a)
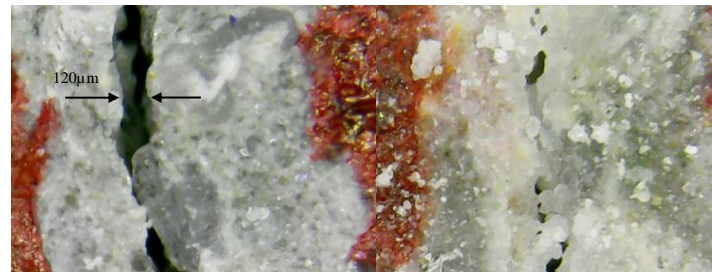
(b)
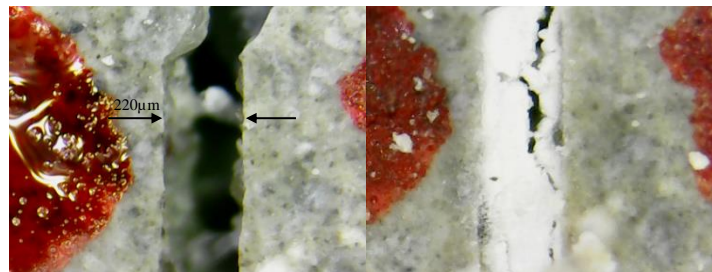
(c)
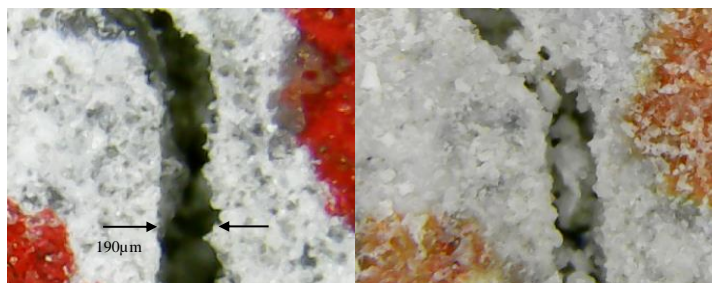
(d)

Figure 5.6 Surface cracks before and after exposure to cyclic wetting and drying of specimens (a) 0% SAP; (b) 0.5% SAP; (c) 1% SAP; and (d) 2% SAP.

Results show that 2% SAP specimens exhibited best healing potential where surface cracks of up to about 220 ± 10 µm in width were completely sealed. In comparison, 0% SAP specimens showed the least self-healing in terms of crack closing. The maximum crack width healed in 0% SAP specimens was 180 ± 10 µm. For 1% SAP and 0.5% SAP specimens, the maximum crack width healed was 205 ± 5 µm and 190 ± 10 µm, respectively. Hence, the ability of crack healing was in the order of 2% SAP > 1% SAP > 0.5% SAP > 0% SAP. These results can be explained by the fact that SAP particles were able to provide water during the dry periods of the wet-dry cycle, therefore increasing the possibility of crack self-healing. Previous study by Snoeck *et al*., (2015-a) investigated the autogenous healing in strain-hardening cementitious composites by using superabsorbent polymers. Their results showed that crack healing was improved by adding SAPs in specimens exposed to wet/dry cycles. Therefore, SAPs can promote crack healing in cement-based materials exposed to cyclic wetting and drying. SEM and EDX analyses also showed that the healing products formed within surface cracks for specimens exposed to wet/dry cycles were mainly $CaCO_3$ (**Fig. 5.7**). This finding agrees with previous studies (Snoeck *et al*., 2014, 2015-b and 2016). Therefore, $CaCO_3$ appears to be the main "permanent" healing product filling cracks in cement-based materials incorporating SAPs and exposed to cyclic wetting and drying.
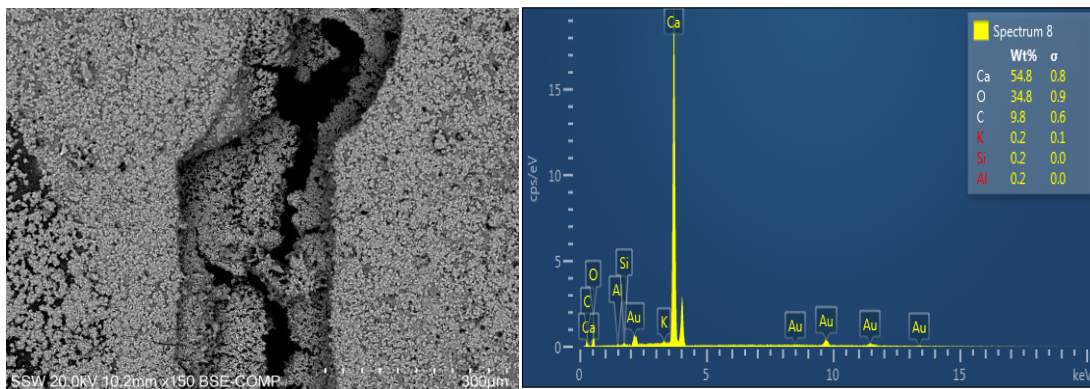
Figure 5.7 SEM micrograph with EDX pattern of products in self-healed cracks of specimens with 1% SAP after cyclic wetting and drying.

5.3.3.3 Cyclic T and RH

Figure 5.8 shows the surface crack healing of specimens after five months of exposure to cyclic T and RH.
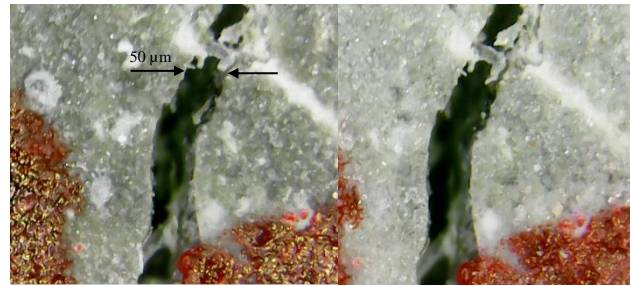
(a)
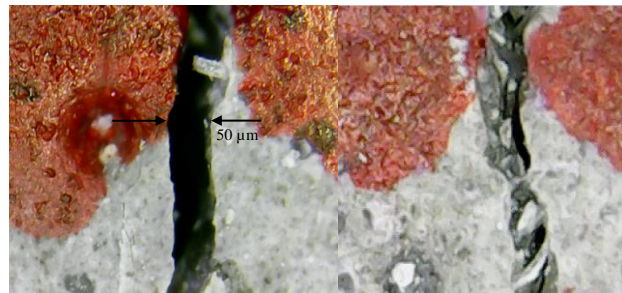
(b)
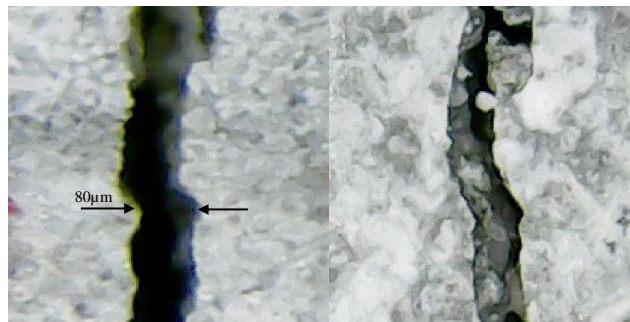
(c)
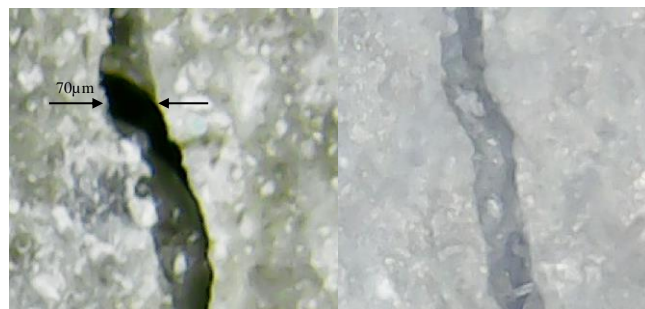
(d)

Figure 5.8 Surface cracks before and after exposure to cyclic T and RH of specimens (a) 0% SAP; (b) 0.5% SAP; (c) 1% SAP; and (d) 2% SAP.

It can be observed that only specimens with SAPs exhibited partial healing. For example, specimens with 2% SAP showed crack closing for up to about 65 ± 10 µm. In comparison, 0% SAP specimens achieved no self-healing in terms of crack closing. For 1% and 0.5% SAP specimens, the maximum crack width healed was 50 ± 10 µm and 20 ± 10 µm, respectively. Therefore, the ability of crack healing was in the order of 2% SAP > 1% SAP > 0.5% SAP > 0% SAP.

Results of EDX analyses **(Fig. 5.9)** reveal that the healing products within the crack were mainly composed of calcium with some carbon and oxygen, indicating that it consists primarily of $CaCO_3$. Apparently, SAP particles were able to absorb moisture and stimulate autogenous healing, even without being in direct contact with water. Due to the drop in relative humidity, swelled SAP particles can release water into the cementitious matrix. Thus, SAPs provide moisture to activate the autogenous self-healing in dry environments (Snoeck *et al*., 2018).
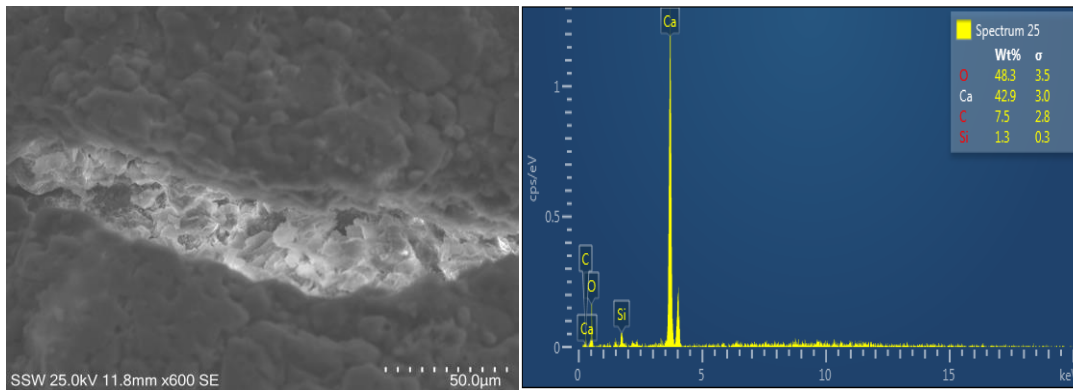
Figure 5.9 SEM micrograph with EDX pattern of products in self-healed cracks of specimens with 1% SAP after exposure to cyclic T and RH.

5.3.4 Crack Quantification Using X-ray Computed Tomography

Figure 5.10 shows 3D-images of the crack profile before and after self-healing. In the present study, 1% SAP specimens with crack width in the range of 150 to 300 µm and exposed to different environmental conditions were selected for X-ray µCT analysis. The selected specimens were scanned before and after self-healing. Two datasets representing the condition before and after self-healing were input into a 3D rendering software (Dragonfly 3.5). **Table 5.3** shows the results of segmentation and quantification analysis of cracks before and after self-healing. For the same specimen, the crack was segmented, and its total volume was measured. Accordingly, the amount of healing product can be quantified by subtracting the volume of crack before and after self-healing. Results show that the healing efficiency was 26.32%, 19.11%, and 6.58% for specimens with 1% SAP exposed to water submersion, cyclic wetting and drying, and cyclic temperature and relative humidity, respectively.

Images from X-ray µCT scans showed most of the healing product is formed at the surface region of the specimens exposed to different environments. On the other hand, at the interior region of the crack, the healing amount was significantly less. Previous study by Wang *et al*. (2014) investigated the self-healing behaviour of concrete specimens incorporating bio-hydrogels (hydrogel encapsulated bacterial spores). Their results showed that complete self-healing was mainly restricted to surface cracks. Similar findings were also reported in other studies (Snoeck *et al*., 2016; Fan and Li, 2014). One possible reason for this phenomenon is that the fast formation of $CaCO_3$ at the surface cracks blocks the water and carbon dioxide from reaching deeper inside the specimen, leading to less healing potential for the interior part of the crack.

Table 5.3: Quantification of cracks before and after self-healing

Environmental exposure	Crack volume (μm^3)		Healing Efficiency (%)
	Before	*After*	
Water submersion	130866367236.4	96420248883.3	26.32
Cyclic W/D	189164338087.4	153014223497.1	19.11
Cyclic T/RH	167845082507.1	156799707845.3	6.581

(a)

Before **After**

Water Submersion

Cyclic W/D

Cyclic T/RH

(b)
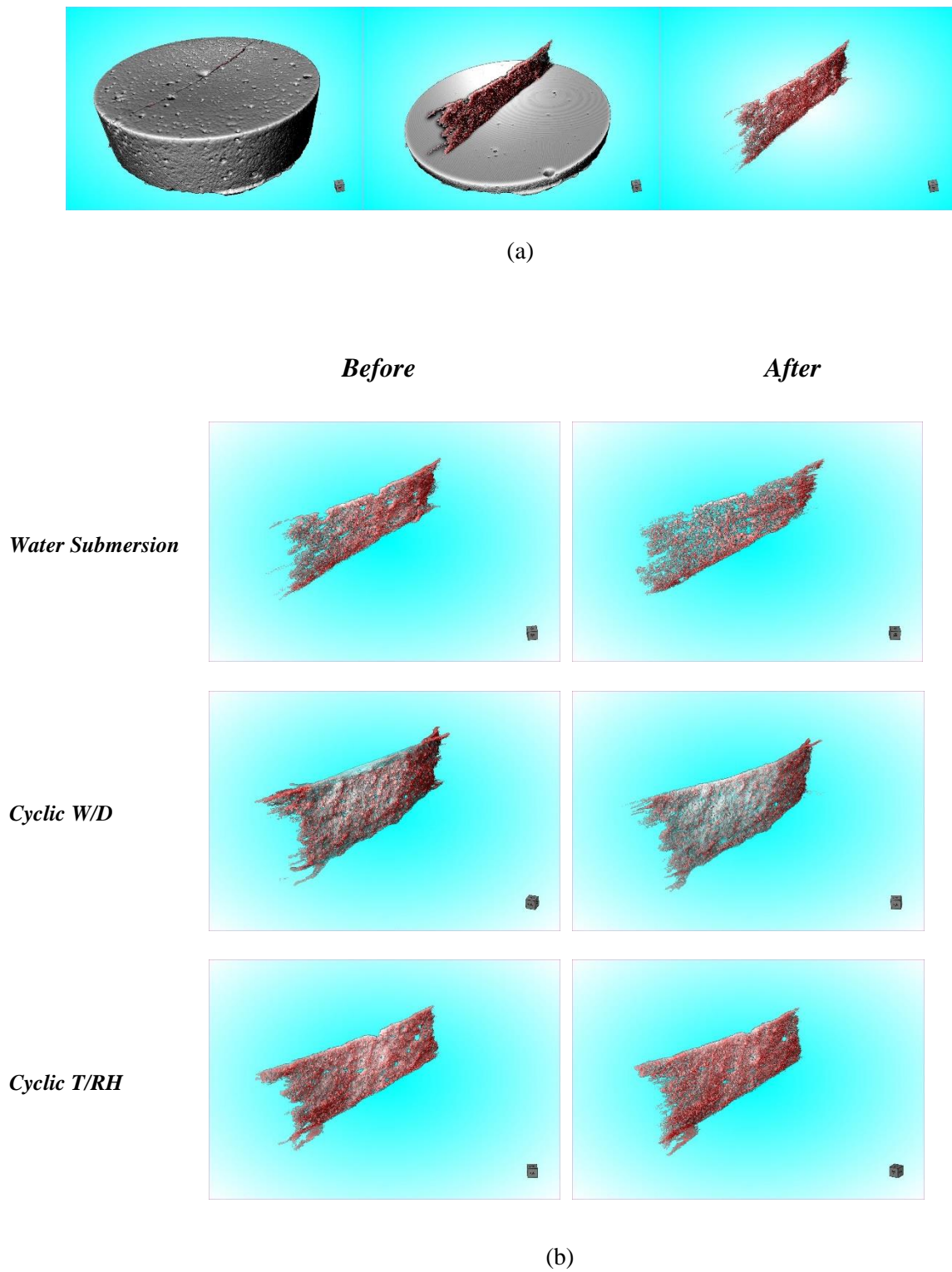
Figure 5.10 3D-images of the (a) crack segmentation, and (b) crack profile before and after self-healing.

5.4 Conclusions

In this chapter, the self-healing of cracks in cement-based materials incorporating superabsorbent polymers was investigated under simulated field conditions. Based on the experimental findings, the following conclusions can be drawn:

- The degree of self-healing depended on the dosage of superabsorbent polymers used and the type of environmental condition applied.

- In specimens containing SAP, the swollen SAP due to water contact formed a soft gel that expanded and temporarily sealed cracks.

- The effect of superabsorbent polymers on permanent crack healing was more pronounced in environments with less direct water contact.

- The main crack healing product formed in cement mortar specimens with and without SAPs was $CaCO_3$.

- X-ray μCT revealed that self-healing of specimens with and without SAPs was restricted to cracks near the surface.

- Based on the segmentation and quantification analysis of the X-ray μCT scans, the healing efficiency was 26.32%, 19.11%, and 6.58% for specimens with 1% SAP exposed to water submersion, cyclic wetting and drying, and cyclic temperature and relative humidity, respectively.

5.5　References

A.M. Soliman and M.L. Nehdi (2013) "Effect of partially hydrated cementitious materials and superabsorbent polymer on early-age shrinkage of UHPC" *Construction and Building Materials*, 41: 270-275.

D. Snoeck, S. Steuperaert, K. Van Tittelboom, P. Dubruel, and N. De Belie (2012) "Visualization of water penetration in cementitious materials with superabsorbent polymers by means of neutron radiography" *Cement and Concrete Research*, 42: 1113-1121.

D. Snoeck, D. Schaubroeck, P. Dubruel, and N. De Belie (2014) "Effect of high amounts of superabsorbent polymers and additional water on the workability, microstructure and strength of mortars with a water-to-cement ratio of 0.50" *Construction and Building Materials*, 72: 148-157.

D. Snoeck and N. De Belie (2015) (a) "Repeated Autogenous Healing in Strain-Hardening Cementitious Composites by Using Superabsorbent Polymers", *Journal of Materials in Civil Engineering*, 28(1): 11p.

D. Snoeck, L.F. Velasco, A. Mignona, S. Van Vlierberghe, P. Dubruel, P. Lodewyckx, N. De Belie (2015) (b) "The effects of superabsorbent polymers on the microstructure of cementitious materials studied by means of sorption experiments" *Cement and Concrete Research*, 77: 26-35.

D. Snoeck, J. Dewanckele, V. Cnudde, and N. De Belie (2016) "X-ray computed microtomography to study autogenous healing of cementitious materials promoted by superabsorbent polymers", *Cement and Concrete Composites*, 65: 83-93.

D. Snoeck, P. Van den Heede, T. Van Mullem, and N. De Belie (2018) "Water penetration through cracks in self-healing cementitious materials with superabsorbent polymers studied by neutron radiography" *Cement and Concrete Research,* 113: 86-98.

E. Özbay, M. Şahmaran, M. Lachemi, and H. E. Yücel (2013) "Self-Healing of microcracks in high-volume fly-ash-incorporated engineered cementitious composites", *ACI Materials Journal*, 110 (1): 33-43.

F. Wang, Y. Zhou, B. Peng, Z. Liu, and S. Hu (2009) "Autogenous Shrinkage of Concrete with Super-Absorbent Polymer" *ACI Materials Journal*, 106(2): 123-127.

H.X.D. Lee, H.S.Wong, and N.R. Buenfeld (2016) "Self-sealing of cracks in concrete using superabsorbent polymers" *Cement and Concrete research*, 97: 194-208.

J. Dang, J. Zhao, and Z. Du (2017) "Effect of Superabsorbent Polymer on the Properties of Concrete" *Polymers*, 9, 672, 17p.

J. Wang, J. Dewanckele, V. Cnudde, S. Van Vlierberghe, W. Verstraete, N. De Belie (2014) "X-ray computed tomography proof of bacterial-based self-healing in concrete" *Cement and Concrete Composites*, 53: 289-304.

K. Sisomphon, O. Copuroglu, and E.A.B. Koenders (2012) "Self-healing of surface cracks in mortars with expansive additive and crystalline additive", *Cement and Concrete Composites*, 34(4): 566-574.

K. Van Tittelboom, E. Gruyaert, H. Rahier, and N. De Belie (2012) "Influence of mix composition on the extent of autogenous crack healing by continued hydration or calcium carbonate formation", *Construction and Building Materials*, 37: 349-359.

S. Fan and M. Li (2014) "X-ray computed microtomography of three dimensional microcracks and self-healing in engineered cementitious composites" *Smart Materials and Structures*, 24: 14p.

S. Mönnig (2005) "Water saturated super-absorbent polymers used in high strength concrete" *Otto-Graf Journal,* 16: 193-202.

M. Sahmaran, G. Yildirim, and T. K. Erdem (2013) "Self-healing capability of cementitious composites incorporating different supplementary cementitious materials" *Cement and Concrete Composites*, 35 (10): 89-101.

M. Roig-Flores, S. Moscato, P. Serna, and L. Ferrara (2015) "Self-healing capability of concrete with crystalline admixtures in different environments", *Constr. & Building Materials*, 86: 1-11.

O.M. Jensen and P.F. Hansen (2001) "Water-entrained cement-based materials I. Principles and theoretical background", *Cement and Concrete Research,* 31: 647-654.

O.M. Jensen and P.F. Hansen (2002) "Water-entrained cement-based materials II. Experimental observations", *Cement and Concrete Research,* 32: 973-978.

Z. Jiang, W. Li and Z. Yuan (2015) "Influence of mineral additives and environmental conditions on the self-healing capabilities of cementitious materials", *Cement and Concrete Composites*, 57: 116-127.

Modeling Self-Healing of Concrete Using Hybrid Genetic Algorithm–Artificial Neural Network*

6.1   Introduction

In recent years, research on the ability of concrete to heal itself has received increasing attention. The inspiration came from the concept of biomimicry and the healing process in living nature (Blaiszik *et al*., 2010; Ghosh, 2009). For instance, when the skin of humans or animals is injured due to cuts, scrapes, or scratches, it can repair itself biologically. Although it is almost impossible to artificially simulate this exact biological healing process in concrete, several studies have proved that a portland cement concrete matrix can heal itself intrinsically (Gagné and Argouges, 2012; Huang and Ye, 2015; Jiang *et al*., 2015; Pang *et al*., 2016; Rahmani and Bazrgar, 2015; Roig-Flores *et al*., 2015; Snoeck and De Belie, 2015; Sisomphon *et al*., 2012; Yang *et al*., 2009).

Different mechanisms are responsible for autogenous (or intrinsic) self-healing in concrete, including (a) further hydration of anhydrous cement or cementitious minerals, (b) carbonation of calcium hydroxide, (c) expansion of the hydrated cement due to the swelling of calcium silicate hydrate, and (d) precipitation of impurities from the ingress water and spalling of loose concrete particles in cracks (Edvardsen, 1999; Hearn, 1998; Jacobsen *et al*., 1995; Ramm and Biscoping, 1998). Nevertheless, both continuous hydration and carbonation of calcium hydroxide are considered as the major mechanisms of autogenous self-healing in concrete (Van Tittelboom *et al.*, 2012).

Autogenous self-healing in concrete can also be stimulated by incorporating different healing agents into the concrete matrix. For instance, previous studies by Termkhajornkit *et al.* (2009), Şahmaran *et al.* (2008) and Van Tittelboom *et al.* (2012)

showed that partially replacing portland cement with supplementary cementitious materials, such as blast-furnace slag and fly ash, can improve the self-healing phenomenon in the cementitious matrix. In addition, a study by Sisomphon *et al.* (2012) reported that using expansive and crystalline additives could also enhance self-healing.

Several other studies investigated the possibility of incorporating bio-chemical self-healing agents in concrete to promote the self-healing efficiency (Chahal *et al*., 2012; Jonkers *et al*., 2010; Khaliq and Ehsan, 2016; Lou *et al*., 2015; Van Tittelboom *et al*., 2010; Wang *et al*., 2012; Wang *et al*., 2014; Wiktor and Jonkers *et al*., 2011, Xu and Yao, 2014). For instance, Jonkers *et al*. (2010) investigated the potential of using a certain type of alkali-resistant spore-forming bacteria as a self-healing agent. Spore-forming bacteria related to the genus *Bacillus* were added into the cementitious material. It was shown that the use of bacteria in concrete can help fill micro-cracks. In addition, a study conducted by Van Tittelboom *et al.* (2010) reported that the use of bacteria can help reduce water permeability into concrete. Wiktor and Jonkers (2011) studied the effect of combining bacteria spores and calcium lactate in concrete. They found that the combined effect can significantly enhance the concrete's ability to self-heal its cracks independently.

Therefore, the development of self-healing in concrete depends on numerous factors and parameters which are highly interdependent and exhibit substantial complexity, having combined roles in the self-healing efficiency of concrete. This makes it difficult to model and predict the self-healing effect of concrete given such complex multitude of parameters.

One promising approach to predicting the self-healing efficiency of concrete is artificial intelligence techniques, such as artificial neural networks (ANNs). According to Adeli (2001), ANNs offer a reliable tool that can model and predict complex problems. It basically consists of computational devices inspired by biological learning in the brain. It has a self-learning capability able to capture complex interactions between different variables. According to Kartam *et al*. (1997), ANNs can be applied to a variety of tasks and problems, such as classification, interpretation, diagnosis, modeling, and control. They are more suitable to problems that are highly complex to solve by mathematical modeling or other classical procedures (Adeli, 2001).

Since 1989 when the first article on the application of ANNs in civil engineering was published, several studies have reported on the excellent ability of ANNs to model and solve complex problems in different civil engineering areas (Adeli and Yeh, 1989; Adeli, 2001). For instance, ANNs have been successfully applied to investigate the concrete's compressive and shear strength, strain, dynamic modulus of elasticity, chloride permeability, crack pattern, and autogenous and drying shrinkage (Bal and Buyle-Bodin, 2013; Duan *et al.*, 2013; Elbahy *et al.*, 2010; El Chabib and Nehdi, 2005; Hegazy *et al.*, 1998; Hossian *et al.*, 2016; Lee, 2003; Mashhadban *et al.*, 2016; Nehdi and Soliman, 2012; Venkiteela *et al.*, 2010; Yeh, 2007; Yeh, 1998). In most cases, the ANN model was trained using the back-propagation (BP) algorithm. Basically, BP is a local search algorithm used in combination with gradient descent to update the weights and biases of the neural network and minimize the performance function (Chandwani *et al.*, 2015). According to Huang *et al.* (2015), training an ANN by BP has been a successful approach that can provide solutions for several engineering applications. However, due to the random initialization of weights and biases, the BP algorithm could be trapped in local optima and may not find the global optimum (Chandwani *et al.*, 2015; Huang *et al.*, 2015).

Recently, a number of studies combined ANN modeling with genetic algorithms (GA) to improve the convergence to global optimum (Rahman and Setu, 2015; Vadood *et al.*, 2015; Yuan *et al.*, 2014). Therefore, in the present chapter, the feasibility of using a hybrid genetic algorithm–artificial neural network (GA–ANN) for predicting the self-healing in concrete is investigated.

6.2 Concept of Neural Network Prediction of Self-Healing in Concrete

Several strategies of self-healing in concrete have been introduced. According to Van Tittelboom and De Belie (2013), such strategies can be classified based on the corresponding healing mechanisms into three groups: intrinsic healing, capsule-based healing and vascular healing. Intrinsic healing includes autogenous healing (further hydration of un-hydrated cement and carbonation of calcium hydroxide) and improved autogenous healing via agents or approaches that can promote further crystallization and cementitious hydration reactions. Strategies such as capsule-based healing (e.g.

microcapsules filled with a healing agent such as epoxy and added during concrete mixing) or vascular healing (networks of hollow tubes built into the cementitious matrix) do not always require interaction with concrete components to promote self-healing. Since each of these self-healing strategies has a different approach and deals with a different mechanism, it is reasonable to model each separately. Thus, in this study, intrinsic self-healing alone will be considered to develop a GA–ANN model capable of predicting the crack-self healing in cementitious materials. Studies retrieved from the literature were carefully selected based on reporting measurements of the change in crack-width due to self-healing under similar environmental conditions (i.e. water submersion). For instance, Özbay *et al*. (2013), Sahmaran *et al*. (2013), and Van Tittelboom *et al*. (2012) investigated crack self-healing under different environmental conditions; however, to obtain reliable model predictions, only results of self-healing obtained for completely water-submerged specimens were retained for developing the GA–ANN model. Sisomphon *et al*. (2012) and Wiktor and Jonkers (2011) also investigated the self-healing potential of cement-based materials under similar environmental conditions and their data were thus used. In addition, different agents were used to promote self-healing. For instance, Özbay *et al*. (2013), Sahmaran *et al*. (2013), and Van Tittelboom *et al*. (2012) investigated the autogenous self-healing of concrete incorporating supplementary cementitious materials. Wiktor and Jonkers (2011) improved the autogenous healing by incorporating bio-chemical self-healing agents. Two biochemical agents consisting of a mixture of bacterial spores and calcium lactate were used. Chahal *et al*. (2012) studied the effect of bacteria on the compressive strength, water absorption and rapid chloride permeability of fly ash concrete. They found that the properties of concrete made with fly ash along with an optimized dose of bacteria could be improved. Sisomphon *et al*. (2012) also studied the self-healing of cement-based materials incorporating calcium sulfo-aluminate-based expansive additive and a crystalline additive. Although in these studies different healing agents were used, the main healing product formed in the cracks were calcium carbonate ($CaCO_3$) and/or calcium silicate hydrate (C–S–H). For example, both Özbay *et al*. (2013) and Sahmaran *et al*. (2013) used scanning electron microscopy (SEM) and X-ray diffraction (XRD) to investigate the mineralogy and chemical composition of the healing product observed in the cracked specimens exposed to continuous curing. They reported the formation of both $CaCO_3$ and C–S–H. In addition, a high amount of $CaCO_3$

was reported in the case of using supplementary materials with higher CaO content. Wiktor and Jonkers (2011) also reported significant formation of $CaCO_3$ as a healing product due to metabolic conversion of calcium lactate and the reaction of metabolically produced CO_2 molecules with $Ca(OH)_2$ minerals present in the concrete. Sisomphon *et al.* (2012) also found that $CaCO_3$ was the major healing product formed in cracks due to the increased release of Ca^{2+} and high pH of the cement mortar specimens incorporating the healing agents. According to Van Tittelboom and De Belie (2013), intrinsic healing can include autogenous healing (further hydration of un-hydrated cement and carbonation of calcium hydroxide) and improved autogenous healing using agents or approaches that promote crystallization and more cementitious hydration reactions. Özbay *et al.* (2013), Sahmaran *et al.* (2013), and Van Tittelboom *et al.* (2012) investigated autogenous self-healing under similar environmental condition and reported practically similar final healing products. Moreover, studies by Sisomphon *et al.* (2012) and Wiktor and Jonkers (2011) investigated the improved autogenous self-healing under similar condition and reported similar final healing products. Hence, developing a model based on artificial neural networks to predict the effect of such agents reported in these studies on crack self-healing was considered a suitable approach.

6.3 Artificial Neural Network (ANN)

6.3.1 Neural Network Approach

Figure 6.1 displays a schematic illustration of both artificial and biological neurons. An artificial neural network is a highly interconnected network of parallel distributed possessors or neurons that has a learning process similar to the extent of the learning procedure in a biological brain (Adeli, 2001; Kartam *et al.*, 1997; Nehdi and Soliman, 2012; Haykin, 1994; Hewayde *et al.*, 2007; Nehdi *et al.*, 2007; Shahriar and Nehdi, 2011; Shahriar and Nehdi, 2013). It operates as a black box through a learning process with the ability to synthesize and memorize complex data structure (Adeli, 2001).

ANN modeling has been applied in almost all engineering fields. For civil engineering in particular, ANN modeling has been employed to solve complex problems in the areas of structural, construction, geotechnical, environmental, and management engineering (Adeli, 2001; Kartam *et al.*, 1997). For instance, Jiang *et al.* (2016) modeled the

microbial-induced corrosion of concrete sewers using the ANN approach. This type of corrosion involves complex mechanisms that are difficult to model analytically. The ANN model provided accurate estimations in comparison to multiple regression models. Similarly, Venkiteela *et al.* (2010) developed an ANN model capable of predicting the dynamic modulus of elasticity of concrete at an early age with reasonable accuracy. Since self-healing in concrete is a multifaceted process that requires a powerful modeling tool, ANN was considered in the present chapter in an attempt to capture the interdependent parameters influencing the self-healing mechanism and its high level of complexity.
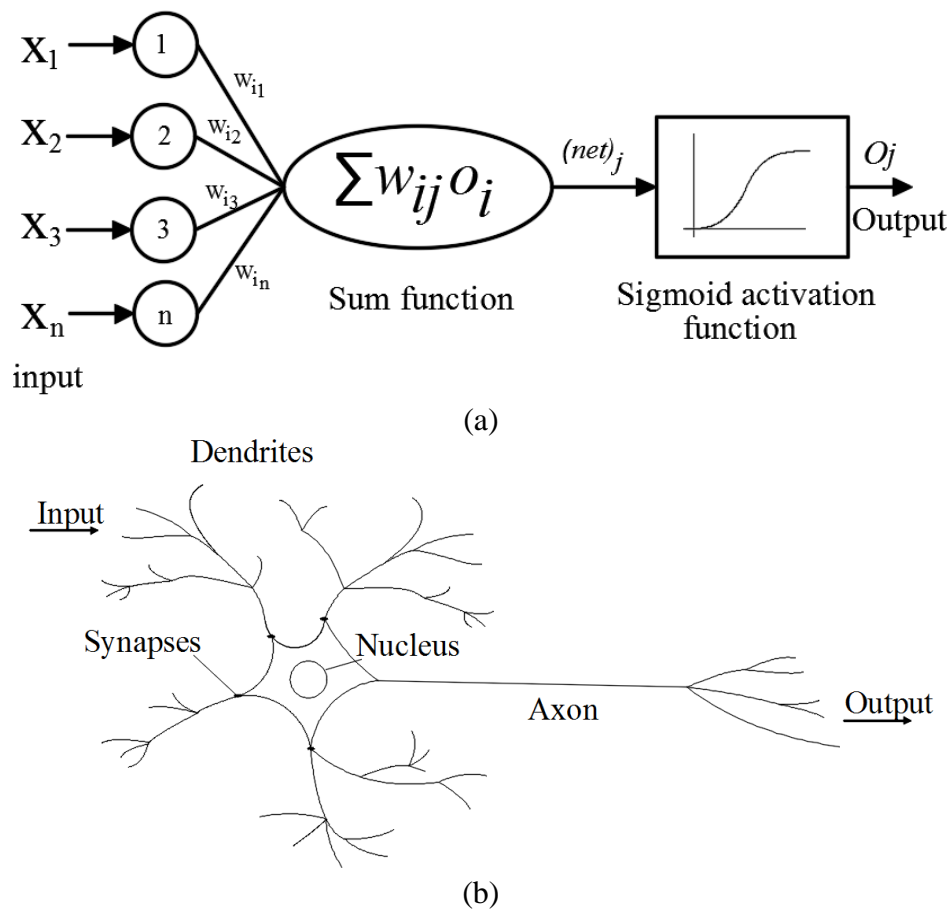
Figure 6.1 Schematic illustration of (a) artificial neuron, and (b) biological neuron.

6.3.2 Neural Network Architectures and Parameters

Since there is no commonly accepted optimal method to determine the best architecture of an ANN, a trial and error approach was adopted. The design of the network architecture started with fewer hidden neurons, and then the number of hidden neurons was adjusted. The network architecture that provided best generalization was retained and is illustrated in **Figure 6.2**. It consisted of 14 input neurons representing the main parameters influencing the self-healing of concrete, along with one hidden layer comprising 16 neurons, and one output layer with a single neuron representing the crack width as an indication of self-healing.
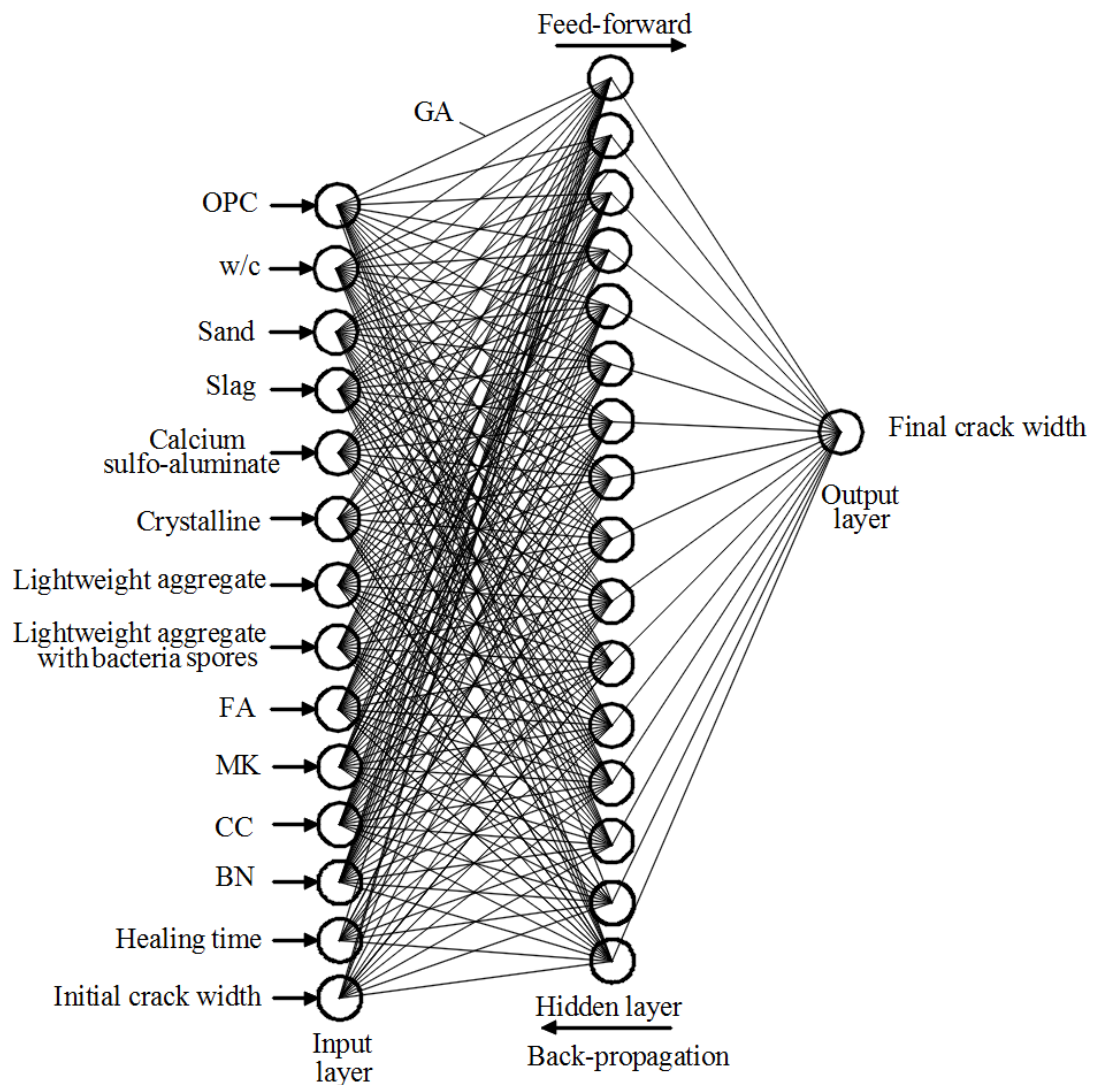
Figure 6.2 Architecture of genetic algorithm–artificial neural network (GA–ANN) model.

There are several different classes of architectures in neural networks in which neurons (nodes) are structured. For instance, in a feed-forward network, nodes are structured in parallel multilayers that can be classified into input layer, hidden layers, and output layer (Mashhadban *et al*., 2016; Nehdi and Soliman, 2012).

Each node mainly consists of three elements where the input information passes through, including connecting links or weights, summing-junction, and activation function (Mashhadban *et al*., 2016; Haykin, 1994; Saridemir, 2009). Weights in a neural network basically represent the strength between the connected nodes. For instance, when a node in the input layer receives information from an external environment, the output will send it as an input to the neighboring node at the next layer (i.e. hidden layer) multiplied by the weight value. Thereafter, the summing-junction combines all the weighted products. **Eq. 6.1** refers to the weighted sums of the input components (Haykin, 1994; Saridemir, 2009; Topcu *et al*., 2007).

$$l_n = \sum_{j=1}^{p} W_{nj}\, x_j + b \qquad\qquad \textbf{(6.1)}$$

where l_n is the weighted sums of the input component, W_{nj} is the weight between neurons, x_j is the input, and b is the bias.

The summation process will form a single input, which will be adjusted by an activation function (Nehdi and Soliman, 2012; Saridemir, 2009; Topcu *et al*., 2007). Basically, the activation function simulates the firing rate of the neuron to axon in the biological brain. Thus, in the computational model, the final single output of a neuron can be calculated based on the following equation:

$$y_n = A_f(l_n) \qquad\qquad \textbf{(6.2)}$$

where y_n is the output of the neuron and A_f is the activation function.

There are several common activation functions that allow neural networks to solve difficult problems, including the sigmoid, ramp, and Gaussian functions. In the case of using a multilayer neural network with receptive fields, using the sigmoid function as an activation function is generally recommended (e.g. Saridemir, 2009). In the current study, the tansigmoid function shown in **Eq. 6.3** was used in the hidden layer and a pure linear transfer function as shown in **Eq. 6.4** was used in the output layer neurons.

$$tansig(x) = \frac{2}{1 + e^{(-2x)}} - 1 \qquad (6.3)$$

$$purelin(x) = x \qquad (6.4)$$

6.3.3 Hybrid Genetic Algorithm–Artificial Neural Network

Table 6.1 shows the values of parameters used in the GA–ANN model. Genetic algorithms are powerful optimization tools based on Darwin's natural selection and evolution theory. It has the capability to find the global optima through stochastic search techniques in a large solution domain. The process of the GA consists of steps including evaluation, selection, crossover, and mutation. Therefore, implementing a GA in ANN can improve the prediction accuracy of the ANN model. Several studies have reported that using GA–ANN can provide a reliable solution for different engineering optimization problems. For instance, Zhang *et al.* (2010) showed that using artificial neural network−genetic algorithm-based optimization provided higher accuracy prediction for the effect of pH, carbodiimide concentration, and coupling time on the activity yield of immobilized cellulose on the smart polymer. Yasin *et al.* (2014) used a hybrid artificial neural network–genetic algorithm approach to optimize the removal of lead ions from aqueous solutions using intercalated Tartrate-Mg–Al layered double hydroxides. It was shown that a small residual error existed between the predicted and experimental values. Ho and Chang (2011) investigated the feasibility of using an artificial neural network model with a genetic algorithm to predict the platelet transfusion requirements for acute myeloblastic leukemia patients. A genetic algorithm was applied in the ANN model to optimize the weights and biases governing the input-output relationship of the ANN model. They found that using a hybrid (GA–ANN)

model effectively predicted the transfusion requirement of the acute myeloblastic leukemia patients.

Table 6.1: Values of parameters used in GA–ANN modeling

Parameter	GA–ANN
Number of input layer neurons	14
Number of first hidden layer neurons	16
Number of output layer neurons	1
MSE goal	13×10^{-5}

In the present chapter, GA was applied to optimize the evolution of weights and biases as shown in **Figure 6.3.** Therefore, mutation and crossover only apply to the weights and biases to find the optimal values. After achieving optimal weights and biases, the model is trained using a BP algorithm.

There are several training paradigms for ANN. For instance, the training can be supervised or unsupervised, i.e. learning with a teacher or learning without a teacher (Hossian *et al*., 2016; Haykin, 1994; Nehdi *et al*., 2001). In the case of supervised learning, the network is trained on certain provided data to a targeted output. Thus, the network can learn in an administered manner. Conversely, in the case of unsupervised learning, the network is guided to learn independently. Thus, it can recognize the analogy among the training pattern on its own.

In the majority of engineering applications of ANNs, the supervised training method based on feed-forward network along with a back-propagation algorithm was implemented (Hossian *et al*., 2016; Saridemir, 2009; Topcu and Saridemir, 2007; Nehdi *et al*., 2001). According to Yeh (2007), developing an ANN model capable of predicting the behavior of a material requires training the network on the targeted data obtained from experimental results of that material. In other words, it requires training the network in a supervised manner. Thus, in the present study, feed-forward neural networks (FFNs) along with back-propagation algorithm was implemented to train the GA–ANN model on predicting self-healing in concrete. The GA–ANN model was trained using 70% of the total database, which was randomly selected to avoid any bias. It includes the influential parameters investigated in the selected studies. Moreover,

15% of the data (also selected randomly) was used for the validation of the model, while the remaining 15% was used for testing the generalization capability of the model.
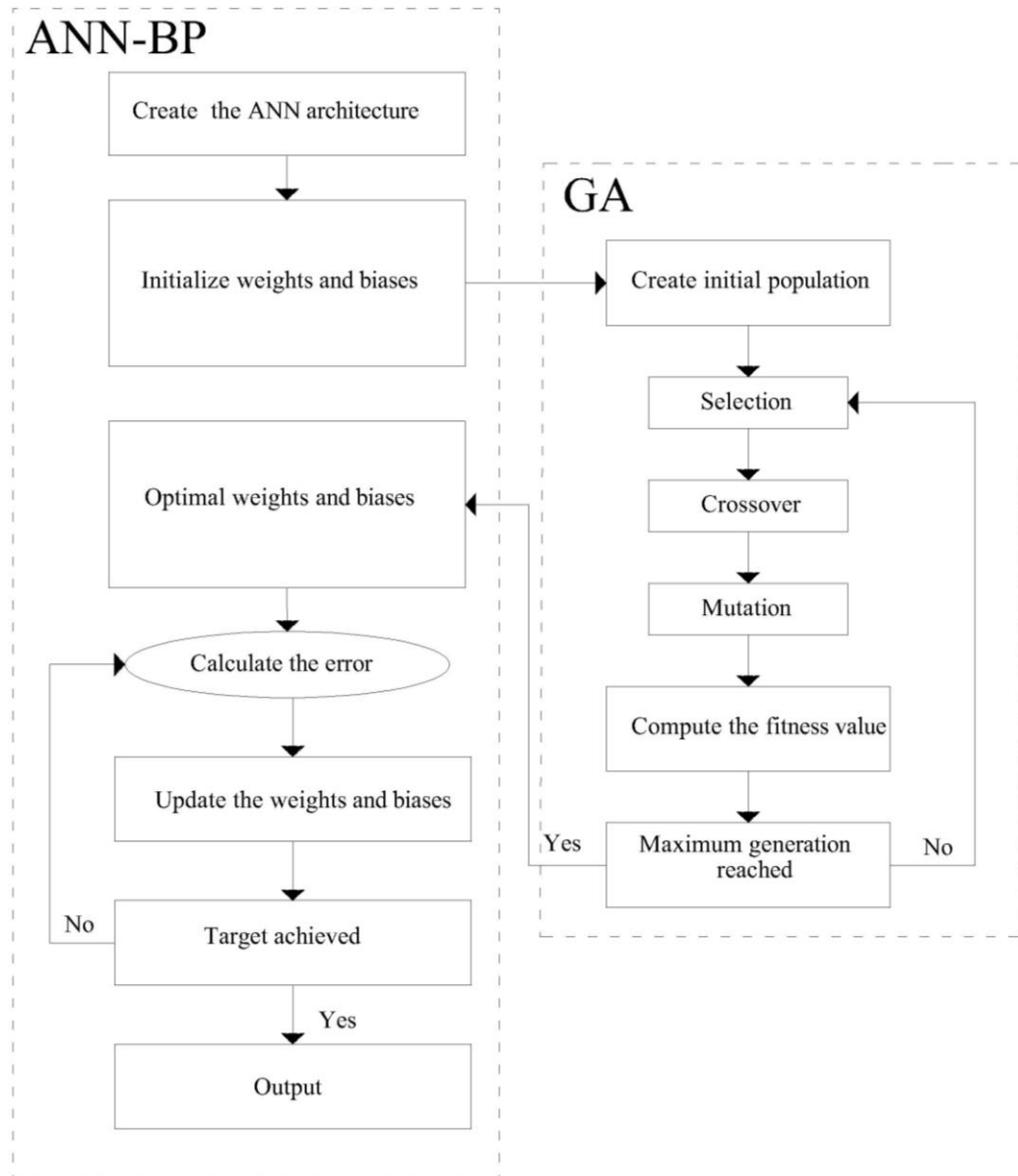
Figure 6.3 Flowchart of artificial neural network–back-propagation (ANN–BP) optimized by GA.

The validation data set is different from the model generalization test set. Validation is regarded as part of the training process. It is used to build the model and determine its parameters in order to avoid overfitting. The non-linear ANN model could get full accuracy on the training data set. This overfitting has been found to lead to very poor

performance on the test data set. Hence, the independent validation data set is used for "cross-validation" to avoid such overfitting. Conversely, the test data set is only used to explore the performance of the trained model on new, unfamiliar data. In other words, the training data set is used for determining the ANN weights and biases to minimize the error function and maximize accuracy in each iteration. The cross-training data set is used to oversee the training process and improve the ANN generalization by minimizing overfitting. An overfitted ANN yields high accuracy on training data, yet fails to generalize from the training data, thus yielding poor performance on new, independent input data. The validation data set thus provides an unbiased estimate of the generalization error of the model.

The back-propagation Levenberg–Marqudt rule (LMA) was used to simplify and shorten the training time. It basically propagates back the calculated error at the output layer to the network based on the Jacobian matrix *J*. The iteration of such an algorithm can be written as follows:

$$w_{j+1} = w_j - [J^T J + \mu I]^{-1} J^T e \qquad (6.5)$$

where w_j is a vector of current weights and biases*; μ is a learning rate; J* is the Jacobian matrix; J^T is the transpose matrix of *J; I* is the identity matrix; and *e* is a vector of network errors.

6.3.4 *Database Sources and Range of Input and Output Variables*

As shown in **Table 6.2**, data from the current study were used. In addition, data were collected from various studies including Wiktor and Jonkers (2011), Sisomphon *et al*. (2012), Van Tittelboom *et al*. (2012), Sahmaran *et al*. (2013) and Özbay *et al*. (2013). The total database included 1612 data points. These reported studies indicated that crack self-healing of cementitious materials is controlled by factors including the binder content, w/c ratio, initial crack width and the healing time. For instance, Sahmaran *et al*. (2013) and Özbay *et al*. (2013) and Van Tittelboom *et al*. (2012) investigated the influence of using alternative binder materials including supplementary cementitious materials on crack self-healing. Cracks were created in mortar cylinders by means of a crack width-controlled splitting test. It was found that cement partial replacement by

blast furnace slag or fly ash improved the crack self-healing. In addition, decreasing the water-to-binder ratio improved the self-healing efficiency.

Sisomphon *et al.* (2012) investigated the potential of promoting self-healing in cementitious materials through crystalline and expansive additives. They used synthetic cementitious materials made of reactive silica and crystalline catalysts as a crystalline additive and calcium sulfo-aluminate as an expansive material. It was found that, within 28 days, pre-cracked specimens were capable of self-healing their cracks with a width of up to 400 µm. Jonkers *et al.* (2010) studied the effect of using a certain type of alkali-resistant spore-forming bacteria in a cementitious material. Lightweight aggregate impregnated with spore-forming bacteria related to the genus Bacillus was added into the cementitious material during the mixing time. Results showed that crack healing occurred for up to 460 µm-wide cracks in specimens incorporating the spore-forming bacteria compared to 180 µm-wide crack healing occurring in control specimens made with ordinary portland cement.

Table 6.2: Database sources and range of input and output variables

Source	No. of data points	
Wiktor and Jonkers (2011)	640	
Sisomphon *et al.* (2012)	594	
Sahmaran *et al.* (2013)	36	
Van Tittelboom *et al.* (2012)	182	
Özbay *et al.* (2013)	10	
Current study	150	
Parameter	**Maximum**	**Minimum**
OPC (mR %)	100	15
w/c (mR %)	60	25
Sand (mR %)	309	200
SG (mR %)	220	0
FA (mR %)	220	0
CC (mR %)	8	0
BN (mR %)	8	0
MK (mR %)	15	0
Calcium sulfo-aluminate (mR %)	10	0
Crystalline additive (mR %)	4	0
LWA (mR %)	76	0
LWA with bacteria spores (mR %)	76	0
Initial crack width (µm)	400	40
Healing time (days)	150	0
Final crack width (µm)*	400	0

mR %: By % of mass ratio of cement. * Output variable

6.3.5 Performance of GA–ANN Model

Figure 6.4 exhibits the results of change in width of the self-healed cracks in concrete predicted by the proposed GA–ANN model versus the corresponding experimental measurements of crack self-healing reported in various studies. The performance of the GA–ANN model mainly depends on its ability to predict the experimental output data with reasonable accuracy. As shown in **Figure 6.4**, the GA–ANN model was able to accurately predict the self-healing of concrete relative to the actual experimental data. For instance, the coefficient of determination (R^2) of model prediction versus experimental data for the training, validation, and test data sets are 0.988, 0.973, and 0.981 respectively. Thus, it can be argued that the proposed GA–ANN model captured the relationships between the provided input and output data with adequate accuracy, which indicates excellent performance.

The reliability of the developed GA–ANN model for the complete data set was also evaluated via the root-mean-square (RMS) error, coefficient of determination (R^2), and mean absolute percentage error (MAPE) between the model's predictions and experimental results, according to **Eqs. 6.6** to **6.8**. The RMS, R^2, and MAPE values were 12.16 µm, 0.985, and 11.14%, respectively, which indicates adequate performance of the GA–ANN model.

$$RMS = \sqrt{\frac{1}{n}\sum_{i=1}^{n}(t_i - o_i)^2} \tag{6.6}$$

$$R^2 = 1 - \left(\frac{\sum_{i=1}^{n}(t_i - o_i)^2}{\sum_{i=1}^{n}(t_i)^2}\right) \tag{6.7}$$

$$MAPE = \frac{1}{n}\frac{\sum_{i=1}^{n}|t_i - o_i|}{\left|\sum_{i=1}^{n}t_i\right|} \tag{6.8}$$

where t_i is the target output; o_i is the predicted output; and n is the number of data point.

The generalization capacity of the GA–ANN model was also evaluated on randomly selected test data (15% of the original database), which was unfamiliar to the model and not previously presented in the training process.
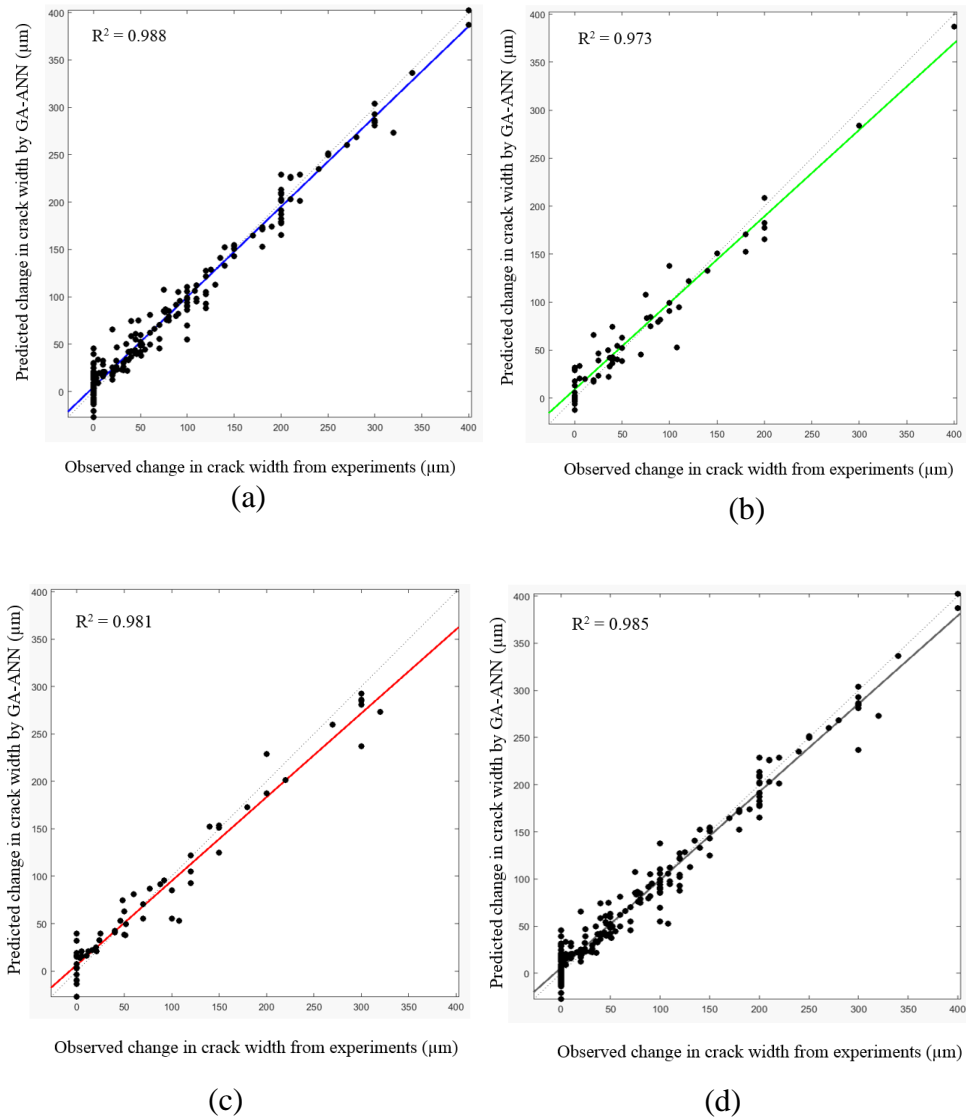
Figure 6.4 Regression plot of GA–ANN predicted change in crack width due to self-healing versus the corresponding experimentally observed change in crack width: (a) training; (b) validation; (c) test; and (d) complete data set.

The fourteen input testing data were introduced to the GA–ANN model to predict the self-healing of concrete. As shown in **Figure 6.4**, the presented GA–ANN model was able to predict the self-healing of concrete relative to the actual experimental data. Furthermore, the model performance on the validation data was comparable to that of the training and testing data, again indicating adequate performance of the GA–ANN model in predicting the complex phenomenon of self-healing as a function of the multitude of interconnected governing variables.

The ability of the GA–ANN model to predict the crack self-healing in cementitious materials was further validated using new experimental data obtained from the lab. Cement mortar specimens were made with ordinary portland cement partially replaced with 20% of fly ash. Water-to-cementitious materials ratio (w/c) of 0.35 and sand-to-cementitious materials ratio (s/c) of 2 by mass were used.

The specimens were cast in plastic containers having a 4 cm diameter and 9 cm height. The specimens were reinforced with a galvanized steel mesh (6 mm × 6 mm with Ø = 1 mm). After 28 days of curing in a moist room at RH ≥ 95% and $T = 21 \pm 1$ °C (68 °F), specimens were cracked by applying a tensile stress. Cracks with a width of 50 ± 10, 100 ± 10, 200 ± 10, 300 ± 10 µm, and 400 ± 10 µm were measured using an optical microscope and marked to evaluate the width change due to self-healing. All specimens were then submerged in water to allow the development of self-healing of cracks. The change in crack width was measured at 15, 21, 28 and 42 days wetting periods. **Figure 6.5** illustrates the healing process of the cracked specimens. It was indicated that complete healing occurred in cracks with small width in comparison to cracks with larger width. The experimental results were compared with the GA–ANN model-predicted results. As shown in **Figure 6.6**, the GA–ANN model was capable of predicting the self-healing of cracks in the tested mortar specimens.

(a)   (b)
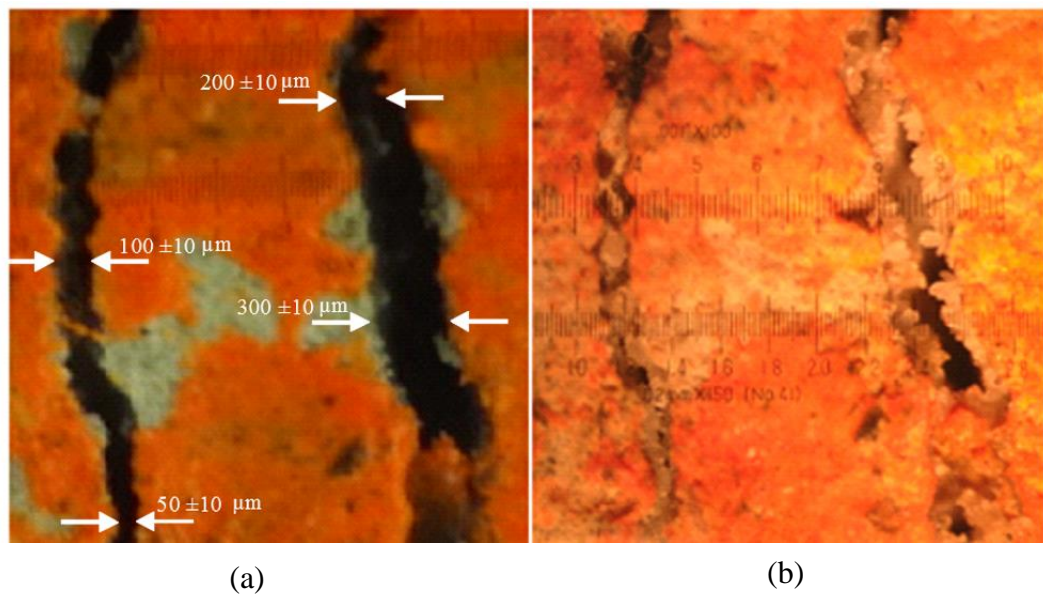
Figure 6.5 Crack healing process: (a) cracks before healing; (b) cracks after 42 days of healing.
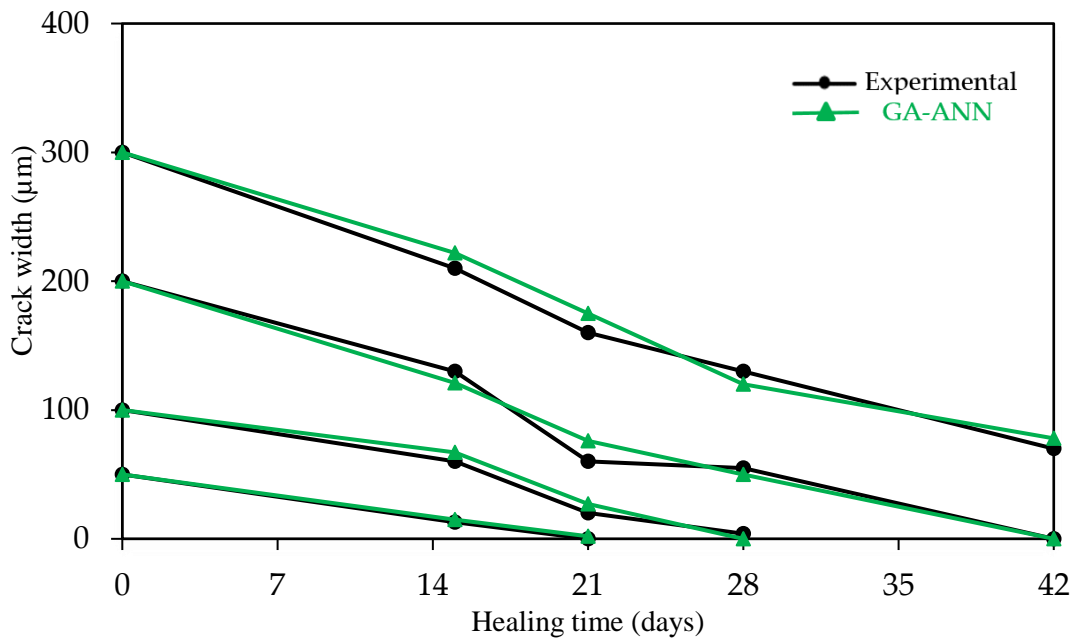
Figure 6.6. GA–ANN model predictions of crack self-healing (reduction in crack
width) of cementitious materials versus corresponding
experimentally measured results.

6.4 Conclusions

In this chapter, a hybrid genetic algorithm–artificial neural network (GA–ANN) model
was developed to predict the self-healing of cracks in cement-based materials. From
this study, the following conclusions can be drawn:

- The developed GA–ANN model represents a powerful computational tool with
  high efficiency providing an alternative solution for the modeling procedure of
  the highly complex self-healing phenomenon in cement-based materials.

- A genetic algorithm was effectively applied in the ANN model to determine the
  optimal weights and biases that govern the input–output relationship of the
  model.

- Training the GA–ANN multilayered feed-forward neural network with a back-
  propagation algorithm showed accurate prediction of the self-healing crack
  ability in cementitious materials, yielding predictions that were close to the
  actual experimental values.

6.5   References

B.J. Blaiszik, S.L.B. Kramer, S.C. Olugebefola, J.S. Moore, N.R. Sottos, White (2010) "Self-healing polymers and composites" *Annu. Rev. Mater. Res*, 40, 179–211.

B. Pang, Z. Zhou, P. Hou, P. Du, L. Zhang, H. Xu, (2016) "Autogenous and engineered healing mechanisms of carbonated steel slag aggregate in concrete" *Construction and Building Materials*, 107, 191–202.

C. Edvardsen, (1999) "Water permeability and autogenous healing of cracks in concrete" *ACI Materials Journal*, 96: 448–454.

D. Snoeck, and N. De Belie, (2015) "From straw in bricks to modern use of microfibers in cementitious composites for improved autogenous healing—A review" *Constr. Build. Mater*, 95: 774–787.

E. Özbay, M. Sahmaran, M. Lachemi, and H.E. Yücel, (2013) "Self-healing of microcracks in high-volume fly-ash-incorporated engineered cementitious composites" *ACI Mater J*, 110: 33–43.

E. Hewayde, M.L. Nehdi, E. Allouche, G. Nakhla, (2007) "Neural network prediction of concrete degradation by sulphuric acid attack" *Str. Inf. Eng*, 3: 17–27.

G. Venkiteela, A. Gregori, Z. Sun, and S.P Shah (2010) "Artificial neural network modeling of early-age dynamic young's modulus of normal concrete" *ACI Mater. J*, 107: 282–290.

G. Jiang, J. Keller, P.L. Bond, and B.Z. Yuan, (2016) "Predicting concrete corrosion of sewers using artificial neural network" *Water Res.*, 92: 52–60.

H. Huang and G. Ye, (2015) "Self-healing of cracks in cement paste affected by additional Ca^{2+} ions in the healing agent" *J. Intell. Mater. Sys. Str*, 26, 309–320.

H. Rahmani, and H. Bazrgar, (2015) "Effect of coarse cement particles on the self-healing of dense concretes" *Magazine Concrete Res*. 67, 476–486.

H. Adeli, (2001) "Neural networks in civil engineering: 1989−2000" *Comp. Aided Civ. Inf. Eng*, 16: 126–142.

H.M. Jonkers, A. Thijssena, G. Muyzerb, O. Copuroglua, E. Schlangena, (2010) "Application of bacteria as self-healing agent for the development of sustainable concrete" *Ecol. Eng*, 36: 230–235.

H. El Chabib, M.L. Nehdi, (2005) "Neural network modeling of properties of cement based materials demystified" *Adv. Cement Res*, 17: 91–102.

H. Adeli, C. Yeh, (1989) "Perceptron learning in engineering design" *Microcomp. Civ. Eng*, 4: 247–256.

H. Mashhadban, S.S Kutanaei, M.A Sayarinejad, (2016) "Prediction and modeling of mechanical properties in fiber reinforced self-compacting concrete using particle swarm optimization algorithm and artificial neural network" *Constr. Build. Mater*, 119: 277–287.

H. Huang, J. Li, C. Xiao, (2015) "A proposed iteration optimization approach integrating backpropagation neural network with genetic algorithm" *Exp. Sys. Appl*, 42: 146–155.

I. B. Topcu and M. Sarıdemir, (2007) "Prediction of properties of waste AAC aggregate concrete using artificial neural network" *Comp. Mater. Sci*., 41: 117–125.

I.C. Yeh, (1998) "Modeling of Strength of high-performance concrete using artificial neural networks" *Cement Concrete Res*, 28: 1797–1808.

I. Yeh, (2007) "Modeling slump flow of concrete using second-order regressions and artificial neural networks" *Cement Concrete Compos*, 29: 474–480.

J. Y. Wang, N. De Belie, W. Verstraete, (2012) "Diatomaceous earth as a protective vehicle for bacteria applied for self-healing concrete" *J. Ind. Microbiol*, 39: 567–577.

J.Y. Wang, H. Soens, W. Verstraete, N. De Belie, (2014) "Self-healing concrete by use of microencapsulated bacterial spores" *Cement Concrete Res*, 56: 139–152.

J. Xu and W. Yao (2014) "Multiscale mechanical quantification of self-healing concrete incorporating non-ureolytic bacteria-based healing agent" *Cement Concrete Res*, 64: 1–10.

K. Sisomphon, O. Copuroglu, and E.A.B Koenders, (2012) "Self-healing of surface cracks in mortars with expansive additive and crystalline additive" *Cement Concrete Compos*,34: 566–574.

K.M.A. Hossian, L.R. Gladson, M.S. Anwar, (2016) "Modeling shear strength of medium- to ultra-high-strength steel fiber-reinforced concrete beams using artificial neural network" *Neural Comp*. Appl, 1–12.

K. Van Tittelboom, E. Gruyaert, H. Rahier, and N. De Belie, (2012) "Influence of mix composition on the extent of autogenous crack healing by continued hydration or calcium carbonate formation" *Construct. Build. Mater*, 37: 349–359.

K. Van Tittelboom, N. De Belie, W. De Muynck, W. Verstraete (2010) "Use of bacteria to repair cracks in concrete" *Cement Concrete Res*, 40: 157–166.

K. Van Tittelboom and N. De Belie, (2013) "Self-healing in cementitious materials—A review. *Materials* 2013, 6, 2182–2217.

L. Bal and F. Buyle-Bodin, (2013) "Artificial neural network for predicting drying shrinkage of concrete" *Constr. Build. Mater*, 38: 248–254.

M. Roig-Flores, S. Moscato, P. Serna, and L. Ferrara, (2015) "Self-healing capability of concrete with crystalline admixtures in different environments" *Constr. Build. Mater*, 86: 1–11.

M. Şahmaran, S.B. Keskin, G. Ozerkan, I.O. Yaman, (2008) "Self-healing of mechanically-loaded self-consolidating concretes with high volumes of fly ash" *Cement Concrete Compos*, 30: 872–879.

M. Lou, C. Qian, R. Li, (2015) "Factors affecting crack repairing capacity of bacteria-based self-healing concrete" *Constr. Build. Mater*, 87: 1–7.

M. M. Rahman, T.A. Setu, (2015) "An implementation for combining neural networks and genetic algorithms" Inter. J. *Comp. Sci. Technol*, 6: 218–222.

M. L. Nehdi and A.M. Soliman, (2012) "Artificial intelligence model for early-age autogenous shrinkage of concrete" *ACI Mater*. J, 109: 353–361.

M. L. Nehdi, H. El Chabib, and A. Said, (2007) "Evaluating shear capacity of FRP reinforced concrete beams using artificial neural networks" *Smart Str. Sys*, 2: 81–100.

M. L. Nehdi, H. El Chabib, and H.M. El Naggar (2001) "Predicting performance of self-compacting concrete mixtures using artificial neural networks" *ACI Mater. J*, 98: 349–401.

M. Vadood, M.S. Johari, and A. Rahai, (2015) "Developing a hybrid artificial neural network-genetic algorithm model to predict resilient modulus of polypropylene/polyester fiber-reinforced asphalt concrete" *J. Text. Inst*, 106: 1239–1250.

M. Sahmaran, G. Yildirim, T.K. Erdem, (2013) "Self-healing capability of cementitious composites incorporating different supplementary cementitious materials" *Cement Concrete Compos*, 35: 89–101.

M. Sarıdemir, (2009) "Predicting the compressive strength of mortars containing metakaolin by artificial neural networks and fuzzy logic" *Adv. Eng. Softw*., 40: 920–927.

N. Chahal, R. Siddique, A. Rajor, (2012) "Influence of bacteria on the compressive strength, water absorption and rapid chloride permeability of fly ash concrete" *Constr. Build. Mater*, 28: 351–356.

N. Hearn, (1998) "Self-healing, autogenous healing and continued hydration: what is the difference?" *Mater. Str*, 31: 563–567.

N. Kartam, I. Flood, H. J. Garret, and G. Agrawal (1997) "Artificial Neural Networks for Civil Engineers: Fundamentals and Applications" *American Society of Civil Engineers*, New York, NY, USA, p. 216.

P. Termkhajornkit, T. Nawa, Y. Yamashiro, T. Saito, (2009) "Self-healing ability of fly ash-cement systems" *Cement Concrete Compos*, 31: 195–203.

R. Gagné and M.A. Argouges, (2012) "Study of the natural self-healing of mortars using air-flow measurements" *Mater. Str*, 45, 1625–1638.

S. Haykin, (1994) "Neural Networks: A Comprehensive Foundation" *Macmillan College Publishing Company*: New York, NY, USA, p.696.

S. Shahriar and M.L. Nehdi, (2011) "Modelling rheological properties of oil well cement slurries using artificial neural networks" *ASCE J. Mater. Civ. Eng*, 23: 1703–1710.

S. Shahriar and M.L. Nehdi, (2013) "Modelling rheological properties of oil well cement slurries using multiple regression analysis and artificial neural networks" *Inter. J. Mate. Sci*, 3: 26–37.

S. K. Ghosh, (2009) "Self-healing Materials: Fundamentals, Design Strategies, and Applications" *Wiley-VCH: Berlin, German*, p. 291.

S. Lee, Prediction of concrete strength using artificial neural networks. *Eng. Str*. 2003, 25, 849–857.

S. Jacobsen, J. Marchand, H. Hornain, (1995) "SEM observation of the microstructure of frost deteriorated and self-healed concretes" *Cement Concrete Res*, 25: 1781–1790.

T. Hegazy, S. Tully, H. Marzouk, (1998) "A neural network approach for predicting the structural behavior of concrete slabs" *Can. J. Civ. Eng*, 25: 668–677.

V. Chandwani, V. Agrawal, R. Nagar, (2015) "Modeling slump of ready mix concrete using genetic algorithms assisted training of artificial neural networks" *Exp.Sys. Appl*, 42: 885–893.

V. Wiktor and H.M.Jonkers (2011) "Quantification of crack-healing in novel bacteria-based self-healing concrete" *Cement Concrete Compos*, 33: 763–770.

W. Ramm and M. Biscoping, (1998) "Autogenous Healing and reinforcement corrosion of water-penetrated separation cracks in reinforced concrete" *Nuclear Eng. Des*, 179: 191–200.

W. Ho and C. Chang, (2011) "Genetic-algorithm-based artificial neural network modeling for platelet transfusion requirements on acute myeloblastic leukemia patients" *Exp. Sys. Appl*, 38: 6319–6323.

W. Khaliq, M.B. Ehsan, (2016) "Crack healing in concrete using various bio influenced self-healing techniques" *Constr. Build. Mater*, 102: 349–357.

Y. Yang, M.D Lepech, E. Yang, V. Li, (2009) "Autogenous healing of engineered cementitious composites under wet–dry cycles" *Cement Concrete Res*. 39: 382–390.

Y.I. Elbahy, M.L Nehdi, and M.A. Youssef, (2010) "Artificial neural network model for deflection analysis of super-elastic shape memory alloy RC beams" *Can. J. Civ. Eng*, 37: 855–865.

Y. Yasin, F.B. Ahmad, M. Ghaffari-Moghaddam, M. Khajeh, (2014) "Application of a hybrid artificial neural network–genetic algorithm approach to optimize the lead ions removal from aqueous solutions using intercalated tartrate-Mg–Al layered double hydroxides" *Environ. Nanotechnol. Monitor. Ma*, 1–2: 2–7.

Y. Zhang, J. Xu, Z. Yuan, H. Xu, and Q. Yu, (2010) "Artificial neural network-genetic algorithm based optimization for the immobilization of cellulose on the smart polymer Eudragit L-100" *Bioresour. Technol*., 101: 3153–3158.

Z. Jiang, W. Li, and Z. Yuan, (2015) "Influence of mineral additives and environmental conditions on the self-healing capabilities of cementitious materials" *Cement Concrete Res*., 57, 116–127.

Z.H. Duan, S.C. Kou, C.S. Poon, (2013) "Using artificial neural networks for predicting the elastic modulus of recycled aggregate concrete" *Constr. Build. Mater*, 44: 524–532.

Z. Yuan, L. Wang, and X. Ji, (2014) "Prediction of concrete compressive strength: research on hybrid models genetic based algorithms and ANFIS" *Adv. Eng. Softw*, 67: 156–163.

<div align="right">

CHAPTER SEVEN

</div>

Conclusions and Recommendations

7.1 Summary and Conclusions

Concrete structures are generally vulnerable to cracking, which can adversely affect its performance and shorten its service life by primarily allowing harmful substances such as chloride ions, sulfates, and carbon dioxide to ingress into to the cementitious matrix. In addition, periodic maintenance and repair can be very costly, especially for large-scale structures. Thus, designing concrete structures with self-healing ability could save billions of dollars in maintenance and repair costs and improve both concrete durability and sustainability, thus leading to eco-friendly civil infrastructure. In the current thesis, self-healing of cracks in concrete under diverse environmental exposure was investigated.

In Chapter 2, the self-healing of surface and interior cracks in cement-based materials exposed to different environmental curing conditions was investigated. Results showed that cracks in cement-based materials exhibited self-healing primarily when the curing environment was conducive to contact with liquid water and no significant self-healing could be identified in the case of specimens exposed to cyclic T and RH. In addition, X-ray computed tomography showed that self-healing was mainly limited to surface cracks. The maximum crack depth that exhibited self-healing was 340 ± 30 µm from the surface of the cracked specimens. The maximum crack width healed in the tested specimens submerged in deionized water in this study was only 300 µm.

In Chapter 3, the self-healing of cracks in cement-based materials incorporating various minerals (i.e., metakaolin as a pozzolanic material, bentonite as a swelling agent, and limestone microfiller as a carbonate mineral) was quantified using X-ray µCT coupled with 3-dimensional quantitative image analysis. Results of optical microscopy showed that the maximum crack width healed for specimens submerged in water was about 330

µm, 290 µm, 260 µm, and 240 µm for specimens incorporating limestone microfiller, ordinary portland cement, bentonite, and metakaolin, respectively. For all specimens, the main crack healing product formed in cracks was $CaCO_3$. Based on image segmentation and quantification analysis, the healing efficiency was 32.26%, 27.27%, 25.6%, and 24.1% for specimens with limestone microfiller, ordinary portland cement, bentonite, and metakaolin, respectively.

In Chapter 4, non-destructive shear wave velocity tests were used to investigate strength recovery due to self-healing of cementitious materials exposed to various environments. In addition, the influence of additives such as silica-based materials, swelling agents, and carbonating minerals on strength recovery under different environmental exposure were evaluated. Results showed that the ability of mechanical strength recovery was in the order of specimens made with fly ash > metakaolin > ordinary portland cement > limestone microfiller > bentonite. This indicates that further hydration and pozzolanic reactions of the un-carked cementitious matrix and pozzolans play a major role in the strength recovery of cement-based materials.

In Chapter 5, the potential of superabsorbent polymers to promote crack self-healing of cement based-materials under simulated field conditions was investigated. Results showed that, under different environmental conditions, all specimens incorporating SAPs exhibited self-healing. The main crack healing product formed in cement mortar specimens with and without SAPs was $CaCO_3$. Based on image segmentation and quantification analysis, the healing efficiency was 26.32%, 19.11%, and 6.581% for specimens with 1% SAP exposed to water submersion, cyclic wetting and drying, and cyclic temperature and relative humidity, respectively.

In chapter 6, a hybrid genetic algorithm–artificial neural network (GA–ANN) model was developed to predict the self-healing of cracks in cement-based materials. Results showed that training the GA–ANN multilayered feed-forward neural network with a back-propagation algorithm achieved accurate prediction of the self-healing crack ability in cementitious materials, yielding predictions that were close to the actual experimental values. Hence, the proposed model was capable of providing accurate predictions for the self-healing ability of a cementitious material, which in turn can be

used to enhance the durability design of concrete, leading to more durable and sustainable structures.

7.2 Limitations of Current Study and Recommendations for Future Work

Based on the findings of the present study, there are several critical points that need improvement or future investigation:

- In the present study, self-healing of concrete was investigated through cracks generated at the age of 28 days. Further research is still required on self-healing of cracks formed at early- and long-term stages of the concrete service life under different environmental conditions.

- In addition, the self-healing process of cement-based materials under the combined actions of environmental conditioning and sustained loading needs to be explored.

- During the current study, crack self-healing and strength recovery were investigated in small specimens. Therefore, full-scale testing is required to evaluate the self-healing in concrete exposed under different environmental exposures.

- The efficiency of autogenous and improved autogenous self-healing to reduce chloride induced reinforcement corrosion also needs dedicated investigation.

- In the current study, results indicated that the presence of water in cracks is an essential factor for promoting both autogenous and improved autogenous self-healing in cement-based materials. However, results from X-ray μCT showed that self-healing was restricted to the surface region of cracks in cement-based materials. A major reason for the limitation of self-healing to near the surface is that this area tends to contain abundant amounts of calcium and carbonate ions. As a result, the surface region of the crack can exhibit faster healing process than the interior regions of the crack, which become isolated from the curing environment and experience restricted access of water. Therefore, it is recommended for future study to investigate combining autogenous healing with the effects of embedded microcapsules filled with a healing agent and quantifying the self-healing of the interior region of the crack using X-ray μCT.

APPENDIX A
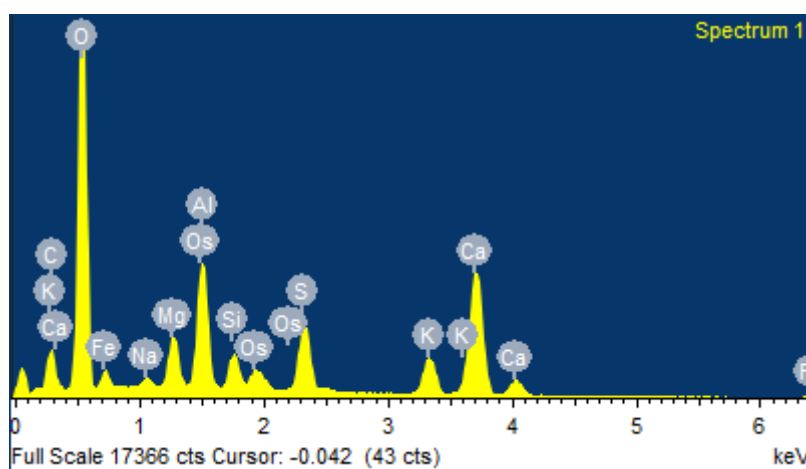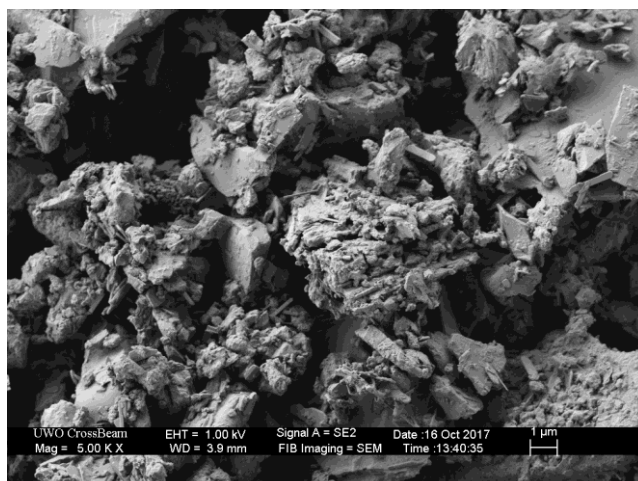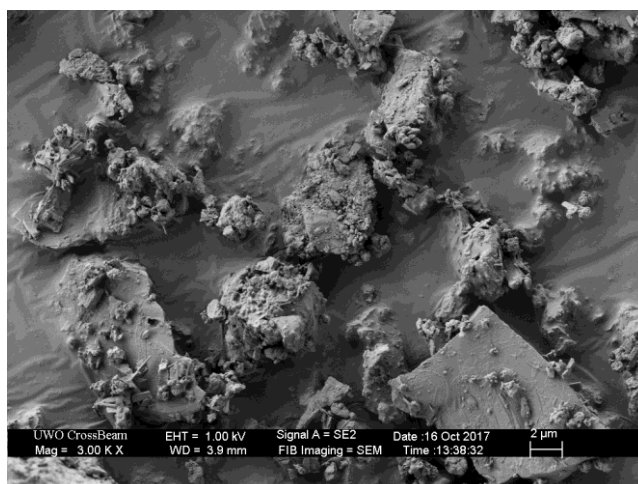
Figure A. 1 SEM micrograph with EDX pattern of the used cement.
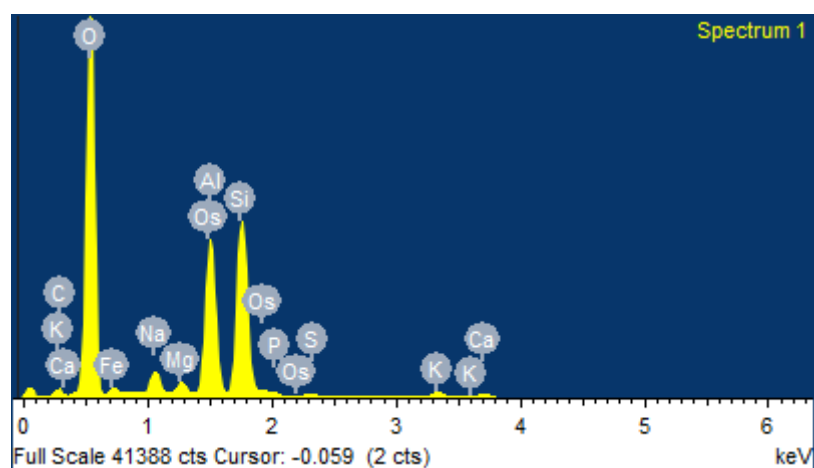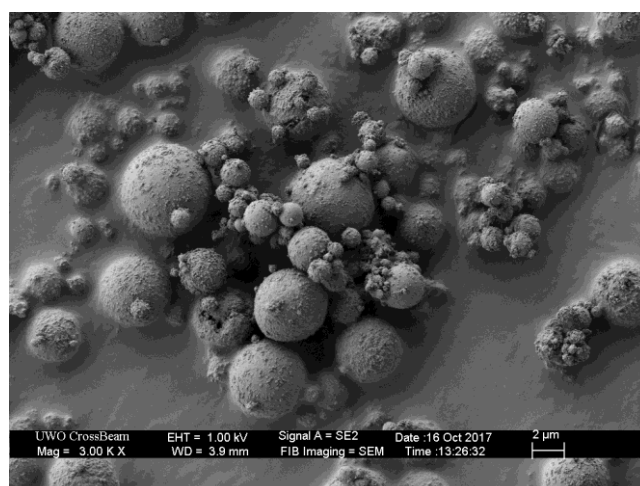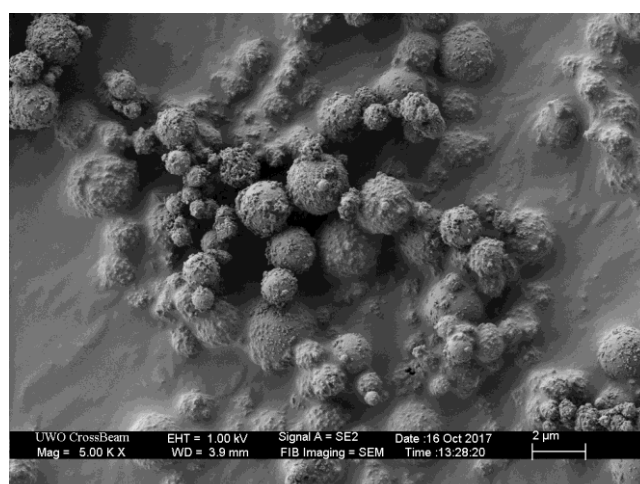
Figure A. 2 SEM micrograph with EDX pattern of the used fly ash.
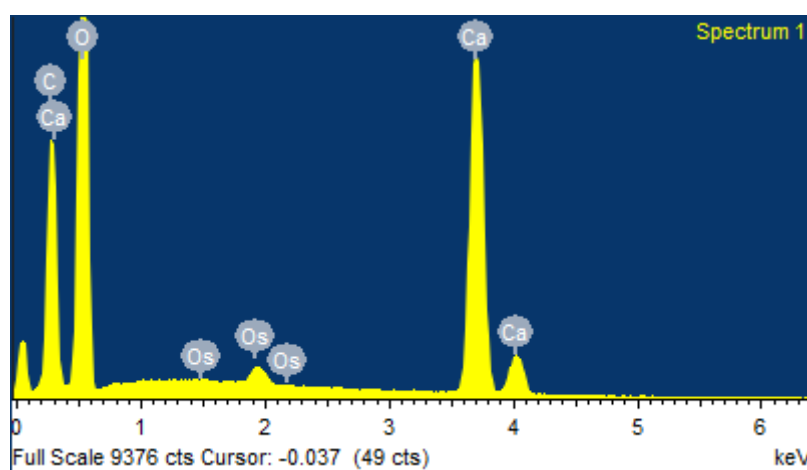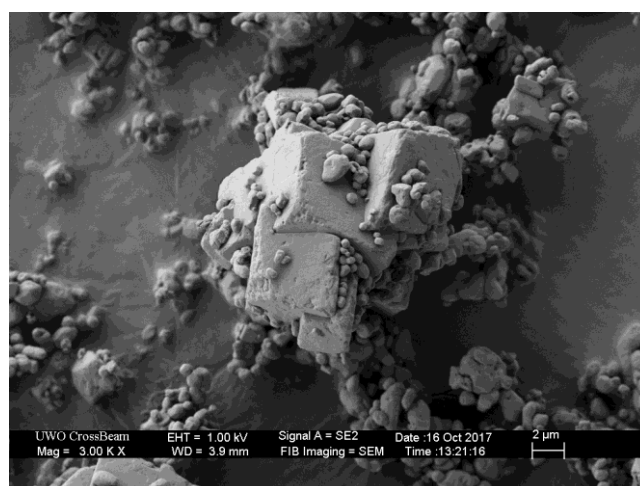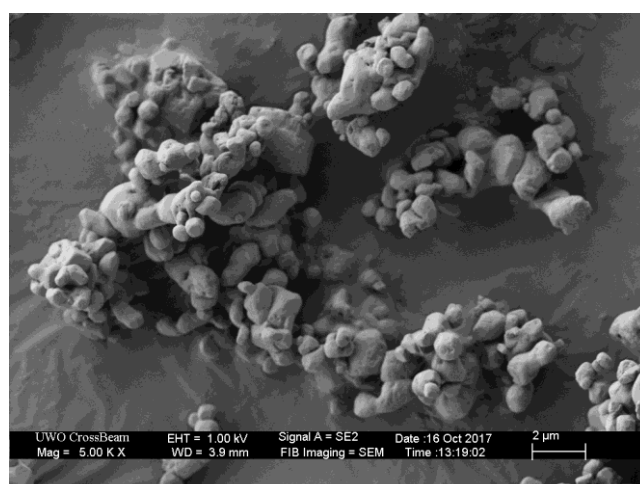
Figure A. 3 SEM micrograph with EDX pattern of the used calcium carbonate microfiller.
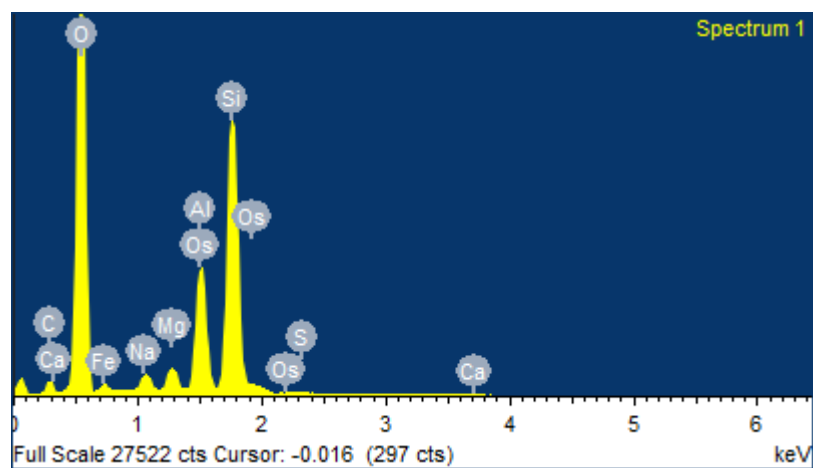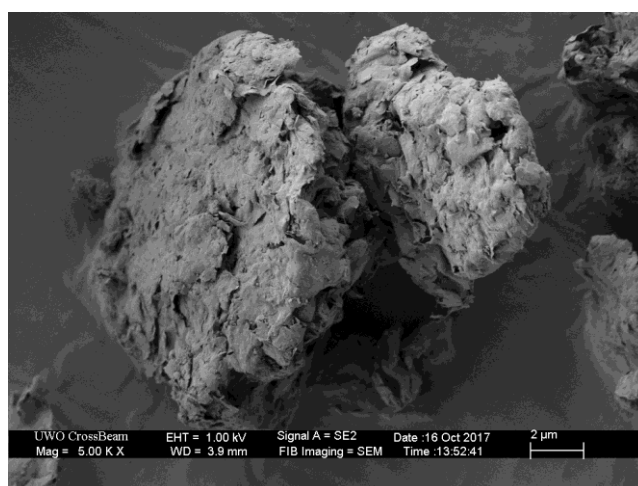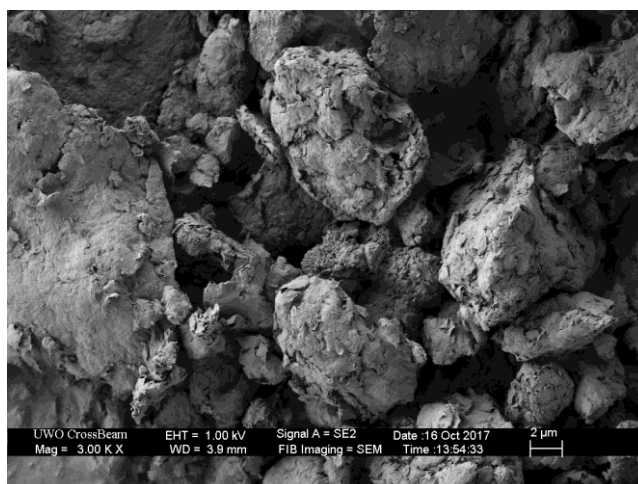
Figure A. 4 SEM micrograph with EDX pattern of the used bentonite.
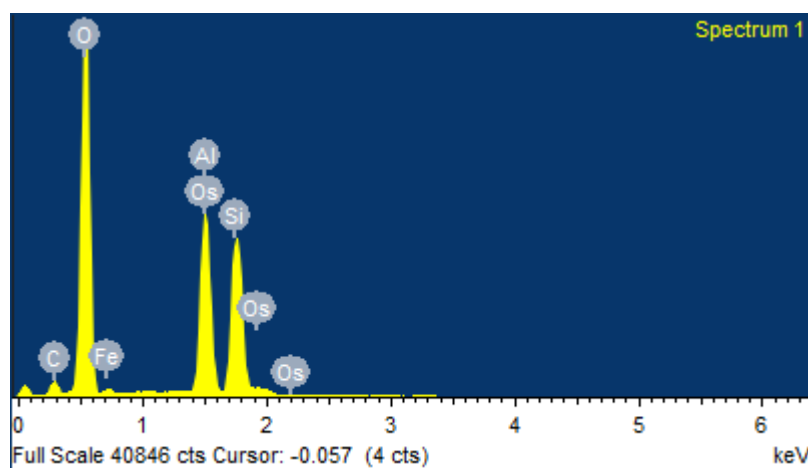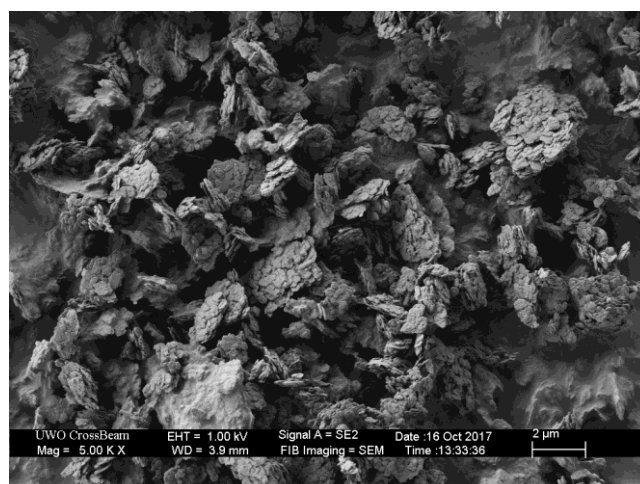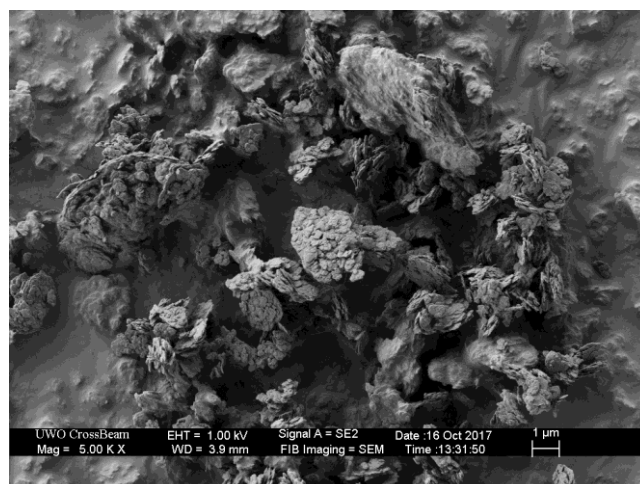
Figure A. 5 SEM micrograph with EDX pattern of the used metakaolin.
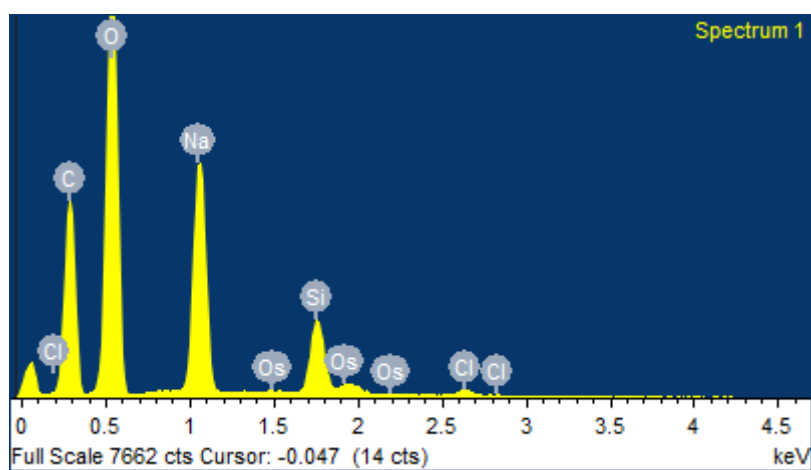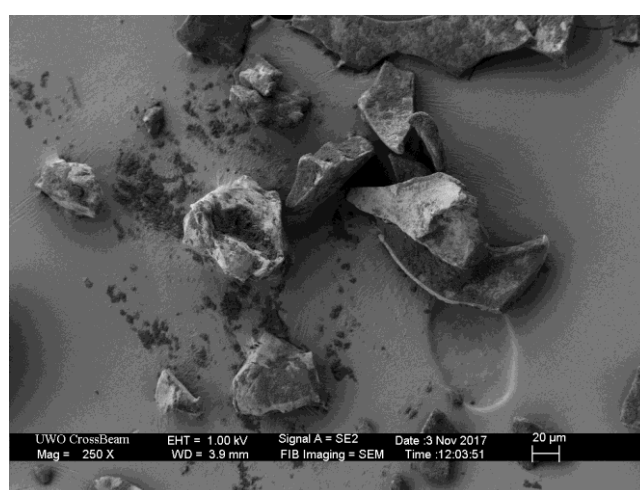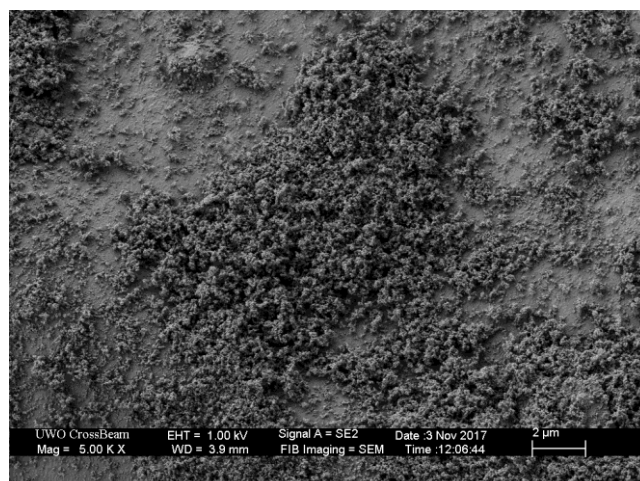
Figure A. 6 SEM micrograph with EDX pattern of the used superabsorbent polymers.

APPENDIX B

Table B. 1: Compressive strength of mortar specimens at
28 days before water submersion

	OPC	*F20*	*MK15*	*CC8*	*BEN8*
	63.08	47.24	92.40	48.05	47.88
	64.48	54.92	92.52	46.16	48.60
	72.68	51.04	85.12	50.96	51.25
Average	66.75	51.07	90.01	48.39	49.24
Coefficient of variation	0.08	0.08	0.05	0.05	0.04

Table B. 2: Compressive strength of mortar specimens at
1 year after water submersion

	OPC	*F20*	*MK15*	*CC8*	*BEN8*
	61.24	65.58	71.45	42.44	23.27
	59.57	47.41	56.10	42.17	25.67
	60.09	59.14	78.54	43.02	39.59
Average	60.30	57.38	68.70	42.54	29.51
Coefficient of variation	0.01	0.16	0.17	0.01	0.30

Table B. 3: Compressive strength of mortar specimens at
28 days before exposure to cyclic T and RH

	OPC	*F20*	*MK15*	*CC8*	*BEN8*
	68.64	59.88	64.36	49.60	51.64
	67.36	52.56	93.00	48.57	52.57
	69.80	56.76	78.80	50.53	50.62
Average	68.60	56.40	78.72	49.57	51.61
Coefficient of variation	0.02	0.07	0.18	0.02	0.02

Table B. 4: Compressive strength of mortar specimens at
1 year after exposure to cyclic T and RH

	OPC	*F20*	*MK15*	*CC8*	*BEN8*
	51.40	59.79	44.96	43.15	44.89
	48.20	55.64	50.96	40.94	35.96
	54.57	43.76	61.76	45.36	36.98
Average	51.39	53.06	52.56	43.15	39.28
Coefficient of variation	0.06	0.16	0.16	0.05	0.12

APPENDIX C

Table C. 1: MIP results for cracked OPC specimen at 28 days

Pore Diameter (µm)	Cumulative Intrusion (mL/g)
107.400375	5.61735E-31
71.35578125	0.001081562
53.66504375	0.001855621
38.97495625	0.003340117
35.70519063	0.003753656
28.56550938	0.004474697
25.19392598	0.004920046
22.54003438	0.005163928
20.39366406	0.005397205
16.4676875	0.005916779
13.37402969	0.006340921
10.68567344	0.007125583
8.549403906	0.007242223
8.109429688	0.007383494
5.032147266	0.007574635
4.560087109	0.007644024
3.808680469	0.007850416
2.95860625	0.008244839
2.469713672	0.008642052
1.901727148	0.009256883
1.538430957	0.009574663
1.237493457	0.010078426
0.985847266	0.010508359
0.794578809	0.01112477
0.652318799	0.011613802
0.509132031	0.012521638
0.412405615	0.013650968
0.335051074	0.014721963
0.267593286	0.015853709
0.216016455	0.01682247
0.178132581	0.017698351
0.142570715	0.01863333
0.112467078	0.019789508
0.090914142	0.021939961
0.07368606	0.023448193
0.059362268	0.025244493
0.047550458	0.028373307
0.038201996	0.033054203
0.030991788	0.039399751
0.024859612	0.046641786
0.020159392	0.052480165
0.016191847	0.057209946
0.014436586	0.059129082
0.013025314	0.06073064
0.010681013	0.063580632
0.008536335	0.066930845
0.007112424	0.067900173
0.006096018	0.069977067
0.005336427	0.071334623
0.004745102	0.072304703
0.004269915	0.073184133
0.00388189	0.073893815
0.003558576	0.074499294

Table C. 2: MIP results for cracked FA20 specimen at 28 days

Pore Diameter (µm)	Cumulative Intrusion (mL/g)
107.400375	7.8796E-31
71.35578125	0.002002837
53.66504375	0.002230432
38.97495625	0.002488373
35.70519063	0.002518719
28.56550938	0.002715968
25.19392598	0.002807006
22.54003438	0.002913217
20.39366406	0.002973909
16.4676875	0.003095293
13.37402969	0.003277369
10.68567344	0.003413927
8.549403906	0.003535311
8.109429688	0.003650068
5.032147266	0.003651798
4.560087109	0.003666169
3.808680469	0.003682165
2.95860625	0.003785059
2.469713672	0.004111217
1.901727148	0.005182841
1.538430957	0.005683891
1.237493457	0.008287688
0.985847266	0.010546259
0.794578809	0.012460239
0.652318799	0.013380523
0.509132031	0.014728237
0.412405615	0.015229498
0.335051074	0.01590452
0.267593286	0.01668134
0.216016455	0.017223068
0.178132581	0.017649895
0.142570715	0.018059349
0.112467078	0.018461142
0.090914142	0.018889701
0.07368606	0.019483155
0.059362268	0.020141793
0.047550458	0.021343958
0.038201996	0.023042794
0.030991788	0.02564013
0.024859612	0.029196382
0.020159392	0.033830326
0.016191847	0.04153702
0.014436586	0.046265636
0.013025314	0.049626444
0.010681013	0.052881781
0.008536335	0.056214094
0.007112424	0.058453566
0.006096018	0.061231246
0.005336427	0.062315646
0.004745102	0.067342367
0.004269915	0.069342444
0.00388189	0.071231232
0.003558576	0.073343245

Table C. 3: MIP results for cracked CC8 specimen at 28 days

Pore Diameter (μm)	Cumulative Intrusion (mL/g)
107.400375	1.53398E-30
71.35578125	0.00110921
53.66504375	0.001780574
38.97495625	0.002714646
35.70519063	0.002831405
28.56550938	0.003094113
25.19392598	0.003648718
22.54003438	0.003969805
20.39366406	0.004057374
16.4676875	0.004787118
13.37402969	0.005516861
10.68567344	0.006071466
8.549403906	0.006098134
8.109429688	0.006098134
5.032147266	0.006306097
4.560087109	0.006464425
3.808680469	0.006747713
2.95860625	0.007409091
2.469713672	0.007735522
1.901727148	0.008357876
1.538430957	0.008942183
1.237493457	0.00954897
0.985847266	0.010567285
0.794578809	0.011971368
0.652318799	0.013434098
0.509132031	0.014545789
0.412405615	0.015439789
0.335051074	0.016822477
0.267593286	0.017698351
0.216016455	0.01863333
0.178132581	0.019789508
0.142570715	0.021939961
0.112467078	0.023448193
0.090914142	0.025244493
0.07368606	0.028373307
0.059362268	0.033054203
0.047550458	0.039399751
0.038201996	0.046641786
0.030991788	0.055256706
0.024859612	0.059195377
0.020159392	0.062532842
0.016191847	0.065014996
0.014436586	0.067061752
0.013025314	0.067909099
0.010681013	0.068668284
0.008536335	0.069970377
0.007112424	0.071300253
0.006096018	0.072376229
0.005336427	0.073434346
0.004745102	0.073992356
0.004269915	0.074234267
0.00388189	0.075343766
0.003558576	0.076534695

Table C. 4: MIP results for cracked MK15 specimen at 28 days

Pore Diameter (µm)	Cumulative Intrusion (mL/g)
107.400375	3.78788E-31
71.35578125	0.001773137
53.66504375	0.002212818
38.97495625	0.002738993
35.70519063	0.002861527
28.56550938	0.003142634
25.19392598	0.003315623
22.54003438	0.003351662
20.39366406	0.003524651
16.4676875	0.003856214
13.37402969	0.004130113
10.68567344	0.004483299
8.549403906	0.005110384
8.109429688	0.005173631
5.032147266	0.005505158
4.560087109	0.005619895
3.808680469	0.005835167
2.95860625	0.006277535
2.469713672	0.00669308
1.901727148	0.007168339
1.538430957	0.007487815
1.237493457	0.007934855
0.985847266	0.008283602
0.794578809	0.008792888
0.652318799	0.009301193
0.509132031	0.009943094
0.412405615	0.010562999
0.335051074	0.011052376
0.267593286	0.011627995
0.216016455	0.012142679
0.178132581	0.012554396
0.142570715	0.013039551
0.112467078	0.013651888
0.090914142	0.014372567
0.07368606	0.015255734
0.059362268	0.016482392
0.047550458	0.01796745
0.038201996	0.01955661
0.030991788	0.020944444
0.024859612	0.022312731
0.020159392	0.023689637
0.016191847	0.026585627
0.014436586	0.029470639
0.013025314	0.032619499
0.010681013	0.038907152
0.008536335	0.044680778
0.007112424	0.048686653
0.006096018	0.051740721
0.005336427	0.054295018
0.004745102	0.056433599
0.004269915	0.058279157
0.00388189	0.059865855
0.003558576	0.061245132

Table C. 5: MIP results for cracked BN8 specimen at 28 days

Pore Diameter (µm)	Cumulative Intrusion (mL/g)
107.400375	7.0922E-31
71.35578125	0.000575664
53.66504375	0.001124553
38.97495625	0.001793931
35.70519063	0.001887643
28.56550938	0.002222332
25.19392598	0.00239637
22.54003438	0.002824771
20.39366406	0.002985422
16.4676875	0.003346886
13.37402969	0.003614636
10.68567344	0.003895775
8.549403906	0.004163526
8.109429688	0.00425157
5.032147266	0.004484235
4.560087109	0.004514362
3.808680469	0.004615491
2.95860625	0.004764879
2.469713672	0.004913052
1.901727148	0.005131667
1.538430957	0.005249713
1.237493457	0.00536455
0.985847266	0.005587744
0.794578809	0.005790376
0.652318799	0.005996684
0.509132031	0.006388302
0.412405615	0.006779795
0.335051074	0.007123871
0.267593286	0.007483243
0.216016455	0.007858754
0.178132581	0.008247287
0.142570715	0.008659406
0.112467078	0.009152651
0.090914142	0.009727927
0.07368606	0.010406638
0.059362268	0.011626573
0.047550458	0.014670506
0.038201996	0.020351894
0.030991788	0.028195594
0.024859612	0.036233231
0.020159392	0.042853039
0.016191847	0.048055701
0.014436586	0.050383225
0.013025314	0.052424498
0.010681013	0.055916596
0.008536335	0.059536584
0.007112424	0.061659392
0.006096018	0.063544646
0.005336427	0.064210489
0.004745102	0.065124854
0.004269915	0.065615386
0.00388189	0.066191479
0.003558576	0.066514961

Table C. 6: MIP results for cracked OPC specimen submerged in water for 1 year

Pore Diameter (μm)	Cumulative Intrusion (mL/g)
107.400375	4.34367E-31
71.35578125	0.000450962
53.66504375	0.00070514
38.97495625	0.001106906
35.70519063	0.001221696
28.56550938	0.001492273
25.19392598	0.001582465
22.54003438	0.001713654
20.39366406	0.001844843
16.4676875	0.002123619
13.37402969	0.002402395
10.68567344	0.002804162
8.549403906	0.003263322
8.109429688	0.003347814
5.032147266	0.003602565
4.560087109	0.003688392
3.808680469	0.003950414
2.95860625	0.004215603
2.469713672	0.004441981
1.901727148	0.004848141
1.538430957	0.005187785
1.237493457	0.00557204
0.985847266	0.005986176
0.794578809	0.006494439
0.652318799	0.007330801
0.509132031	0.00840274
0.412405615	0.009569586
0.335051074	0.010831573
0.267593286	0.012432171
0.216016455	0.014171109
0.178132581	0.015843777
0.142570715	0.017781366
0.112467078	0.0195482
0.090914142	0.021126416
0.07368606	0.02262222
0.059362268	0.024296455
0.047550458	0.026691858
0.038201996	0.030829821
0.030991788	0.037199762
0.024859612	0.044666231
0.020159392	0.050197288
0.016191847	0.053954776
0.014436586	0.055145916
0.013025314	0.05633606
0.010681013	0.058343943
0.008536335	0.060367879
0.007112424	0.062136278
0.006096018	0.063319907
0.005336427	0.064498551
0.004745102	0.065416619
0.004269915	0.066269144
0.00388189	0.066884838
0.003558576	0.067549698

Table C. 7: MIP results for cracked FA20 specimen submerged in water for 1 year

Pore Diameter (µm)	Cumulative Intrusion (mL/g)
107.400375	4.47427E-31
71.35578125	0.000633437
53.66504375	0.00091215
38.97495625	0.001106404
35.70519063	0.001157079
28.56550938	0.001325996
25.19392598	0.001385116
22.54003438	0.001435791
20.39366406	0.001494912
16.4676875	0.001613154
13.37402969	0.001731395
10.68567344	0.001841191
8.549403906	0.002018554
8.109429688	0.002036577
5.032147266	0.002315852
4.560087109	0.002366149
3.808680469	0.002446773
2.95860625	0.002728407
2.469713672	0.002933918
1.901727148	0.003170935
1.538430957	0.003520319
1.237493457	0.004016642
0.985847266	0.004391892
0.794578809	0.004738504
0.652318799	0.005028315
0.509132031	0.005318911
0.412405615	0.005707133
0.335051074	0.006072398
0.267593286	0.006392987
0.216016455	0.006677078
0.178132581	0.006871209
0.142570715	0.007052721
0.112467078	0.007345518
0.090914142	0.007635584
0.07368606	0.007948921
0.059362268	0.008357663
0.047550458	0.009034752
0.038201996	0.009130273
0.030991788	0.009740457
0.024859612	0.010987064
0.020159392	0.012519431
0.016191847	0.014128021
0.014436586	0.016618814
0.013025314	0.01800617
0.010681013	0.019035453
0.008536335	0.021901734
0.007112424	0.025089469
0.006096018	0.027838547
0.005336427	0.029315902
0.004745102	0.030052152
0.004269915	0.030572118
0.00388189	0.031020388
0.003558576	0.031029427

Table C. 8: MIP results for cracked CC8 specimen submerged in water for 1 year

Pore Diameter (μm)	Cumulative Intrusion (mL/g)
107.400375	0.000705149
71.35578125	0.001106906
53.66504375	0.001221696
38.97495625	0.001492273
35.70519063	0.001582465
28.56550938	0.001713654
25.19392598	0.001844843
22.54003438	0.002123619
20.39366406	0.002402395
16.4676875	0.002804162
13.37402969	0.003263322
10.68567344	0.003347814
8.549403906	0.003602565
8.109429688	0.003688392
5.032147266	0.003950414
4.560087109	0.004215603
3.808680469	0.004441981
2.95860625	0.004848141
2.469713672	0.005187785
1.901727148	0.005572039
1.538430957	0.005986176
1.237493457	0.006494439
0.985847266	0.007330801
0.794578809	0.008402739
0.652318799	0.008923279
0.509132031	0.009121337
0.412405615	0.011231311
0.335051074	0.011829876
0.267593286	0.013032327
0.216016455	0.013623223
0.178132581	0.013982325
0.142570715	0.015932325
0.112467078	0.016723232
0.090914142	0.017823236
0.07368606	0.021546547
0.059362268	0.025876686
0.047550458	0.028808678
0.038201996	0.033451729
0.030991788	0.037945032
0.024859612	0.041551374
0.020159392	0.044296458
0.016191847	0.046713226
0.014436586	0.047813356
0.013025314	0.048749104
0.010681013	0.050362404
0.008536335	0.052906971
0.007112424	0.053053461
0.006096018	0.053608026
0.005336427	0.055472285
0.004745102	0.056790136
0.004269915	0.058244459
0.00388189	0.059932467
0.003558576	0.061486341

Table C. 9: MIP results for cracked MK15 specimen submerged in water for 1 year

Pore Diameter (μm)	Cumulative Intrusion (mL/g)
107.400375	4.47427E-31
71.35578125	0.000434214
53.66504375	0.000791802
38.97495625	0.001226016
35.70519063	0.001379268
28.56550938	0.001685772
25.19392598	0.001847538
22.54003438	0.001983762
20.39366406	0.002111472
16.4676875	0.002409462
13.37402969	0.002673396
10.68567344	0.003065041
8.549403906	0.003771703
8.109429688	0.00380082
5.032147266	0.004018551
4.560087109	0.004083383
3.808680469	0.00422608
2.95860625	0.004979126
2.469713672	0.005346131
1.901727148	0.005727673
1.538430957	0.00619274
1.237493457	0.006542131
0.985847266	0.007095855
0.794578809	0.007627993
0.652318799	0.008205418
0.509132031	0.008779768
0.412405615	0.009262306
0.335051074	0.009671317
0.267593286	0.010115859
0.216016455	0.010459162
0.178132581	0.010742397
0.142570715	0.011058903
0.112467078	0.011406707
0.090914142	0.011750335
0.07368606	0.012077958
0.059362268	0.012411039
0.047550458	0.012904899
0.038201996	0.013555972
0.030991788	0.014606568
0.024859612	0.01488398
0.020159392	0.016573492
0.016191847	0.018251911
0.014436586	0.020432819
0.013025314	0.021852149
0.010681013	0.023367202
0.008536335	0.026624138
0.007112424	0.030611582
0.006096018	0.033583798
0.005336427	0.035816975
0.004745102	0.037473381
0.004269915	0.038774591
0.00388189	0.039843209
0.003558576	0.040821236

Table C. 10: MIP results for cracked BN8 specimen submerged in water for 1 year

Pore Diameter (µm)	Cumulative Intrusion (mL/g)
107.400375	4.1198E-31
71.35578125	0.000572283
53.66504375	0.001097528
38.97495625	0.001983391
35.70519063	0.002116662
28.56550938	0.002532155
25.19392598	0.002673266
22.54003438	0.002853574
20.39366406	0.003018203
16.4676875	0.003308265
13.37402969	0.003614005
10.68567344	0.003990299
8.549403906	0.004437151
8.109429688	0.004537663
5.032147266	0.004880073
4.560087109	0.004957018
3.808680469	0.005155305
2.95860625	0.005469104
2.469713672	0.005702171
1.901727148	0.006166504
1.538430957	0.006357367
1.237493457	0.006632225
0.985847266	0.006915031
0.794578809	0.007156235
0.652318799	0.007612618
0.509132031	0.007999594
0.412405615	0.008480576
0.335051074	0.009037078
0.267593286	0.009532553
0.216016455	0.010072369
0.178132581	0.010584999
0.142570715	0.010921728
0.112467078	0.011373143
0.090914142	0.011890666
0.07368606	0.01247651
0.059362268	0.013199539
0.047550458	0.014657727
0.038201996	0.016945252
0.030991788	0.020295665
0.024859612	0.025533577
0.020159392	0.032042149
0.016191847	0.038998522
0.014436586	0.042558059
0.013025314	0.045241371
0.010681013	0.04887474
0.008536335	0.052033316
0.007112424	0.054057941
0.006096018	0.055888202
0.005336427	0.057141617
0.004745102	0.05805191
0.004269915	0.058784913
0.00388189	0.059356827
0.003558576	0.059828155

Table C. 11: MIP results for cracked OPC specimen exposed to Cyclic T and RH for 1 year

Pore Diameter (μm)	Cumulative Intrusion (mL/g)
107.400375	7.96115E-31
71.35578125	0.00101499
53.66504375	0.001393718
38.97495625	0.002348111
35.70519063	0.002454155
28.56550938	0.002954076
25.19392598	0.003120716
22.54003438	0.003272207
20.39366406	0.003438847
16.4676875	0.003817575
13.37402969	0.004226601
10.68567344	0.004438688
8.549403906	0.004787118
8.109429688	0.004840058
5.032147266	0.005078446
4.560087109	0.005111271
3.808680469	0.005221411
2.95860625	0.005372891
2.469713672	0.005639228
1.901727148	0.006208073
1.538430957	0.006631969
1.237493457	0.007018149
0.985847266	0.007758843
0.794578809	0.008500334
0.652318799	0.009731044
0.509132031	0.012010189
0.412405615	0.014834999
0.335051074	0.018353845
0.267593286	0.020905871
0.216016455	0.022766773
0.178132581	0.023897567
0.142570715	0.025161639
0.112467078	0.026562455
0.090914142	0.028321298
0.07368606	0.030759124
0.059362268	0.035082755
0.047550458	0.046556011
0.038201996	0.047588899
0.030991788	0.053609777
0.024859612	0.05810843
0.020159392	0.062003743
0.016191847	0.065303318
0.014436586	0.068398476
0.013025314	0.069966748
0.010681013	0.071325779
0.008536335	0.073807858
0.007112424	0.076464415
0.006096018	0.078617692
0.005336427	0.080615871
0.004745102	0.082524635
0.004269915	0.084263689
0.00388189	0.086130857
0.003558576	0.087798402

Table C. 12: MIP results for cracked FA20 specimen exposed to Cyclic T and RH for 1 year

Pore Diameter (μm)	Cumulative Intrusion (mL/g)
107.400375	5.87199E-31
71.35578125	0.000256995
53.66504375	0.000670421
38.97495625	0.001139716
35.70519063	0.001195585
28.56550938	0.001374364
25.19392598	0.001452579
22.54003438	0.001519622
20.39366406	0.001575497
16.4676875	0.001709574
13.37402969	0.001988917
10.68567344	0.002245912
8.549403906	0.002469386
8.109429688	0.002478231
5.032147266	0.002567565
4.560087109	0.002600541
3.808680469	0.002924048
2.95860625	0.003216583
2.469713672	0.003499123
1.901727148	0.003929735
1.538430957	0.004391319
1.237493457	0.004790718
0.985847266	0.005116957
0.794578809	0.005436663
0.652318799	0.005767438
0.509132031	0.006347644
0.412405615	0.007061518
0.335051074	0.007546029
0.267593286	0.007959058
0.216016455	0.008454827
0.178132581	0.008996091
0.142570715	0.009618786
0.112467078	0.010516032
0.090914142	0.012352719
0.07368606	0.016582971
0.059362268	0.024670264
0.047550458	0.039834484
0.038201996	0.041314822
0.030991788	0.044043675
0.024859612	0.046230834
0.020159392	0.047978323
0.016191847	0.049312085
0.014436586	0.050514132
0.013025314	0.051107913
0.010681013	0.051709153
0.008536335	0.052532081
0.007112424	0.053498622
0.006096018	0.054330207
0.005336427	0.055111959
0.004745102	0.055893652
0.004269915	0.056698117
0.00388189	0.057533767
0.003558576	0.058430053

Table C. 13: MIP results for cracked CC8 specimen exposed to Cyclic T and RH for 1 year

Pore Diameter (µm)	Cumulative Intrusion (mL/g)
107.400375	5.7402E-31
71.35578125	0.000720912
53.66504375	0.001267057
38.97495625	0.00187874
35.70519063	0.002173658
28.56550938	0.003091182
25.19392598	0.003342409
22.54003438	0.003560867
20.39366406	0.003801171
16.4676875	0.004270856
13.37402969	0.004827924
10.68567344	0.005308532
8.549403906	0.006215133
8.109429688	0.006301783
5.032147266	0.006900132
4.560087109	0.007304648
3.808680469	0.007881993
2.95860625	0.008644421
2.469713672	0.009226599
1.901727148	0.010634919
1.538430957	0.012171453
1.237493457	0.013545764
0.985847266	0.015565654
0.794578809	0.016545406
0.652318799	0.017693438
0.509132031	0.019843736
0.412405615	0.021311336
0.335051074	0.021734343
0.267593286	0.024343867
0.216016455	0.026323276
0.178132581	0.028756379
0.142570715	0.035232563
0.112467078	0.039823562
0.090914142	0.048232678
0.07368606	0.052122468
0.059362268	0.059385259
0.047550458	0.062210362
0.038201996	0.064246528
0.030991788	0.065905631
0.024859612	0.067515962
0.020159392	0.068974309
0.016191847	0.070631973
0.014436586	0.071532227
0.013025314	0.072383441
0.010681013	0.073947847
0.008536335	0.075621843
0.007112424	0.076848991
0.006096018	0.077793658
0.005336427	0.078633986
0.004745102	0.079339914
0.004269915	0.079977468
0.00388189	0.080583572
0.003558576	0.081278585

Table C. 14: MIP results for cracked MK15 specimen exposed to Cyclic T and RH for 1 year

Pore Diameter (μm)	Cumulative Intrusion (mL/g)
107.400375	7.02543E-31
71.35578125	0.000477414
53.66504375	0.000808952
38.97495625	0.001193536
35.70519063	0.001246582
28.56550938	0.001432243
25.19392598	0.001525074
22.54003438	0.00157812
20.39366406	0.001697473
16.4676875	0.00184335
13.37402969	0.00228098
10.68567344	0.002652302
8.549403906	0.003076671
8.109429688	0.003114415
5.032147266	0.003325447
4.560087109	0.003365906
3.808680469	0.004570746
2.95860625	0.005456939
2.469713672	0.005837401
1.901727148	0.006425841
1.538430957	0.006885772
1.237493457	0.007537016
0.985847266	0.009069112
0.794578809	0.010396504
0.652318799	0.011338308
0.509132031	0.012900095
0.412405615	0.014429938
0.335051074	0.015698785
0.267593286	0.016806103
0.216016455	0.017743587
0.178132581	0.018377917
0.142570715	0.018964104
0.112467078	0.019707007
0.090914142	0.020455556
0.07368606	0.021419089
0.059362268	0.024735855
0.047550458	0.031678617
0.038201996	0.036328085
0.030991788	0.039843041
0.024859612	0.042947173
0.020159392	0.045286734
0.016191847	0.047314286
0.014436586	0.048363645
0.013025314	0.049340226
0.010681013	0.051233437
0.008536335	0.054088879
0.007112424	0.056109149
0.006096018	0.057657544
0.005336427	0.058912776
0.004745102	0.059979449
0.004269915	0.060973379
0.00388189	0.061794793
0.003558576	0.062801198

Table C. 15: MIP results for cracked BN8 specimen exposed to Cyclic T and RH for 1 year

Pore Diameter (µm)	Cumulative Intrusion (mL/g)
107.400375	6.81013E-31
71.35578125	0.000751614
53.66504375	0.001218133
38.97495625	0.002112295
35.70519063	0.002371472
28.56550938	0.003187879
25.19392598	0.003615523
22.54003438	0.003939494
20.39366406	0.004237548
16.4676875	0.004833655
13.37402969	0.005533434
10.68567344	0.006272089
8.549403906	0.006984827
8.109429688	0.007051026
5.032147266	0.007517645
4.560087109	0.007617138
3.808680469	0.007990307
2.95860625	0.008351832
2.469713672	0.008597724
1.901727148	0.009298428
1.538430957	0.009740438
1.237493457	0.010183628
0.985847266	0.010878659
0.794578809	0.012092284
0.652318799	0.014075756
0.509132031	0.016005704
0.412405615	0.017519612
0.335051074	0.018633472
0.267593286	0.019329621
0.216016455	0.019900188
0.178132581	0.020437934
0.142570715	0.021092707
0.112467078	0.022146536
0.090914142	0.023711829
0.07368606	0.028220113
0.059362268	0.039021928
0.047550458	0.039746527
0.038201996	0.047153018
0.030991788	0.051729269
0.024859612	0.055027369
0.020159392	0.057759181
0.016191847	0.059801676
0.014436586	0.061579064
0.013025314	0.062413189
0.010681013	0.063165434
0.008536335	0.064678349
0.007112424	0.066398047
0.006096018	0.067876562
0.005336427	0.069104843
0.004745102	0.070184797
0.004269915	0.071143016
0.00388189	0.072043777
0.003558576	0.072847933

CURRICULUM VITAE

EDUCATION

Ph.D. Civil and Environmental Engineering   **2019**
University of Western Ontario, London, ON
Thesis: Self-healing of Concrete Under Diverse Environmental Exposure

MESc. Civil and Environmental Engineering   **2014**
University of Western Ontario, London, ON
Thesis: Physical Sulphate Attack on Concrete

BSc. Civil Engineering   **2004**
University of Benghazi, Libya
Project: Design of Crane-Supporting Steel Structure

RELATED RESEARCH EXPERIENCE

Graduate Research Assistant   **2012 - 2019**
University of Western Ontario, London, ON

- Investigated the mechanism of concrete durability exposed to physical and chemical sulfate attack.
- Simulated field exposure of concrete to severe natural environment in the lab.
- Proposed solutions to mitigate concrete exposed to physical sulfate attack.
- Investigated the potential alkali-reactivity of different aggregates.
- Explored the effect of using different materials including bentonite, nano-silica, fly ash, superabsorbent, and calcium carbonite in concrete exposed to cyclic temperature and relative humidity.
- Collaborated with other graduate student researchers from State University of Northern Rio de Janeiro in investigating the effect of using sugarcane bagasse ash in hydrated cement paste.
- Developed a hybrid artificial intelligence-based model to accurately predict the concrete's capability to heal its own cracks.
- Investigated the effect of environmental exposure on self-healing of cracks in cement-based materials.

Reviewer   **2019**
CSCE Annual Conference

- Acted as a reviewer in CSCE annual conference, 7th international conference on engineering mechanics and materials.

RELATED TEACHING EXPERIENCE

Instructor
EPIC Training, Mississauga, ON   **2019 - Present**

- Worked as an instructor for the courses: (a) Diagnosing Defects in Aging Concrete Structures and Developing Effective Repair Solutions, and (b) Formwork for Concrete Structures.

Lecturer
University of Western Ontario, London, ON   **2018 -2019**

- Worked as a lecturer for the course CEE 3369B: Materials for Civil Engineering at Western University for the 2018-2019 academic year.
- Supervised and trained teaching assistants assigned to the course.
- Worked in tandem with the lab supervisor to orchestrate four lab sections for undergraduate students.

Teaching Assistant   **2012 - 2019**
University of Western Ontario, London, ON

- Coordinated tutorials and laboratory sessions for the civil engineering courses CEE 3369B: Materials for Civil Engineering, CEE 2202A: Mechanics of Materials, and ES 1022: Engineering Statics.
- Planned and directed tutorial and laboratory sessions for hundreds of undergraduate students.
- Conducted pre-laboratory discussion, detailing safety precautions, and ensured safe laboratory techniques were employed by undergraduate students.
- Delivered presentations and lectures to assist students in their term project.

RELATED INDUSTRIAL EXPERIENCE

QA-QC Lead Engineer   **2008- 2009**
Man Enterprise (off-shore), Tripoli/Libya

- Supervised sub-contractor on implementing the project in terms of constructing deep foundations, diaphragm walls, and managing the dewatering system.
- Supervised and monitored the quality of concrete and steel reinforcement used in construction of the Intercontinental Hotel and Tripoli Tower project.
- Implemented standard quality assurance and quality control of materials used in constructions.
- Prepared daily and monthly reports and revised the sub-contractor's technical reports for approval.
- Maintained coordination of the project implementation with consultant and sub-contractors.

Supervisor and Designer Engineer   **2004 - 2008**
Alemaad consultant Engineers, Tripoli/Libya

- Supervised the construction of 66Kv and 400Kv overhead transmission line project for the Libyan Ministry of Energy
- Supervised the design and construction of steel building with double overhead cranes.
- Tested the properties of concrete and steel reinforcement used in various projects.
- Prepared the specification and the detailed drawings for three high-way concrete bridges for the Libyan Ministry of Transportation.
- Designed and supervised the maintenance of multi-story concrete structures in the old city of Tripoli.
- Designed various concrete and steel structures.
- Reviewed and checked structural design and geotechnical investigation for various projects.

AWARDS

- CEE Teaching Assistant Excellence Awards **2017 - 2018**
- Ontario Graduate Scholarship **2016 - 2017**
- Graduate Scholarship in Structural Engineering **2016**

LIST OF RELATED PUBLICATIONS
Journal Papers

- **A. R. Suleiman**, A. Nelson, and M. L. Nehdi, (2019) "Visualization and quantification of crack self-healing in cement-based materials incorporating different minerals", *Cement and Concrete composites*", *Cement and Concrete Composites*, 103:49-58.
- **A. R. Suleiman** and M. L. Nehdi, (2018) "Effect of environmental exposure on autogenous self-healing of cracked cement-based materials", *Cement and Concrete Research.* 111:197-208
- **A. R. Suleiman** and M. L. Nehdi (2017) "Modeling self-healing of concrete using hybrid genetic algorithm–artificial neural network", *Materials*, 10: 135.
- **A. R. Suleiman** and M. L. Nehdi, (2017) "Exploring effects of supplementary cementitious materials in concrete exposed to physical salt attack", *Magazine of Concrete Research.* 69(11): 576 -585.
- P. Andreao**, A. R. Suleiman,** G. C. Cordeiro and M. L. Nehdi, (2019) "Exploring effects of sugarcane bagasse ash in cement-based materials", *Green Materials*. 10p.
- P. Andreao**, A. R. Suleiman,** G. C. Cordeiro and M. L. Nehdi, (2019) "Benefciation of sugarcane bagasse ash: pozzolanic activity and leaching behavior", *Waste and Biomass Valorization*. 10p.
- **A. R. Suleiman**, A.M. Soliman, and M.L.Nehdi, (2014) "Effect of Surface Treatment on Durability of Concrete Exposed to Physical Sulfate Attack", *Construction & Building Materials*. Vol. 73: 674-681.
- M. L. Nehdi, **A. R. Suleiman**, and A. M. Soliman (2014) "Investigation of concrete exposed to dual sulfate attack", *Cement and Concrete Research*. Vol. 64: 42-53.

Conference Papers

- **A. R. Suleiman** and M. L. Nehdi, (2019) "Self-Healing Behaviour of Cracks in Cement-Based Materials Exposed to Cyclic Temperature and Relative Humidity", *The 7th International Conference on Engineering Mechanics and Materials*, Proceeding of the Annual Conference of the Canadian Society for Civil Engineering, Laval, Canada.
- **A. R. Suleiman** and M. L. Nehdi, (2018) "Effect of Environmental Exposure on Formation of Self-Healing Product in Cracked Cement Based Materials. *The 7th International Materials Specialty Conference, Proceeding of the Annual Conference of the Canadian Society for Civil Engineering*, Fredericton, Canada.
- **A. R. Suleiman** and M. L. Nehdi, (2017) "Predicting Self-healing in Concrete Using Artificial Neural Networks. *The 6th International Conference on Engineering Mechanics and Materials, Proceeding of the Annual Conference of the Canadian Society for Civil Engineering*, Vancouver, BC, Canada.
- **A. R. Suleiman** and M. L. Nehdi, (2016) **"**Effect of pore structure on concrete deterioration by physical sulphate attack. *The 5th International Materials Specialty Conference, Proceeding of the Annual Conference of the Canadian Society for Civil Engineering*, London, ON, Canada.
- **A. R. Suleiman** and M. L. Nehdi, (2016) "Alkali-silica reactivity in Southwestern Ontario aggregates. *The 5th International Materials Specialty Conference, Proceeding of the Annual Conference of the Canadian Society for Civil Engineering*, London, ON, Canada.